

DEMOCRATIC AND POPULAR REPUBLIC OF ALGERIA
MINISTRY OF HIGHER EDUCATION AND SCIENTIFIC
RESEARCH

MOHAMED KHIDER UNIVERSITY OF BISKRA
FACULTY OF EXACT SCIENCES, SCIENCES OF NATURE AND LIFE
DEPARTMENT OF MATTER SCIENCES
Applied Chemistry Laboratory (LCA)



DISSERTATION

Presented by

BACHIR Nassima

To obtain the degree of

Doctorate in Chemistry

Option:

Pharmaceutical chemistry

Entitled:

**Searching for Neutralisers of Energetic Organic
Compounds: A Theoretical Approach from the
Perspective of Quantum Chemistry**

Publicly defended on: 29th February 2024

In front of the jury composed of:

Mr. CHADLI Abdelhakim	MCA	University of Biskra	President
Mr. KENOUCHE Samir	MCA	University of Biskra	Supervisor
Mr. MELKEMI Nadjib	Prof.	University of Biskra	Co-Supervisor
Mr. MESSAOUDI Abdelatif	Prof.	University of Batna 1	Examiner
Mr. DAOUD Ismail	MCA	University of Biskra	Examiner

*This work is dedicated to my dearly beloved parents
To my dear brothers and sisters
To my dear brother's wife and uncle
To my dear, precious and wonderful nephews and nieces
To all my family and everyone who is dear to me*

Acknowledgments

First and foremost, I would like to express my heartfelt gratitude and praise to Allah Almighty for bestowing upon me the strength, patience, and determination to overcome challenges and reach this momentous day that I eagerly anticipated.

I want to express my deep appreciation and extend my sincere thanks to my supervisor, **Dr. KENOUCHE Samir**, under whose guidance I had the privilege to work. I deeply appreciate his exceptional competence, remarkable expertise, and consistent professionalism. Thank you for the invaluable assistance, guidance, encouragement, and insightful advice throughout these three years. I am grateful for the time he dedicated to me despite his numerous commitments. I learned and benefited greatly from him during this experience.

I would also like to convey my sincere appreciation to **prof. Martínez-Araya Jorge Ignacio** at Andrés Bello University-Chile for the technical support that significantly enhanced our work and saved us considerable time. Your valuable comments and advice were instrumental, and it was an honor to collaborate with someone of your caliber. Also, thanks to my co-supervisor **Prof. MELKEMI Nadjib** for his valuable advice, guidance, and encouragement.

I extend my sincere gratitude to the respected jury members: **Dr. CHADLI Abdelhakim** of Biskra University, **Prof. MESSAOUDI Abdelatif** of Batna 1 University, and **Dr. DAOUD Ismail** of Biskra University for accepting the responsibility of evaluating this dissertation and for generously dedicating their precious time.

My profound appreciation goes to all my teachers who played a crucial role in supporting my academic journey. To my colleagues and friends, with whom I shared moments of joy, faced challenges together, engaged in meaningful discussions, and received valuable advice, I express my heartfelt thanks and extend my best wishes to each and every one of you.

To my dear parents, words cannot fully capture the depth of my gratitude for your unwavering support. Everything I have achieved today is a testament to your hard work, dedication, and prayers. I extend my warmest thanks and profound appreciation to both of you.

To my family, my brothers and sisters, thank you for your encouragement, assistance, and constant presence by my side. A special acknowledgment goes to my dear brothers Khaled and Nasreddine for their unwavering support and encouragement which have consistently motivated me.

Finally, I express my gratitude to everyone who played a part, whether big or small, in my career.

Thanks greatly
Nassima Bachir

List of works

International publications:

1. **Bachir N**, Kenouche S, and Martínez-Araya J.I., Theoretical investigation of the effect of $O \cdots M = \{Ti, Zr, Hf\}$ interactions on the sensitivity of energetic N-nitro compounds. *Journal of Molecular Graphics and Modelling*, **2023**. 118: p. 108341. <https://doi.org/10.1016/j.jmgm.2022.108341>
2. **Bachir N**, Kenouche S, and Martínez-Araya J. I., The effect of $\{O,N\} = X \cdots M = \{Ti,Zr,Hf\}$ interactions on the sensitivity of C-NO₂ trigger bonds in FOX-7: Approach based on the QTAIM/EDA-NOCV analysis. *Journal of Molecular Graphics and Modelling*, **2024**. 126, 108645. <https://doi.org/10.1016/j.jmgm.2023.108645>
3. Kenouche S, **Bachir N**, and Martínez-Araya J.I., Explaining the High Catalytic Activity in Bis (indenyl) methyl Zirconium Cation Using Combined EDA-NOCV/QTAIM Approach. *ChemPhysChem*, **2023**. 24(2): p. e202200488. <https://doi.org/10.1002/cphc.202200488>
4. Kenouche S, **Bachir N**, Bouchal W and Martínez-Araya J.I., Aromaticity of Six-membered Nitro Energetic Compounds Through Molecular Electrostatic Potential, Magnetic, Electronic Delocalisation and Reactivity-based Indices. *Journal of Molecular Graphics and Modelling*, **2024**. 129, 108728 <https://doi.org/10.1016/j.jmgm.2024.108728>

International conferences:

1. **Bachir N**, Kenouche S, Stabilizing the N-NO₂ trigger bonds through intermolecular interactions: theoretical approach based on DFT calculations. *The 6th International Chemistry Symposium (CIC-6)*. University of Batna 1- Algeria (**oral**).
2. **Bachir N**, Kenouche S, Effect of Intermolecular Interactions on the Sensitivity of Some Energetic Compounds Using DFT Calculations. *1st International Con-*

ference on Materials Sciences and Technology (MatScience-2022). University of Khenchela- Algeria (**oral**).

3. **Bachir N**, Kenouche S, Understanding electron density imbalance in energetic materials through molecular electrostatic potential. *International Seminar on Chemical Process and Environment (ISCPE2022)* .University of Biskra-Algeria (**poster**).

National conferences:

1. **Bachir N**, Kenouche S, Unraveling Electron Density Disparity in Nitrobenzene Compounds: A comprehensive Molecular Electrostatic Potential Investigation with Insights into the Impact of Amino Groups. *The 2nd Study Day on Materials: Synthesis and Energy Applications (2nd SDMSEA2023)*. University of Biskra-Algeria (**poster**).
2. **Bachir N**, Kenouche S, Intermolecular interactions for stabilizing trigger bonds in energetic compounds: topological analysis using DFT calculations. *The 1st Scientific Days on Materials and Their Applications (SDMA'2023)*. University of Biskra- Algeria (**poster**).
3. **Bachir N**, Kenouche S, Theoretical investigation of the effect of intermolecular interactions in stabilizing the C-NO₂ trigger bonds in FOX-7. *2nd National Conference on Materials, Energy & Environment (NCMEE'2024)*. University of Biskra- Algeria (**poster**).

List of abbreviations and acronyms

ECs: Energetic Compounds

MMCs: Metallocene Methyl Cations

BP: Black Powder

BC: Before Christ

NC: Nitrocellulose

NG: Nitroglycerine

NQ: Nitroguanidine

AN: Ammonium nitrate

AP: Ammonium perchlorate

HF: Hartree-Fock theory

HP: Hartree Product

DFT: Density Functional Theory

SD: Slater determinant

KS: Kohn-Sham method

MEP: Molecular Electrostatic Potential

EDA-NOCV: Energy Decomposition Analysis-Natural Orbitals for Chemical Valence

QTAIM: Quantum Theory of Atoms In Molecules

AIM: Atoms In Molecules

CPs: Critical Points

BCP: Bond Critical Points

NCP: Nuclear Critical Points

RCP: Ring Critical Points

CCP: Cage Critical Points

IRI: Interaction Region Indicator

RDX: 1,3,5-trinitro-1,3,5-triazinane, also known as hexogen

HMX: 1,3,5,7-tetranitro-1,3,5,7-tetrazocane, also known as octogen

FOX-7: 1,1-diamino-2,2-nitroethylene, also known as DADNE

Abstarct

Neutralising energetic molecules is a valuable approach to minimize the risks of unpredictable explosions and associated tragic events. Quantum chemical methods offer highly efficient and effective tools for studying these compounds. The main objective of this dissertation is to quantify the impact of intermolecular interactions on the sensitivity of energetic compounds. Concerning the cyclic compounds RDX (1,3,5-trinitro-1,3,5-triazinane) and HMX (1,3,5,7-tetranitro-1,3,5,7-tetrazocane), a quantitative analysis with MEP evidenced anomalies arising from the marked depletion of negative charge distribution. The EDA-NOCV results reveal that the electrostatic and orbital contributions are the dominant factors driving the assembly of the $M = \{\text{Ti, Zr, Hf}\}$ -based complexes. The chemical nature of the $\text{O} \cdots M = \{\text{Ti, Zr, Hf}\}$ bonding has been investigated by using the QTAIM theory. Additionally, the topological properties of the $\text{N}-\text{NO}_2$ trigger bonds were quantified before and after the $\text{O} \cdots M$ interaction. These intermolecular interactions strengthens the trigger bonds, revealing an increased stability to decomposition. The IRI-based analysis was carried out to further investigate the electronic properties of group 4 transition metals in coordination environments. With regard to the aliphatic compound FOX-7 (1,1-diamino-2,2-nitroethylene), we examined three types of interactions: oxygen and nitrogen from a nitro group interacting with the metal atom, as well as nitrogen from an amino group interacting with the same metal atom. The local chemical reactivity of FOX-7 was elucidated through a quantitative study of MEP. Results derived from QTAIM showed that the $\text{C}-\text{NO}_2$ bonds are influenced by the $\text{O} \cdots M = \{\text{Ti, Zr, Hf}\}$ bonding. Furthermore, this interaction rules the complex formation when a nitro group interacts with MMCs. The interaction energies calculated by EDA-NOCV revealed that the $(\text{H}_2\text{N})_2\text{C}=\text{C}(\text{NO}_2)-(\text{O})\text{NO} \cdots \text{Cp}_2\text{MCH}_3^+$ complexes are significantly more structurally stable (by about 21.8 kcal/mol) than the $(\text{O}_2\text{N})_2\text{C}=\text{C}(\text{NH}_2)-\text{H}_2\text{N} \cdots \text{Cp}_2\text{MCH}_3^+$ complexes. This work is crucial to validate the proposal of using MMCs (metallocene methyl cations) as a neutraliser of energetic molecules.

Keywords: Energetic molecules, neutralisers, metallocene methyl cations, sensitivity, MEP/ EDA-NOCV/ QTAIM/ IRI analysis, trigger bonds.

Contents

I	Bibliographic study on energetic organic compounds	1
I.1	Brief history of energetic compounds	8
I.2	What is an energetic compound?	10
I.3	Classification of energetic compounds	10
I.3.1	Depending on their chemical composition	10
I.3.1.1	Pure single energetic compounds	10
I.3.1.2	Energetic mixtures	13
I.3.2	Depending on their intended use	14
I.3.2.1	Explosives	14
I.3.2.2	Propellants	15
I.3.2.3	Pyrotechnics	15
I.4	Decomposition of energetic compounds	16
I.4.1	Decomposition regimes	16
I.4.1.1	Detonation	17
I.4.1.2	Deflagration	17
I.4.1.3	Combustion	17
I.5	Civil applications of energetic compounds	17
I.6	Sensitivity of energetic compounds	18
I.7	Factors affecting the sensitivity of energetic compounds	19
I.7.1	Molecular indices related with sensitivity	19
I.8	Reducing sensitivity: a major challenge	20
I.9	Efforts towards sensitivity reduction	21
I.10	Safety of energetic compounds:	23
I.11	Some of history's serious accidents caused by energetic compounds	24
I.12	Trigger linkage concept	25
I.13	Neutralisation of energetic compounds by using MMCs	26

II	Quantum chemical methods	28
II.1	The Schrödinger equation	39
II.2	Hartree-Fock theory	40
II.2.1	The Hartree-Fock equations	42
II.3	Post Hartree-Fock methods	45
II.4	Density Functional Theory (DFT)	45
II.4.1	Kohn-Sham equations	46
II.4.2	The main exchange-correlation density functionals of DFT	48
II.4.2.1	Local Density Approximation	48
II.4.2.2	Generalized Gradient Approximation (GGA) and Hybrid Functionals	48
II.5	Molecular Electrostatic Potential (MEP)	49
II.6	Energy Decomposition Analysis-Natural Orbitals for Chemical Valence (EDA-NOCV)	50
II.7	Quantum Theory of Atoms In Molecules (QTAIM)	51
II.8	Interaction Region Indicator (IRI)	53
III	Theoretical Investigation of the Effect of $O \cdots M = \{Ti, Zr, Hf\}$ Interactions on the Sensitivity of RDX and HMX	54
III.1	Introduction	60
III.2	Computational details	61
III.3	Results and discussion	61
III.3.1	MEP analysis	61
III.3.2	EDA-NOCV	63
III.3.3	QTAIM analysis	67
III.3.4	IRI analysis	70
III.4	Conclusion	72
IV	The effect of $\{O, N\} = X \cdots M = \{Ti, Zr, Hf\}$ interactions on the sensitivity of C-NO₂ trigger bonds in FOX-7.	81
IV.1	Introduction	86
IV.2	Computational details	88
IV.3	Results and discussion	89
IV.3.1	Electrostatic potential analysis	89
IV.3.2	Topological analysis of electron density	91
IV.3.3	Bond length	96
IV.3.4	EDA-NOCV analysis	98
IV.4	Conclusion	102

List of Figures

I.1	Some molecular structures of common energetic compounds.	9
I.2	Classification of pure single energetic compounds	12
I.3	Classification of energetic mixtures	14
I.4	Classification of energetic compounds according to their intended use .	14
I.5	Molecular structure-sensitivity relationships	19
I.6	Some pictures from the Beirut explosion	25
II.1	IRI colorbar	53
III.1	1,3,5-trinitro-1,3,5-triazinane and 1,3,5,7-tetranitro-1,3,5,7-tetrazocane also known as RDX and HMX, respectively.	60
III.2	MEP-mapped van der Waals surfaces (<i>kcal/mol</i>) using a colour scale ranging from red (negative MEP), through white (neutral MEP) to blue (positive MEP). The blue regions are prone to nucleophilic attack, and the red regions are sites for electrophilic attack. The grid spacings were set to 0.2 bohr and the van der Waals surface denotes the isosurface of $\rho = 0.001 e/\text{bohr}^3 \equiv a.u.$ Values with a star indicate global surface extrema. The bold numbers in the bottom right-hand corner are the posi- tive MEP variance (σ_+^2), negative MEP variance (σ_-^2), positive surface area (A_+) and negative surface area (A_-) whose units are $(\text{kcal/mol})^2$, \AA^2 , respectively.	62
III.3	Models of interactions between methyl metallocene cations (MMCs) and RDX/HMX	63
III.4	Bond distances (\AA) for trigger bonds in RDX- $\text{Cp}_2\text{M}(\text{CH}_3)^+$ and HMX- $\text{Cp}_2\text{M}(\text{CH}_3)^+$	63
III.5	EDA-NOCV deformation densities of RDX- $\text{Cp}_2\text{M}(\text{CH}_3)^+$ complexes. A: RDX- $\text{Cp}_2\text{Ti}(\text{CH}_3)^+$, B: RDX- $\text{Cp}_2\text{Zr}(\text{CH}_3)^+$ and C:RDX- $\text{Cp}_2\text{Hf}(\text{CH}_3)^+$. The direc- tion of the negative charge flow is from the red to the blue region.	67
III.6	EDA-NOCV deformation densities of HMX- $\text{Cp}_2\text{M}(\text{CH}_3)^+$ complexes. A: HMX- $\text{Cp}_2\text{Ti}(\text{CH}_3)^+$, B: HMX- $\text{Cp}_2\text{Zr}(\text{CH}_3)^+$ and C:HMX- $\text{Cp}_2\text{Hf}(\text{CH}_3)^+$. The direction of the negative charge flow is from the red to the blue region. . . .	67

III.7	Molecular graph obtained by QTAIM topological analysis. Brown lines denote bond paths and the bond critical points (BCPs) are represented by orange circles. Only the (3,-1) critical points have been displayed. Percentage changes in electron density ($\Delta\rho(\mathbf{r}_B)$ %) and total electron energy ($\Delta H(\mathbf{r}_B)$ %) are shown at BCPs of $O\cdots M = \{Ti, Zr, Hf\}$. Colour-coded by element: C = iceblue, H = white, O = red, N = blue, Ti = yellow, Zr = green, Hf = cyan.	68
III.8	Isosurface map of IRI = 1.0 for the studied complexes. Colour-coded by element: C = iceblue, H = white, O = red, N = blue, Ti = yellow, Zr = green, Hf = cyan. The black arrow refers to the $O\cdots M = \{Ti, Zr, Hf\}$ bonding.	70
III.9	Scatter plot of IRI = 1.0 for the studied complexes using a grid spacing of 0.08 bohr. The points intersecting with the red line at IRI = 1.0 visualized on the scatter plots correspond to the grid points forming the isosurfaces.	72
IV.1	Structural formula of FOX-7, also known as DADNE.	86
IV.2	Interaction $O\cdots M$ leading to the complex of type $(H_2N)_2C=C(NO_2)-(O)NO\cdots Cp_2MCH_3^+$.	87
IV.3	Interaction $N\cdots M$ leading to the complex of type $(O_2N)_2C=C(NH_2)-H_2N\cdots Cp_2MCH_3^+$.	88
IV.4	ESP-mapped van der Waals surface (kcal/mol) using a colour scale ranging from red (negative ESP), through white (neutral ESP) to blue (positive ESP). The blue regions are prone to nucleophilic attack, and the red regions are sites for electrophilic attack. The grid spacings were set to 0.2 Bohr and the van der Waals surface denotes the iso-surface of $\rho = 0.001 e/Bohr^3 \equiv 0.001 a.u.$ Values with a star indicate global surface extreme. The bold numbers in the bottom right-hand corner are the positive ESP variance (σ_+^2), negative ESP variance (σ_-^2), positive surface area (A_+) and negative surface area (A_-) whose units are $(Kcal/mol)^2 \text{ \AA}^2$, respectively.	90
IV.5	Molecular graph of the $(H_2N)_2C=C(NO_2)-(O)NO\cdots Cp_2MCH_3^+$ complexes obtained by QTAIM topological analysis. Brown lines denote bond paths and the bond critical points (BCPs) are represented by orange circles. Only the (3,-1) critical points have been displayed. Color-coded by element: C = iceblue, H = white, O = red, N = blue, Ti = yellow, Zr = green, Hf = cyan.	92

IV.6	Molecular graph of the $(\text{O}_2\text{N})_2\text{C}=\text{C}(\text{NH}_2)-(\text{H})\text{HN}\cdots\text{Cp}_2\text{MCH}_3^+$ complexes obtained by QTAIM topological analysis. Brown lines denote bond paths and the bond critical points (BCPs) are represented by orange circles. Only the (3,-1) critical points have been displayed. Color-coded by element: C = iceblue, H = white, O = red, N = blue, Ti = yellow, Zr = green, Hf = cyan.	93
IV.7	Bond lengths (\AA) in FOX-7 and the studied complexes. Coloured-coded by element: C=gray, H=white, O=red, N=blue, Ti=yellow, Zr=green, Hf=cyan.	97
IV.8	ETS-NOCV deformation densities in complexes $(\text{H}_2\text{N})_2\text{C}=\text{C}(\text{NO}_2)-(\text{O})\text{NO}\cdots\text{Cp}_2\text{MCH}_3^+$. (A): $(\text{H}_2\text{N})_2\text{C}=\text{C}(\text{NO}_2)-(\text{O})\text{NO}\cdots\text{Cp}_2\text{TiCH}_3^+$, (B): $(\text{H}_2\text{N})_2\text{C}=\text{C}(\text{NO}_2)-(\text{O})\text{NO}\cdots\text{Cp}_2\text{ZrCH}_3^+$ and (C): $(\text{H}_2\text{N})_2\text{C}=\text{C}(\text{NO}_2)-(\text{O})\text{NO}\cdots\text{Cp}_2\text{HfCH}_3^+$. The red and blue contours correspond to accumulation and depletion of electron density, respectively. Direction of the negative charge flow: red \rightarrow blue. The eigenvalues $ \nu $ yield the extent of the charge flow. The deformation densities were plotted with the contour values 0.002 a.u. for $\Delta\rho(\mathbf{r})^{(1)}$ and 0.0006 a.u. for $\Delta\rho(\mathbf{r})^{(2)}$	100
IV.9	ETS-NOCV deformation densities in complexes $(\text{O}_2\text{N})_2\text{C}=\text{C}(\text{NH}_2)-\text{H}_2\text{N}\cdots\text{Cp}_2\text{MCH}_3^+$. (A): $(\text{O}_2\text{N})_2\text{C}=\text{C}(\text{NH}_2)-\text{H}_2\text{N}\cdots\text{Cp}_2\text{TiCH}_3^+$, (B): $(\text{O}_2\text{N})_2\text{C}=\text{C}(\text{NH}_2)-\text{H}_2\text{N}\cdots\text{Cp}_2\text{ZrCH}_3^+$ and (C): $(\text{O}_2\text{N})_2\text{C}=\text{C}(\text{NH}_2)-\text{H}_2\text{N}\cdots\text{Cp}_2\text{HfCH}_3^+$. The red and blue contours correspond to accumulation and depletion of electron density, respectively. Direction of the negative charge flow: red \rightarrow blue. The eigenvalues $ \nu $ yield the extent of the charge flow. The deformation densities were plotted with the contour values 0.002 a.u. for $\Delta\rho(\mathbf{r})^{(1)}$ and 0.0006 a.u. for $\Delta\rho(\mathbf{r})^{(2)}$	101

List of Tables

I.1	Some significant discoveries in the history of ECs.	9
I.2	Classification of organic energetic compounds	11
I.3	Classification of metal-containing energetic compounds	12
I.4	Most explosophoric groups used in energetic compounds	16
III.1	Results of the EDA-NOCV calculations of the studied complexes at the DFT/revPBE-D3(BJ)/TZ2P level of theory. All the values are in <i>kcal/mol</i>	65
III.2	Orbital interaction energies of σ -donation ($\Delta E_{orb}^{(1)}$) and π -backdonation ($\Delta E_{orb}^{(2)}$) with the respective charge transfer.	66
III.3	Topological properties of the electron density calculated at the (3,-1) bond critical point for the $O \cdots M = \{Ti, Zr, Hf\}$ bonding.	68
III.4	Topological properties of the electron density calculated at the (3,-1) bond critical point of the N-NO ₂ bonds.	68
IV.1	Topological properties of the electron density calculated at the (3,-1) bond critical point for the $\{O, N\} = X \cdots M = \{Ti, Zr, Hf\}$ bonding at DFT/CAM-B3LYP level of theory. The vector \mathbf{r}_B locates the position of the critical point.	94
IV.2	Topological properties of the electron density calculated at the (3,-1) bond critical point of the C-NO ₂ and C-NH ₂ bonds at the DFT/CAM-B3LYP level of theory. bonding at DFT/CAM-B3LYP level of theory.	95
IV.3	Results of the EDA-NOCV calculations at the DFT/revPBE-D3(BJ)/TZ2P level of theory ^a . All the values are in <i>kcal/mol</i>	98

General introduction

Energetic compounds (ECs) are a class of compounds that can release chemical energy stored in their molecular structure under the effect of an external stimulus, in a short time [1]. The history of ECs, their chemistry and application are as old as 220 years BC (Before Christ), when black powder was accidentally discovered by the Chinese [2]. Although being initially known for its use in the military and despite their potential risks, ECs play a crucial role in our daily lives. They are utilized in a wide range of civil applications [3, 4]. It is widely acknowledged that the quality of an EC is determined by two key properties: energy and safety, both of which guide its applicability. Otherwise, a new energetic molecule will be rejected due to insufficient energy and lacking safety [5, 6]. Nevertheless, it is well understood that safety is extremely critical, even more vital than high energy output for ECs [6]. Numerous novel ECs have been recently developed; however, due to their high sensitivity, only a few of them are utilized [7]. Since ECs are frequently exposed to various external influences all over manufacturing, transportation, and storage processes, a more sensitive EC can readily ignite, potentially leading to catastrophic events [8]. In fact, over the last few decades, specific safety issues have frequently arisen during the manufacturing, storage, and utilization of such compounds [9, 10].

We have many examples of such accidents, most spectacular, the one that took place on August 4, 2020 in Beirut Port, Lebanon, when approximately 2,750 tons of ammonium nitrate stored in a warehouse detonated. This tragic event claimed the lives of 204 individuals and left more than 7,000 others injured [11, 12]. Another explosion occurred on March 21, 2019 at a chemical warehouse in China, where dinitrobenzene and substandard nitro compounds were being stored. This unintentional explosion led to a tragic outcome, causing more than 617 injuries and claiming the lives of 78 individuals [13]. In addition, traditional ECs like RDX (1,3,5-trinitro-1,3,5-triazinane) and HMX (1,3,5,7-tetranitro-1,3,5,7-tetrazocane) can also have negative effects on the environment, potentially contaminating soil and water and harming ecosystems and wildlife over the long run [14, 15].

Sensitivity to detonation is an essential characteristic of ECs. This property refers to the vulnerability of these compounds to unexpected detonation due to an involuntary stimulus (sparks, friction, shock, heat etc) [2, 16]. The sensitivity to various external influences originates at the molecular level from molecular stability. Many studies have used the trigger mechanism to gain insight about sensitivity [17, 18, 19].

Trigger linkage represents a fundamental concept in the breakdown of ECs. It is frequently employed to elucidate the spontaneous decomposition that characterizes such compounds when adequately stimulated [20, 21]. In this concept, specific types of bonds are more vulnerable to disruption due to external energy input. When these bonds rupture, they "triggers" an additional exothermic and self-sustaining decomposition, specific of detonation process [22]. The trigger linkage approach allows to understand the sensitivity of ECs from a molecular structure perspective. Numerous correlations between sensitivity and the strength of the trigger bond were identified using this approach [21]. Lower sensitivity indicates greater chemical stability. As a result, a weaker trigger linkage results in increased sensitivity [17].

Neutralising ECs by selecting specific chemical compounds to react on certain sites of an energetic molecule, can be used to prevent the latter from following its normal explosion channel. The formation of such complexes may reinforce the trigger bonds within the EC and therefore reduce its sensitivity to detonation. Thus, we define a neutraliser as a molecule able to form a complex with an EC and prevents its explosion. The neutralisation of ECs may contribute to public security by designing insensitive ECs, thereby minimising the risks of possible unpredictable explosions and their associated tragic events. The sensitive nature of ECs makes experimental investigations a very difficult and dangerous task, as the detonation process occurs almost instantaneously and is highly exothermic. Accordingly, theoretical studies using quantum chemical methods can be a very useful way to study such compounds.

In our work, we have selected three commonly used reference energetic molecules : RDX, HMX, and FOX-7 (1,1-diamino-2,2-nitroethylene). We tested group IV methyl metallocene cations, MMCs (chemical formula $Cp_2MCH_3^+$) with $M = \{ Ti, Zr, Hf \}$ as potential neutralisers. The rationale for this choice will be elucidated in the first chapter.

Main objectives of this dissertation:

1. Develop innovative approaches for neutralising energetic molecules using the conceptual tools of quantum chemistry.
2. Understand the influence of intermolecular interactions on the sensitivity of energetic molecules.
3. Quantify the effect of these interactions on the stabilization of trigger bonds.

This dissertation is divided into four chapters:

1. **In chapter I:** We conduct a bibliographic study on ECs, covering topics such as their definition, classification, fields of application, their sensitivity and the concept of trigger bonds.
2. **In chapter II:** We present the theoretical background of the different quantum chemical methods used in our work.
3. **In chapter III:** We study the effect of $O \cdots M = \{Ti, Zr, Hf\}$ interactions on the sensitivity of energetic N-nitro compounds and the role of these intermolecular interactions in stabilising the N-NO₂ trigger bonds in RDX and HMX.
4. **In chapter IV:** We highlight the effect of $\{O, N\} = X \cdots M = \{Ti, Zr, Hf\}$ interactions on the sensitivity of C-NO₂ trigger bonds in FOX-7.

Finally, this manuscript will end by a general conclusion that summarizes the main results we have obtained and some perspectives on future possible recommendations.

Bibliography

- [1] Yu Ma, Anbang Zhang, Chenghua Zhang, Daojian Jiang, Yuanqiang Zhu, and Chaoyang Zhang. Crystal packing of low-sensitivity and high-energy explosives. *Crystal Growth & Design*, 14(9):4703–4713, 2014.
- [2] Thomas M Klapötke. *Chemistry of High-Energy Materials*. Walter de Gruyter GmbH & Co KG, 2019.
- [3] K-J Kim and H-S Kim. Coating of energetic materials using crystallization. *Chemical Engineering & Technology: Industrial Chemistry-Plant Equipment-Process Engineering-Biotechnology*, 28(8):946–951, 2005.
- [4] Philip F Pagoria, Gregory S Lee, Alexander R Mitchell, and Robert D Schmidt. A review of energetic materials synthesis. *Thermochimica acta*, 384(1-2):187–204, 2002.
- [5] Rupeng Bu, Ying Xiong, and Chaoyang Zhang. π - π stacking contributing to the low or reduced impact sensitivity of energetic materials. *Crystal Growth & Design*, 20(5):2824–2841, 2020.
- [6] AK Sikder and Nirmala Sikder. A review of advanced high performance, insensitive and thermally stable energetic materials emerging for military and space applications. *Journal of hazardous materials*, 112(1-2):1–15, 2004.
- [7] Yanfei Cheng, Xiang Chen, Na Yang, Yazhou Zhang, Haixia Ma, and Zhaoqi Guo. Sandwich-like low-sensitive nitroamine explosives stabilized by hydrogen bonds and π - π stacking interactions. *CrystEngComm*, 23(9):1953–1960, 2021.
- [8] LQ Xiao, Y Zhao, XL Fu, WX Xie, and XZ Fan. Mechanical sensitivity reduction of energetic materials by using carbon nanomaterials. In *Journal of Physics: Conference Series*, volume 2478, page 032010. IOP Publishing, 2023.
- [9] Christer B Aakeröy, Tharanga K Wijethunga, and John Desper. Crystal engineering of energetic materials: Co-crystals of ethylenedinitramine (edna) with modified performance and improved chemical stability. *Chemistry–A European Journal*, 21(31):11029–11037, 2015.

- [10] Zhen Xu, Guangbin Cheng, Shunguan Zhu, Qiuhan Lin, and Hongwei Yang. Nitrogen-rich salts based on the combination of 1, 2, 4-triazole and 1, 2, 3-triazole rings: a facile strategy for fine tuning energetic properties. *Journal of Materials Chemistry A*, 6(5):2239–2248, 2018.
- [11] Giorgia Guglielmi. Why beirut’s ammonium nitrate blast was so devastating. *Nature*, 2020.
- [12] Gending Yu, Yulan Wang, Liang Zheng, Jiale Huang, Jingling Li, Lingzhu Gong, Rongguo Chen, Wei Li, Jiulai Huang, and Yih-Shing Duh. Comprehensive study on the catastrophic explosion of ammonium nitrate stored in the warehouse of beirut port. *Process Safety and Environmental Protection*, 152:201–219, 2021.
- [13] Xiaodong Yang, Yongzhao Li, Yangqing Chen, Yuqi Li, Libo Dai, Ren Feng, and Yih-Shing Duh. Case study on the catastrophic explosion of a chemical plant for production of m-phenylenediamine. *Journal of Loss Prevention in the Process Industries*, 67:104232, 2020.
- [14] Dimitrios Kalderis, Albert L Juhasz, Raj Boopathy, and Steve Comfort. Soils contaminated with explosives: environmental fate and evaluation of state-of-the-art remediation processes (iupac technical report). *Pure and Applied Chemistry*, 83(7):1407–1484, 2011.
- [15] Liudmyla K Sviatenko, Leonid Gorb, Danuta Leszczynska, Sergiy I Okovytyy, Manoj K Shukla, and Jerzy Leszczynski. Application of computational approaches to analysis of multistep chemical reactions of energetic materials: Hydrolysis of hexahydro-1, 3, 5-trinitro-1, 3, 5-triazine (rdx) and octahydro-1, 3, 5, 7-tetranitro-1, 3, 5, 7-tetrazocine (hmx). *Practical Aspects of Computational Chemistry V*, pages 215–232, 2022.
- [16] Scott A Shackelford. Role of thermochemical decomposition in energetic material initiation sensitivity and explosive performance. *Central European Journal of Energetic Materials*, 5(1):75–101, 2008.
- [17] Gang Li and Chaoyang Zhang. Review of the molecular and crystal correlations on sensitivities of energetic materials. *Journal of Hazardous Materials*, 398:122910, 2020.
- [18] Jinshan Li. Relationships for the impact sensitivities of energetic c-nitro compounds based on bond dissociation energy. *The Journal of Physical Chemistry B*, 114(6):2198–2202, 2010.

- [19] Bisheng Tan, Xinping Long, Rufang Peng, Hongbo Li, Bo Jin, Shijin Chu, and Haishan Dong. Two important factors influencing shock sensitivity of nitro compounds: Bond dissociation energy of x-no₂ (x= c, n, o) and mulliken charges of nitro group. *Journal of hazardous materials*, 183(1-3):908–912, 2010.
- [20] MJ Kamlet and HG Adolph. The relationship of impact sensitivity with structure of organic high explosives. ii. polynitroaromatic explosives. *Propellants, Explosives, Pyrotechnics*, 4(2):30–34, 1979.
- [21] Ying Xiong, Kai Zhong, and Chao-yang Zhang. Trigger linkage mechanism: Two or multiple steps initiate the spontaneous decay of energetic materials. *Energetic Materials Frontiers*, 3(1):38–46, 2022.
- [22] Peter Politzer and Jane S Murray. Detonation performance and sensitivity: a quest for balance. In *Advances in quantum chemistry*, volume 69, pages 1–30. Elsevier, 2014.

Chapter I

Bibliographic study on energetic organic compounds

I.1 Brief history of energetic compounds

The history of energetic compounds (ECs) may be traced back to ancient times. In ancient China, the first EC was developed when a group of Chinese alchemists made black powder (BP) by accident while separating silver from gold. Chinese alchemists began experimenting with heating saltpeter and sulfur mixtures around 220 BC (Before Christ). In the seventh century, saltpeter, sulfur, and charcoal were combined to make an explosive called black powder (also known as gunpowder). It was first used for fireworks, but soon it became more and more important for a variety of military purposes [1, 2, 3].

In the 17th century, BP was initially used in mining and civil engineering. Until Edward Charles Howard's discovery of mercury (II) fulminate in 1799, gunpowder served as the foundation for all ECs that were actually put to use. BP was not introduced into Europe until the 13th century when Roger Bacon and Berthold Schwarz experimented with the basic components of BP and produced this compound. By the end of the 13th century, numerous countries were utilizing BP as a military weapon to breach castle and city walls. In any case, the main upset in the advancement of ECs since the revelation of explosive began with the creations of nitrocellulose (NC) and nitroglycerine (NG) in 1846. NC was mostly used as an explosive, while NG was used as a propellant. Compared to gunpowder, these compounds performed significantly better. Alfred Nobel came up with the first version of dynamite in 1866. It was a mixture of 75% NG and 25% kieselguhr with a small amount of sodium carbonate added. In contrast to pure NG, it was relatively safe to handle and transport and had a much lower sensitivity. Nobel later combined NG and NC in a jelly to create gelatinous dynamite. In addition to improving safety, this substance performed significantly better than the original dynamite [1, 2, 3].

Many ECs were prepared after that, as indicated in Table I.1 and Figure I.1. Among them PETN, TNT, HMX, and RDX,...etc. It should be noted that the latter was initially prepared for medicinal use, and its explosive value was not recognized until 1920 by Herz [1, 3].

Table I.1: Some significant discoveries in the history of ECs.

EC	Acronym	Development	First prepared by
Blackpowder	BP	1250–1320	Chinese alchemists
Nitroglycerine	NG	1846	Ascanio Sobrero
Dynamite	Dy	1867	Nobel
Picric acid	PA	1885–1888	Turpin
Nitroguanidine	NQ	1877	Jousselin
Trinitrotoluene	TNT	1880	Wilbrand
Nitropenta	PETN	1894	Panpushko
Hexogen	RDX	1920–1940	Henning
Octogen	HMX	1943	Bachmann
Hexanitrostilbene	HNS	1913	Shipp
Triaminotrinitrobenzene	TATB	1888	Jackson and Wing
HNIW	CL-20	1987	Arnie Nielsen

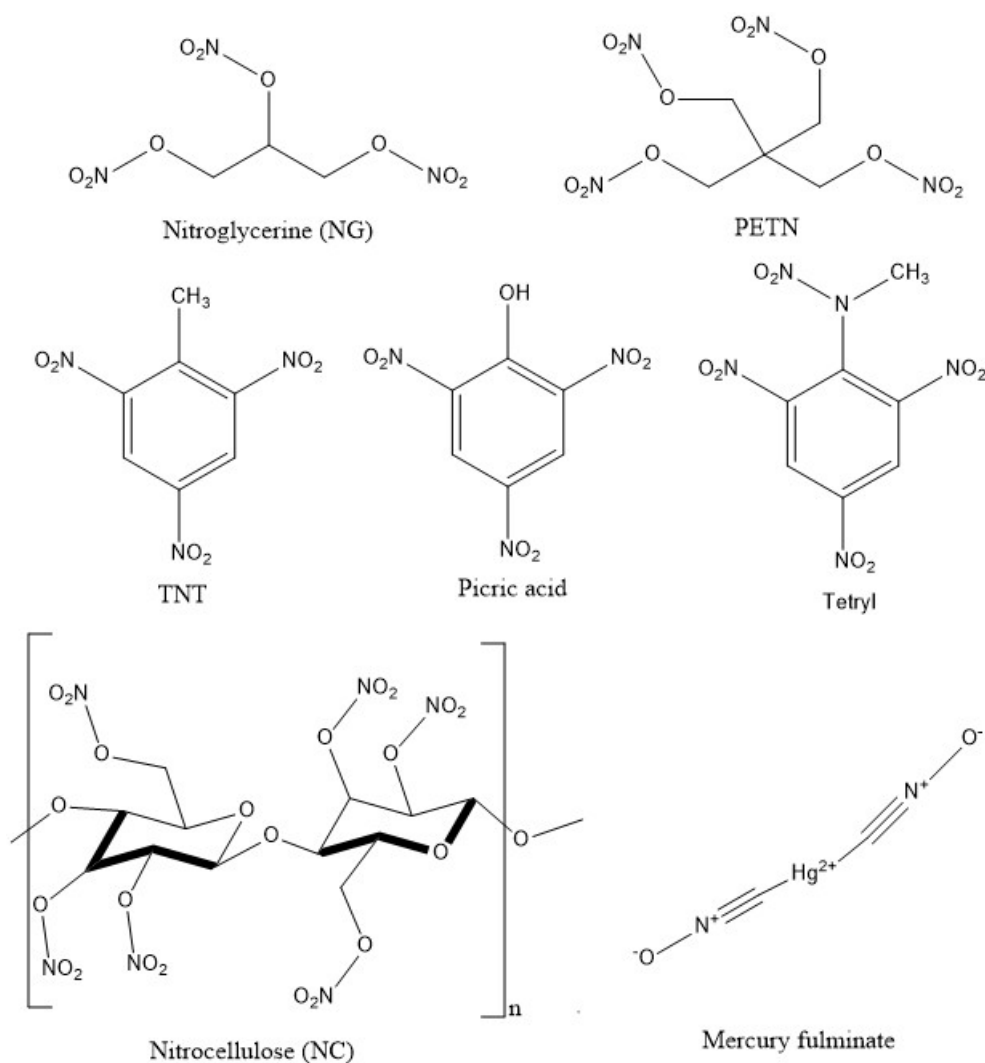


Figure I.1: Some molecular structures of common energetic compounds.

I.2 What is an energetic compound?

Energetic compounds are substances that store a large amount of chemical energy and are able to release this energy in a very short time (less than a few fractions of a second) in the form of heat and pressure under the influence of a mechanical or thermal stimulus. These compounds contain oxidizing and reducing elements that will react violently with each other via an exothermic reaction [4, 5, 6].

I.3 Classification of energetic compounds

ECs can be categorized in a number of different ways. Here are some typical classification schemes:

I.3.1 Depending on their chemical composition

A large number of classifications of ECs based on their chemical composition are found in the literature [7, 8, 9]. Recently, F. Zapata et al. [10] proposed a more useful and organized chemical categorization of ECs, which we have relied upon in this section. Based on their molecular structure, ECs are chemically classified into two large categories: pure single energetic compounds and energetic mixtures.

I.3.1.1 Pure single energetic compounds

Pure single ECs, often known as "molecular ECs" are any energetic molecules whose unimolecular breakdown reactions can result in an explosion. These compounds are classified into two types based on the nature of their constituent elements: organic and inorganic compounds.

I.3.1.1.A Organic energetic compounds: These are energetic molecules that have at least one carbon atom and no atoms of any other element besides C, H, O, N, or halogens. Because numerous organic ECs are available, they are often grouped into six types, as illustrated in Table I.2 [10].

Table I.2: Classification of organic energetic compounds

class		Structural feature	Examples
Nitro-compounds	Nitro-aromatic	C(aromatic)-NO ₂	TNT, TATB
	Nitro-aliphatic	C(aliphatic)-NO ₂	Nitromethane, FOX-7
	Nitramine	N-NO ₂	RDX, HMX, CL-20
	Nitrate ester	O-NO ₂	PETN, NC
Peroxide compounds		Peroxide group(-OO-)	TATP , HMTD
Organic azides		Azide group (-N ₃)	Cyanuric triazide (C ₃ N ₁₂)
Organic halogen amino compounds		Halogen-amino group (-NX ₂)	Methyldichloramine (CH ₃ NCl ₂)
Azo/diazo energetic compounds		Azo/diazo groups (-N=N- /N≡N)	Diazomethane (CH ₂ N ₂)
Other organic energetic compounds		Some compounds that does not contain the previous chemical groups	Tetracene(C ₁₈ H ₁₂), fulminic acid (HCNO)

I.3.1.1.B Inorganic energetic compounds: These are ECs that either do not have any carbon atoms, e.g., lead azide (Pb(N₃)₂) or nitrogen trichloride (NCl₃), or have at least one atom that is not carbon, hydrogen, oxygen, nitrogen, or halogen (in most cases, a metal element), such as silver fulminate (AgCNO), lead picrate (PbC₁₂H₄N₆O₁₄). Typically, these compounds are classified into two types:

1. Nonmetal inorganic energetic compounds: These compounds have no carbon or metal atoms in their chemical structure. This class include:
 - (a) Ammonium nitrate (NH₄NO₃)
 - (b) Ammonium dinitramide
 - (c) Ammonium chlorate/perchlorate (NH₄ClO₃/NH₄ClO₄).
 - (d) Nitrogen halides
 - (e) Hydrazine and derivatives (N₂H₄)
2. Metal-containing energetic compounds: These compounds have at least one metal atom in their molecular structure. All the various types of compounds within this class are categorized in Table I.3 [10].

Table I.3: Classification of metal-containing energetic compounds

class	Structural feature	Examples
Nitro-phenyl salts, nitramine salts, benzofuroxan salts, etc.	Every energetic salt that results from the hydrogen-metal replacement in an organic EC	lead picrate), silver methylene-dinitramine
Metal azides	Metal element+an azide group(-N ₃)	sodium azide (NaN ₃) , lead azide (Pb(N ₃) ₂)
Metal fulminates	a metal element and a fulminate group (-CNO)	silver fulminate (AgCNO) ,mercury fulminate (Hg(CNO) ₂)
Metal acetylides	a metal element and an acetylide group (-C≡C-)	cuprous acetylide (Cu ₂ C ₂)
Organo-metallic complexes	Organo-metallic complexes with explosive properties	tetrazole-ring containing cobalt perchlorate complexes

Figure I.2 [10] summarizes all details we have discussed regarding the classification of pure single ECs.

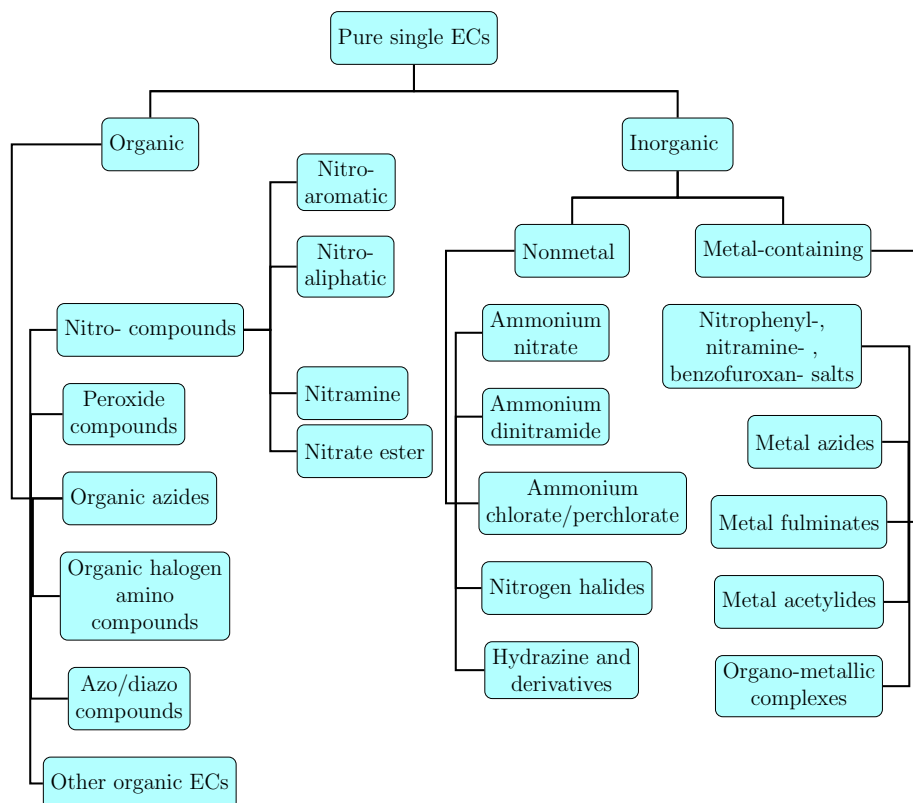


Figure I.2: Classification of pure single energetic compounds

I.3.1.2 Energetic mixtures

1. Mixture of several single ECs: such as Composition B =RDX (60%) + (40%), pentolite =PETN (50%) + TNT (50%)
2. Mixture of one/ several single ECs with added fuels/oxidizers/binders/ plasticizers: It is uncommon to utilize a single energetic component or a combination of several single ECs alone. Multiple additives, such as plasticizers, binders, fuels, and/or oxidizers, are commonly introduced to individual ECs in order to enhance various characteristics. Four main categories can be recognized within this group:
 - (a) Plastic bonded explosives: A combination of one or more high-energy secondary explosives (usually organic nitro-energetic compounds) in significant proportions (>80%), along with supplementary substances that serve as binders and plasticizers in smaller quantities (20%). For instance, PG-2 plastic explosive (91% RDX).
 - (b) AN-based explosives: These are all explosive mixtures in which ammonium nitrate serves as the primary component (40-95%). Additional constituents encompass fuels, binders, plasticizers, supplementary explosives, and more. for example: ANAl (80–85% AN + 15–20% aluminum powder).
 - (c) Nitrocellulose-based propellants: These are energetic formulations characterized by a significant content (>90%) of NC (either NC alone or in conjunction with other organic nitro-explosives), accompanied by a minor fraction (<10%) of other compounds that function as binders, plasticizers, stabilizers, etc.
 - (d) AP-containing propellants: These represent a form of composite propellant comprising nearly 70% ammonium perchlorate, in addition to other components such as metal powders (e.g., aluminum) and polymers (e.g., carboxy-terminated polybutadiene).
3. Oxidizer-fuel energetic composite : This group encompasses every combination of two or more non-ECs that, through their redox reaction, have the potential to generate an explosion. One of the components functions as an oxidizing agent, while the other acts as a reducing agent. The explosive nature of these chemicals originated from the rapid combustion of the fuel upon contact with the oxidizing agent. Due to the prevalence of fuels over energetic salts used as oxidizers, these compounds can be categorized based on the oxidizer as: Nitrate-, Chlorate-, and Perchlorate-based energetic composite.

As before, Figure I.3 [10] summarizes all details regarding the classification of energetic mixtures.

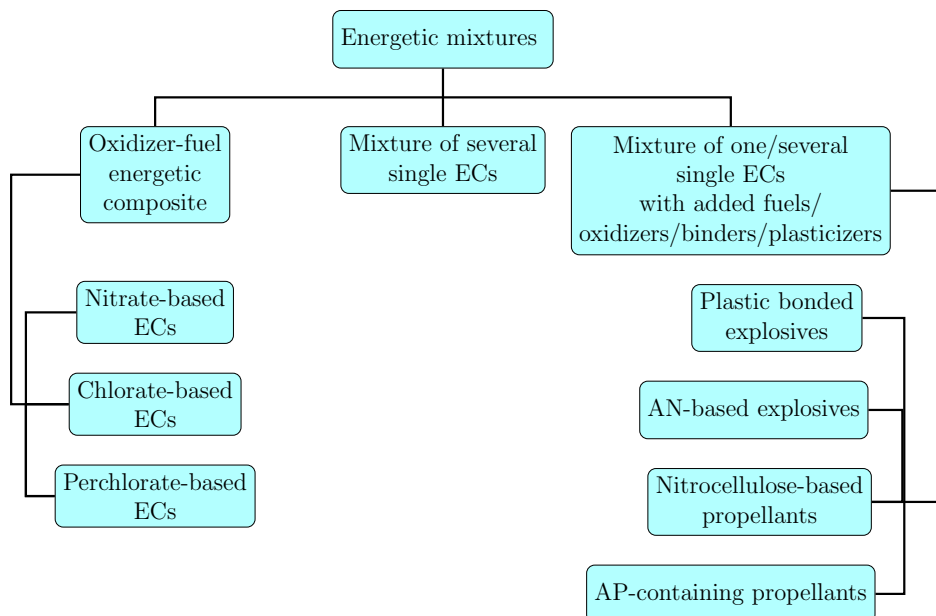


Figure I.3: Classification of energetic mixtures

I.3.2 Depending on their intended use

ECs may be categorized based on their intended application into several classes, namely, explosives, propellants and pyrotechnics [3], as illustrated in Figure I.4. The aim of explosives and propellants is to transform stored chemical energy into macroscopic kinetic energy. While, the intended use of pyrotechnics is to convert this energy into distinct visual and auditory effects [11, 12].

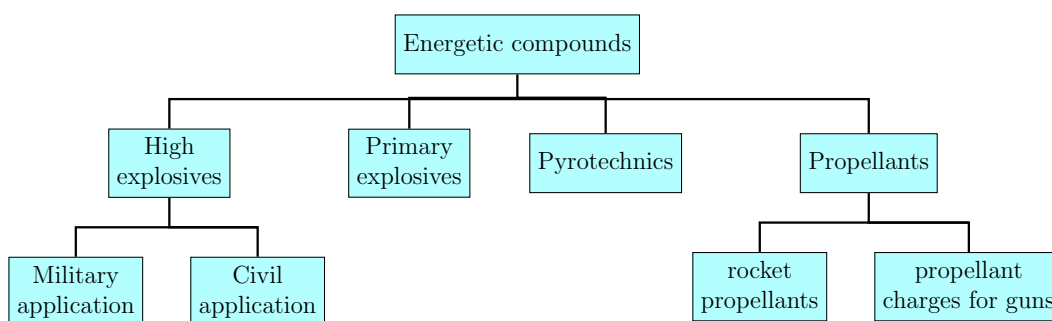


Figure I.4: Classification of energetic compounds according to their intended use

I.3.2.1 Explosives

Explosives are frequently defined as solid or liquid substances capable of generating gas through a chemical reaction at temperatures, pressures, and velocities sufficient to cause significant damage to the surroundings. Explosives, in turn, are categorized into two groups: primary and secondary explosives. The main characteristic of pri-

mary explosives is their susceptibility to initiation to detonations as a result of a very rapid intrinsic evolution from burning to deflagration to detonation. which is usually induced by a mechanical, electrostatic, or thermal stimulation. Secondary explosives, in contrast, need a far larger stimulus to detonate than primary explosives. Despite being harder to detonate, secondary explosives have substantially greater performances meaning they release much more energy at a faster rate than primary explosives. two forms of secondary explosives (High Energy Density Materials, HEDMs, and Low Performance Energetic Materials, LPEMs) have recently received a lot of attention. The goal of the former is to achieve the highest achievable performance, whereas the goal of the latter is to sacrifice a small portion of performance in order to achieve the lowest attainable sensitivity [11, 12].

I.3.2.2 Propellants

Propellants are substances that burn quickly or release a substantial amount of gas at a rate adequate to elevate pressure and generate propulsive power or impulse. Propellants can also be classified according to their usage and construction into: single, double, and triple base solid propellants, composite propellants, and liquid mono- and bipropellants. Single, double and triple base solid propellants contain one, two or three energetic components, respectively. Single, double, and triple base solid propellants consist of one energetic component (NC), two energetic components (NC+NG), or three energetic components (NC+NG+NQ), respectively. Modern composite propellants, which incorporate a secondary explosive, are also extensively employed. A variety of compounds, such as stabilizers, plasticizers, coolants, lubricants, and anti-wear agents, are added to the energetic component in traditional solid propellants. Solid propellants are utilized in a range of applications, encompassing small and large caliber weapons, rocketry, and space exploration, where liquid propellants are also employed. Liquid propellants can exist as monopropellants, comprising a single ingredient like hydrogen peroxide, or bipropellants, which involve combinations of a liquid fuel and a liquid oxidizer [11, 12].

I.3.2.3 Pyrotechnics

Pyrotechnics derive their name from the ancient Greek words "*pyr*" (meaning fire) and "*tekhnikos*" (meaning made by art), it refers to substances that emit distinctive colors, heat, sounds, or smoke. The most well-known civil application of pyrotechnics is fireworks used during ceremonies and festivals. In the military context, pyrotechnics are utilized for various purposes, such as signal flares, smoke screens for concealment, and decoy devices. Pyrotechnical formulations are primarily made up of an oxidizer such as nitrates or perchlorates, along with a metal as fuel, like magnesium or aluminum. A

coloring ingredient, such as strontium or lithium, is added to formulations that produce a color effect [3].

I.4 Decomposition of energetic compounds

ECs are typically organic compounds comprising backbones and explosophoric groups (Table I.4) [8, 13]. Various backbones have been proposed, including aromatic, aliphatic, and caged carbon structures, as well as heterocyclic frameworks. Typically, the backbone acts as fuel and has no explosive qualities. The energy is provided by explosophoric groups (mostly $-\text{NO}_2$ groups) and moieties (e.g, NHNO_2) that can be covalently or ionically bonded to the backbone of a molecule [14, 15]. An explosophore provides the needed oxygen to turn the EC into small molecules (N_2 , CO , H_2O , and other small molecules depending on the energetic molecule structure). Especially, the $-\text{NO}_2$ and $-\text{ONO}_2$ groups are the primary oxygen sources in energetic molecules, which play an important role in the decomposition process [16]. When ECs decompose, they generate energy through a process known as oxidation, which is the chemical reaction that occurs when fuel burns or an explosive detonates [16, 17].

Table I.4: Most explosophoric groups used in energetic compounds

Explosophoric group	Sum Formula (M.w)	Explosophoric group	Sum Formula (M.w)
$-\text{NO}_2$	NO_2 (46.01)	$-\text{OCIO}_3$	ClO_4 (99.45)
$-\text{ONO}_2$	NO_3 (62.00)	$=\text{NClO}_3$	ClNO_3 (97.46)
$=\text{NNO}_2$	N_2O_2 (60.01)	$-\text{NF}_2$	NF_2 (52.00)
$-\text{C}(\text{NO}_2)_3$	CN_2O_2 (150.03)	$-\text{N}=\text{N}(\text{O})\text{F}$	N_2OF (82.01)
$-\text{C}(\text{NO}_2)_2\text{F}$	$\text{CN}_2\text{O}_4\text{F}$ (123.02)	$-\text{N}(\text{O})=\text{NOCH}_3$	$\text{CH}_3\text{N}_2\text{O}_2$ (75.05)
$-\text{C}(\text{NO}_2)_2\text{NF}_2$	$\text{CN}_3\text{O}_4\text{F}_2$ (156.03)	$-\text{N}(\text{O})=\text{NCN}$	CN_3O (70.03)
$-\text{C}(\text{NO}_2)_2\text{N}_3$	CN_5O_4 (146.04)	$-\text{N}=\text{N}-$	N_2 (28.01)
$-\text{C}(\text{NO}_2)_2\text{NH}_2$	$\text{CH}_4\text{N}_3\text{O}_4$ (122.06)	$-\text{N}=\text{N}(\text{O})-$	N_2O (44.01)
$-\text{N}(\text{O})=\text{NNO}_2$	N_3O_3 (90.02)	$-\text{N}=\text{N}-\text{N}=\text{N}-$	N_3 (42.02)
$-\text{N}=\text{N}(\text{O})\text{C}(\text{NO}_2)_3$	CN_5O_7 (194.04)		
$-\text{N}=\text{N}(\text{O})\text{C}(\text{NO}_2)_2\text{F}$	$\text{CN}_4\text{O}_5\text{F}$ (167.03)		
$-\text{ClO}_3$	ClO_3 (83.45)		

M.w: molecular weight (in g/mol)

I.4.1 Decomposition regimes

For the decomposition reaction of an EC, three distinct regimes can be distinguished: detonation, deflagration, and combustion. The three terms refer to exothermic oxidation processes. The distinction among them lies in their reaction velocities [18]. Explosion is another common word that lacks a precise scientific definition. An explosion occurs when a significant quantity of accumulated energy is rapidly liberated. The origin of the released energy could be physical, chemical, or nuclear. it may be

beneficial to characterize the decomposition reaction of energetic compounds in terms of the velocity by which chemical energy is released [19, 12].

I.4.1.1 Detonation

Detonation represents the most rapid release of chemical energy, propagating through a supersonic shockwave that traverses the substance at several thousands of meters per second. The swift release of chemical energy immediately behind the wave front sustains the propagation of the shockwave. The resultant destructive or propulsive force arises from the shockwave as it exits the substance. Explosives can release their energy in the form of a detonation [19, 12].

I.4.1.2 Deflagration

Deflagration processes are primarily propagated by heat transfer as they move through ECs at somewhat subsonic linear rates. The propagation velocity varies from a few millimeters per second and thousands of meters per second. Deflagration is a state that exists between detonation and combustion. As a result of a deflagration, propellants mostly release their energy through gas production [19, 12].

I.4.1.3 Combustion

Combustion, also known as simple burning, occurs at a slower rate and is characterized as a complex self-sustaining exothermic oxidation reaction. (the propagation rate is in the range of a few millimeters per second). This type of reaction is used to generate heat, noise, smoke, or sound, and the substances used for such an action are known as pyrotechnic compounds [19, 12].

I.5 Civil applications of energetic compounds

In addition to their common and main applications in the military sector, primarily as explosives and propellants, ECs are also used in numerous civilian fields [20]. This duality in their usage categorizes these compounds as what are known as "***dual-use chemicals***" [21, 22]. In this section, we will review the most prominent and significant civilian uses of ECs:

1. Mining: Minerals, ores, metals, exploration of oil and gas, and other resources located deep underground require specific extraction methods. Explosives are utilized in blast mining to eliminate hard rock layers, dislodge rocks, and create access to subterranean mining sites [20, 23].

2. Aerospace: Aerospace uses ECs like AP for rocket propulsion, satellite launches, and space exploration [20].
3. Civil engineering: Explosives are utilized in public works projects that require the breaking of rocks, such as railways, paths, reservoirs, tunnels, docks, ports, and building destruction [20, 24].
4. Automotive: To inflate the airbags, sodium azide within the airbags reacts with a propellant. Due to the brief time available for inflation during a crash, the airbag circuit triggers a chemical explosion to facilitate their rapid deployment [20].
5. Agriculture: Certain energetic chemicals find common applications in agriculture. Ammonium nitrate, despite its role as an industrial explosive, is extensively used as a chemical fertilizer in agriculture due to its high nitrogen concentration. It is also employed as an insecticide and herbicide, functions as an oxidizer in rocket propellants, and serves as a nutrient in the production of antibiotics and yeast [20, 25, 26].
6. Medicine: Nitroglycerin tablets have been used to rapidly widen blood vessels, lower blood pressure, and provide immediate relief from angina. However, as alternatives to NG, various nitric acid esters such as erythritol tetranitrate and PETN are being utilized. Additionally, explosives are being explored for their potential applications in medicine and surgery. For instance, a group of researchers at a Japanese University has devised a novel technique for eliminating large stones (mineral deposits) in the kidney and bladder. This method involves the use of micro-explosive charges, without requiring surgery [20]. Another example is pentaerythritol nitrate, which finds application in medicine for treating chronic coronary insufficiency and angina pectoris. It is also utilized in the production of capsule detonators. Furthermore, compounds including the furoxan ring demonstrate a variety of biological actions, including anti-tuberculosis, anti-tumor, anti-inflammatory, anti-aggregant, and anti-aggregant, and can also be employed as an EC [21, 13]. In addition, Hydrogen peroxide is employed as a precursor in the synthesis of ECs, and it finds application in the medical and agricultural sectors [22].

I.6 Sensitivity of energetic compounds

Sensitivity to detonation is an essential characteristic of EC. This property refers to the vulnerability of these compounds to unexpected detonation due to an involuntary stimulus (sparks, friction, shock, heat, ...etc) [27, 18, 28].

I.7 Factors affecting the sensitivity of energetic compounds

Sensitivity comprehension is largely a chemical issue [29, 30]. It is a complex characteristic that are influenced by several chemical, structural, and physical factors [31]. Among these factors, molecular structure (encompassing chemical composition, molecular geometry, and stability) and crystal structure (including crystal size, shape, defects and strength) are inherent for an EC and are also considered crucial for sensitivity. Consequently, endeavors to establish a link between sensitivity and a specific molecular or crystal characteristic have at times been met with skepticism. Nevertheless, these initiatives have frequently been very effective and have given rise to significant predictive abilities [32]. Such correlations are crucial for comprehending sensitivities and developing new ECs. Although the fact that, as Brill and James noted, a correlation does not always indicate a causal link and may instead only be symptomatic [32]. The sensitivity to various external influences originates at the molecular level from molecular stability. Many studies have used the trigger mechanism to gain insight about sensitivity. There were many sensitivity correlations based on molecule stability suggested as a result. Lia et al. recently published a noteworthy review summarizing key sensitivity correlations in molecules, as depicted in Figure I.5 [33].

I.7.1 Molecular indices related with sensitivity

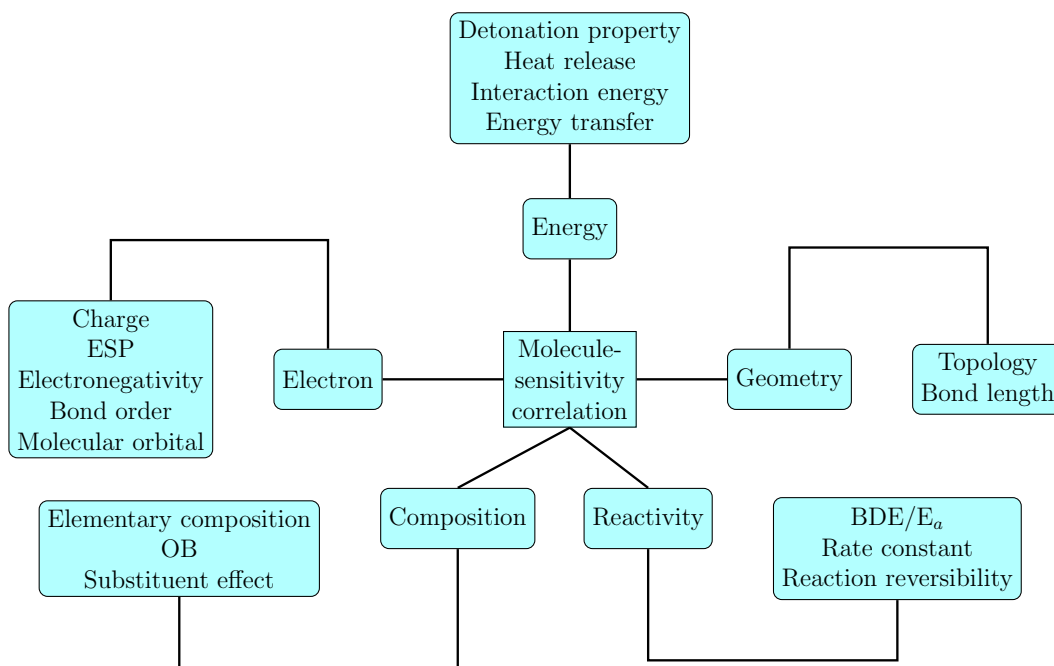


Figure I.5: Molecular structure-sensitivity relationships

1. **Molecular composition indices:** such as Oxygen balance (OB) and substituent effect. OB indicate the ratio of oxidizer elements (O) to reducer (C and H) elements in the system. Increased OB infers reduced stability of the molecule and increased sensitivity to some extent. The substituent effect can be attributed to either reinforcing the trigger bond (we will discuss later) or not, which therefore affects sensitivity. Naturally, this effect relies on the type, quantity, and positioning of substituents [33].
2. **Molecular electronic structure indices:** The molecular electronic structure encompasses six main parameters, comprising electron density, charge distribution, electrostatic potential (ESP), electronegativity, bond order (BO), and molecular orbitals. These indicators are interconnected with the electron density, which can be employed to estimate the other indices. Electron density can be determined through both experimental and computational methods. Typically, it is computed from the wave function using Bader’s Theory of Atoms in Molecules (AIM) [34]. Evidently, higher density implies stronger bonding, better stability, and lower sensitivity [33]. Molecular orbital features, such as BO, conjugation, HOMO and LUMO, and their gap, are further correlated with sensitivity [33].
3. **Molecular reactivity indices:** Indices such as reaction activation energy (E_a) or bond dissociation energy (BDE), and rate constant of molecular decomposition (k) were used to understand and anticipate sensitivity [33].
4. **Molecular energy indices:** interaction energy also influences sensitivity. A greater negative interaction energy (indicating attraction) is linked to heightened stability and reduced sensitivity. Enhanced intermolecular attraction contributes to diminished sensitivity [33, 35].
5. **Molecular geometry:** include bond length that can serve as an indicator of bond strength and can thus be related to sensitivity [33].

It’s important to recognize that the deduced molecular sensitivities might not perfectly align with experimental values due to the presence of numerous influencing factors that remain unknown until the substance is synthesized and characterized. Nevertheless, they offer a valuable evaluation of the sensitivity’s magnitude [33].

I.8 Reducing sensitivity: a major challenge

Reduced sensitivity to unintentional detonations caused by unwanted stimuli is an important and ongoing goal in the field of ECs [32, 36]. It is widely acknowledged that

the quality of an EC is determined by two key properties: energy and safety, both of which guide its applicability. Otherwise, a new energetic molecule will be rejected due to insufficient energy and lacking safety [37, 38]. This is one of the key reasons why, in comparison to the huge number of ECs designed in previous decades, only a limited number of ECs are employed in practice [39]. Unfortunately, the two characteristics are inherently conflicting, resulting in the so-called energy-safety contradiction. That is, stronger energy performance comes with greater risk [28, 40, 41, 42, 43, 44, 45].

The challenge is to bring together low sensitivity with high performance [16, 46]. In other words, balance the required metastability with the intended insensitivity. Essentially, they need to be unstable enough to rapidly release a significant amount of energy, while remaining stable enough to refrain from doing so until it is intended [47]. It is well understood that safety is extremely critical, even more vital than high energy output for ECs [38]. Numerous novel ECs have been recently developed; however, due to their high sensitivity, only a few of them are utilized [48]. Because ECs are frequently exposed to impacts, friction, and various external influences all over manufacturing, transportation, and storage processes, a more sensitive EC can readily ignite, potentially leading to catastrophic events [49]. In fact, over the last few decades, specific safety issues have frequently arisen during the manufacturing, storage, and utilization of such compounds [50, 51].

I.9 Efforts towards sensitivity reduction:

Efforts towards sensitivity reduction have been a priority focus in the field of ECs. The goal is to improve safety with maintaining the desired performance. Extensive investigations have been carried out to identify innovative approaches for minimising the sensitivity of such compounds. Several strategies have been analyzed, including modifications to the molecular structure of ECs and the employment of advanced manufacturing techniques such as coating and co-crystallization. Structural modification offers a means to mitigate the sensitivities of ECs [52]. In this context, we highlight certain strategies from the literature that depend on modifications to the chemical structure:

- Reducing mechanical sensitivity by incorporating methyl groups is an interesting strategy. For instance, incorporating a methyl group into the bis-triazole fused backbone has proven to be an efficient approach to diminish the sensitivity of ECs. By methylating the imino group of 5-nitro-3-trinitromethyl-1H-[1,2,4]triazole, the resultant compound demonstrates decreased sensitivity [53, 54].
- Tang et al, found that the replacement of a nitro group in FOX-7 with a nitrogen-rich heterocyclic ring increases stability and adjusts the sensitivity of the product

due to the emergence of a planar structure [55]. Tsyshevsky et al; noted that the sensitivity of oxadiazole-based ECs can be efficiently regulated by replacing nitro groups with amino groups and replacing the core 1,2,5-oxadiazole ring with the 1,2,4-oxadiazole ring [56].

- An effective strategy relies on combining a nitro group or an N-O group with an amino group to generate new ECs with limited sensitivity [57, 48]. Pang et al, proposed a substitution of one C-NO₂ of PTX (3,7,8-trinitropyrazolo[5,1-c][1,2,4] triazin-4-amine) with an N-O moiety [58].
- Another approach is the incorporation of a few of the same or distinct heterocyclic subunits into a molecule. 5 nitro-2-hydroxytetrazole, for example, is a very sensitive molecule; however, by introducing a triazole ring to produce 5-(3-nitro-1,2,4-1H-triazol-5-yl)tetrazol-1-ol, sensitivity to external stimuli is significantly decreased [59]. Furthermore, the combination of furazan and 1,2,4-oxadiazole may be advantageous for generating low sensitive ECs [60].
- To improve thermal sensitivity of ECs, four general approaches were proposed : introduction of amino groups; condensation with a triazole ring; salt formation; introduction of conjugation [61, 62, 63]. Moreover, the addition of amino-groups to a polynitroaromatic reduces sensitivity when compared to the analogous H-atom-substituted molecules. As a result of the increased hydrogen bonding between the NH₂ and NO₂ groups [44].
- Recent studies have revealed that carbon nanomaterials, such as fullerenes, graphite, carbon nanotubes, and graphene, can effectively decrease the mechanical sensitivity of ECs [64, 49]. Different types of carbon nanomaterials have varying effects on the desensitization of ECs. Functionalizing copper azide with a carbon nanomaterial, for instance, constitutes a feasible technique to enhance its sensitivity [65, 66, 52].

The pursuit of desensitization technology for ECs remains a focal point of research. Several approaches, including refining, coating, and co-crystallization, have been effectively explored to mitigate the sensitivity of ECs [67]. The application of a polymer coating onto EC particles aims to diminish the likelihood of hot-spot formation on the crystal surface when subjected to shock loading, and also to shield the resultant substances from adverse environmental influences. Polymer coating has conventionally been employed to enhance the mechanical insensitivity of ECs [68].

- HMX particles have undergone various coating techniques. The physicochemical characteristics of the resultant composite are distinctly influenced by the choice of polymer employed. A variety of polymers were used to significantly reduce

HMX sensitivity to mechanical stimulation such as polymethyl acrylate (PMA), ethyl cellulose (EC) and polylactide (PLA),...etc [68].

- When RDX combined with a molded polymer explosive PBX, the impact sensitivity was decreased. Sayles and Dhar noted that the use of glycidyl azide polymer (GAP) decreases the impact sensitivity of composite propellants containing ammonium perchlorate (AP)/RDX [69]. Certain researchers have even taken the step of designing a nanocomposite diamond layer to mitigate the reactivity of RDX [70].

I.10 Safety of energetic compounds:

Accidents regarding the detonation of huge amounts of ECs can lead to significant practical consequences, including substantial loss of life, destruction of infrastructure, and severe financial damage. Instances of such incidents took place in both industrial and military environments, leading to explosions that vary from minor to catastrophic. Producing, storing, and transporting ECs has long been a risky occupation. Even though the risks are well-recognized, and despite advancements in security measures, incidents and accidents still happen, particularly when these substances are manufactured, transported, or stored [71, 72].

According to statistics, In 2015, the Joint Research Center of the European Union (JRC) released a report, illustrating that the manufacturing and storage of explosives contributed to 43% of the 47 major accidents involving explosives in industrial activities. As per the report, accidents involving explosives have continued to happen regularly, with an average of two to four incidents occurring almost every year since 2000. Furthermore, in recent years, news reports have reported a number of tragic events related to the production of explosives, occurring in countries such as Germany, the United Kingdom, and Poland [72]. In the United States, according to the United States Bomb Data Center's Explosive Incident Report (USBDC-EIR), there were 860 explosive events recorded in the year 2021, resulting in 100 casualties and 27 deaths. Out of these 860 incidents, 381 were categorized as bombings, 226 as accidental, 213 as undetermined, and the remaining cases were either not defined or were currently under investigation [73].

I.11 Some of history's serious accidents caused by energetic compounds

Although many explosions are meticulously planned, throughout history, there have been numerous instances of severe explosions that have resulted in catastrophic consequences, which were caused by ECs. Here, we present some of the most tragic cases:

1. On August 4, 2020, in Beirut Port, Lebanon, a catastrophic explosion occurred when approximately 2,750 tons of ammonium nitrate stored in a warehouse detonated. This tragic event claimed the lives of 204 individuals and left more than 7,000 others injured. Furthermore, around 300,000 Lebanese residents were compelled to evacuate their destroyed homes, resulting in an estimated property damage cost of approximately US\$15 billion [74, 75, 76].
2. On March 21, 2019, a significant explosion occurred at a chemical warehouse in China, where dinitrobenzene and substandard nitro compounds were being stored. This unintentional explosion led to a tragic outcome, causing more than 617 injuries and claiming the lives of 78 individuals [74, 77].
3. On August 12, 2015, a series of massive explosions blasted through a container storage station in Tianjin, China. Hundreds of people died and hundreds more received injuries in the explosions [74].
4. On July 11, 2011, a devastating incident took place at a naval base in Cyprus, where military munitions and high explosives detonated. Tragically, multiple individuals lost their lives in this catastrophe. The explosion's estimated TNT equivalent yield was around 480 tonnes, marking it as the most significant military disaster ever documented on the island [74].
5. On December 6, 1917, a French cargo ship carrying a substantial load of high explosives erupted in a violent explosion known as the Halifax explosion in Nova Scotia. This devastating explosion ravaged Halifax's Richmond neighborhood, killing around 2,000 people [74].
6. On November 27, 1944, an accidental detonation occurred in the United Kingdom involving a stockpile of approximately 4,000 tons of military weapons. During the same year, another unintended military munition explosion took place in Port Chicago, California. In this incident, a cargo ship was in the process of being loaded when the explosives unexpectedly detonated, resulting in the tragic deaths of hundreds of sailors and civilians [74].
7. On September 21, 1921, a catastrophic explosion occurred near Oppau, Germany, involving a stockpile of ammonium sulfate and ammonium nitrate fertilizer.

While estimates differ, approximately 4,500 tonnes of this substance detonated, causing the loss of hundreds of lives and injuring thousands [74].



Figure I.6: Some pictures from the Beirut explosion

I.12 Trigger linkage concept

When an EC undergoes a mechanical or thermal stimulus, its deformation leads to elevated hot-spot temperatures, as postulated by the hot-spot theory [78]. If these temperatures surpass a critical threshold, the compound will undergo decomposition [79]. Trigger linkage, initially introduced by Kamlet and Adolph in 1979 [80], represents a fundamental concept in the breakdown of ECs. It is frequently employed to elucidate the spontaneous decomposition that characterizes such compounds when adequately stimulated [80, 81]. In this concept, specific types of bonds are more vulnerable to disruption due to external energy input. When these bonds rupture, they "triggers" an additional exothermic and self-sustaining decomposition, specific of detonation process [47]. C-NO₂ in nitroaromatics, nitroaliphatics, and nitroheterocycles; N-NO₂ in nitramines; O-NO₂ in nitrate esters; and N-N₂ in organic azides are examples

of often believed trigger bonds [36, 46]. It is important to note that the breaking of trigger bonds is not the only process that could lead to the initiation of detonation, undoubtedly, there exist additional possibilities [46]. Nevertheless, nearly all these mechanisms typically require the participation of nitro groups in combination with other substituents, often those in ortho positions [82].

The trigger linkage approach allows to understand the sensitivity of ECs from a molecular perspective. Numerous correlations between sensitivity and the strength of the trigger bond were identified using this approach. Lower sensitivity indicates greater chemical stability. As a result, a weaker trigger linkage results in greater sensitivity. Nitro ECs are of great significance, in such compounds, the X-NO₂ (X = C, N or O) is usually a trigger bond. The link between the strength of the C-NO₂/N-NO₂ bonds and sensitivity to detonation has been extensively studied both theoretically and experimentally [83, 84, 85, 86, 87, 88, 89]. It was revealed that as bond strength increases, the sensitivity to detonation decreases.

I.13 Neutralisation of energetic compounds by using MMCs

Neutralising ECs by selecting specific chemical compounds to react on certain sites of an energetic molecule, can be used to prevent the latter from following its normal explosion channel. The formation of such complexes may reinforce the trigger bonds within the EC and therefore reduce its sensitivity to detonation. Thus, we define a neutraliser as a molecule able to form a complex with an EC and prevents its explosion. The intrinsic value of this work appears in two main aspects:

1. Humanitarian demining: These types of complexes could potentially find utility in non-explosive reaction channels for the decomposition of ECs, which have been proposed [46, 90, 91]. If the interaction of an EC with a neutraliser is strong sufficiently to avoid an explosion pathway, a competent operator will be capable of safely removing the mine [92].
2. Enhanced security in the manufacturing, storage, transportation and use of ECs: The synthesis of these complexes might be helpful in the development of more stable and less sensitive compounds. This, in turn, would improve safety in the use of ECs in a variety of practical applications, successfully preventing accidents caused by such compounds.

Metallocene methyl cations (MMCs) are prominent organometallic compounds originally involved in the polymerization processes for their catalytic properties exerted on

π -electron bearing monomers through the Cossè-Arlman mechanism [93, 94] which can be explained by mean of a coordination of these monomers on metallic center of the MMCs. Because nitro groups are present in nearly all ECs, a hypothesis regarding the potential for favorable interactions arose. This encouraged to explore MMCs coordinating behavior as a way of preventing the explosion of ECs. MMCs were theoretically assessed as possible neutralisers of FOX-7 [92]. This energetic molecule is a derivative of ethylene, was thought to be highly reactive against MMCs through double bond π -electrons. However, after proper investigations, we realised that π -electrons from the double bond were less reactive when compared against those of oxygens of nitro groups. We found that a stable complex between FOX-7 and MMCs is formed. Such finding serves as the motivation behind this work and opened the possibility to explore interactions with any EC bearing at least one nitro group under the assumption that this substituent group can favourably interact with a cation like MMCs. If so, we can postulate MMCs as neutralisers of any energetic organic molecule.

In our work, the objective being to exploit the coordination capacity of MMCs to avoid the explosion channel. Nitro energetic molecules can interact with MMCs through its nucleophilic regions (lone pair electrons of NO_2) according to an electrophilic addition reaction. The chemical bond between a transition metal and oxygen holds an important place in several applications in chemistry, especially in catalytic processes [95, 96, 97, 98, 99]. Within the context of ECs, the oxygen atom, very active in the NO_2 group, plays an essential role in the sensitivity of ECs. To our knowledge, the role of intermolecular interactions on the sensitivity of ECs is limited to hydrogen bonds [6, 100, 101]. The role of intermolecular interactions involving transition metals in rationalising the sensitivity of ECs has not received much interest, which is likely related to the correlation between these intermolecular interactions and the sensitivity-related features of energetic molecules. This type of interaction is supported by the Gas-Phase Ion Chemistry investigation performed by M3 and Y3nez [102, 103, 104].

In summary, the formation of such complexes can enhance the trigger bond strength. Therefore, the sensitivity of the EC decreases. Thus, supporting the use of MMCs as possible neutralisers of ECs.

Bibliography

- [1] J Akhavan. Royal society of chemistry (great britain). *The chemistry of explosives*, 2004.
- [2] Tore Brinck. Introduction to green energetic materials. *Green Energetic Materials*, pages 1–14, 2014.
- [3] TM Klapötke. Chemistry of high energy materials, 5th edn., chapter 1.3, 2019.
- [4] Didier Mathieu. *Matériaux énergétiques*. Ed. Techniques Ingénieur, 2004.
- [5] Sergei G Zlotin, Aleksandr M Churakov, Mikhail P Egorov, Leonid L Fershtat, Michael S Klenov, Ilya V Kuchurov, Nina N Makhova, Gennady A Smirnov, Yury V Tomilov, and Vladimir A Tartakovsky. Advanced energetic materials: Novel strategies and versatile applications. *Mendeleev Communications*, 31(6):731–749, 2021.
- [6] Yu Ma, Anbang Zhang, Chenghua Zhang, Daojian Jiang, Yuanqiang Zhu, and Chaoyang Zhang. Crystal packing of low-sensitivity and high-energy explosives. *Crystal Growth & Design*, 14(9):4703–4713, 2014.
- [7] JACQUELINE AKHAVAN. The chemistry of explosives, 2004.
- [8] Tadeusz Urbanski, Sylvia Laverton, and Wladyslaw Ornaf. *Chemistry and technology of explosives*, volume 1. pergamon press Oxford, 1964.
- [9] Tenney L Davis. *The chemistry of powder and explosives*. Pickle Partners Publishing, 2016.
- [10] Félix Zapata and Carmen García-Ruiz. Chemical classification of explosives. *Critical Reviews in Analytical Chemistry*, 51(7):656–673, 2021.
- [11] Anthony J Bellamy. Fox-7 (1, 1-diamino-2, 2-dinitroethene). *High energy density materials*, pages 1–33, 2007.
- [12] Jan Welch. *Low sensitivity energetic materials*. PhD thesis, lmu, 2008.

- [13] Shijie Zhang, Zhenguo Gao, Di Lan, Qian Jia, Ning Liu, Jiaoqiang Zhang, and Kaichang Kou. Recent advances in synthesis and properties of nitrated-pyrazoles based energetic compounds. *Molecules*, 25(15):3475, 2020.
- [14] Tore Brinck and Martin Rahm. Theoretical design of green energetic materials: predicting stability, detection, synthesis and performance. *Green Energetic Materials*, pages 15–44, 2014.
- [15] Haixiang Gao, Qinghua Zhang, and M Shreeve Jean’ne. Fused heterocycle-based energetic materials (2012–2019). *Journal of Materials Chemistry A*, 8(8):4193–4216, 2020.
- [16] DM Badgujar, MB Talawar, SN Asthana, and PP Mahulikar. Advances in science and technology of modern energetic materials: an overview. *Journal of hazardous materials*, 151(2-3):289–305, 2008.
- [17] Paul W Cooper. *Explosives Engineering*. John Wiley & Sons, 1996.
- [18] Thomas M Klapötke. *Chemistry of high-energy materials*. Walter de Gruyter GmbH & Co KG, 2022.
- [19] Jimmie C Oxley. The chemistry of explosives. In *Explosive effects and applications*, pages 137–172. Springer, 1998.
- [20] Jai Prakash Agrawal. *High energy materials: propellants, explosives and pyrotechnics*. John Wiley & Sons, 2010.
- [21] Elena Chugunova, Timur Shaekhov, Ayrat Khamatgalimov, Vladimir Gorshkov, and Alexander Burirov. Dft quantum-chemical calculation of thermodynamic parameters and dsc measurement of thermostability of novel benzofuroxan derivatives containing triazidoisobutyl fragments. *International Journal of Molecular Sciences*, 23(3):1471, 2022.
- [22] Fadi Malak, Ahmad Rifai, Rana Baydoun, Bilal Nsouli, and Dimitar Dimitrov. Chemical safety and security after beirut port explosion: Part1-state of the art of legal framework and authorization policy. *Safety science*, 144:105456, 2021.
- [23] Christopher McFadden. Mining tools in 2022—a guide to mining equipment and mining machines, 2021.
- [24] J Lorimer. Some uses of explosives in civil engineering. works construction paper no 3. *Journal of the Institution of Civil Engineers*, 26(5):50–87, 1946.
- [25] Prathibha S Rao. Ammonium nitrate. 2014.

- [26] Awais Shakoor, Sher Muhammad Shahzad, Taimoor Hassan Farooq, and Fatima Ashraf. Future of ammonium nitrate after beirut (lebanon) explosion. *Environmental Pollution*, 2020, vol. 267, 115615, 2020.
- [27] Scott A Shackelford. Role of thermochemical decomposition in energetic material initiation sensitivity and explosive performance. *Central European Journal of Energetic Materials*, 5(1):75–101, 2008.
- [28] Laurence E Fried, M Riad Manaa, Philip F Pagoria, and Randall L Simpson. Design and synthesis of energetic materials. *Annual Review of Materials Research*, 31(1):291–321, 2001.
- [29] CB Storm, JR Stine, and JF Kramer. Sensitivity relationships in energetic materials. *Chemistry and physics of energetic materials*, pages 605–639, 1990.
- [30] Svatopluk Zeman. Sensitivities of high energy compounds. *High energy density materials*, pages 195–271, 2007.
- [31] D Mathieu. Theoretical shock sensitivity index for explosives. *The Journal of Physical Chemistry A*, 116(7):1794–1800, 2012.
- [32] Jane S Murray, Monica C Concha, and Peter Politzer. Links between surface electrostatic potentials of energetic molecules, impact sensitivities and c–no₂/n–no₂ bond dissociation energies. *Molecular Physics*, 107(1):89–97, 2009.
- [33] Gang Li and Chaoyang Zhang. Review of the molecular and crystal correlations on sensitivities of energetic materials. *Journal of Hazardous Materials*, 398:122910, 2020.
- [34] RFW Bader et al. A quantum theory. *Clarendon: Oxford, UK*, 1990.
- [35] Hai-bin Wang, Wen-jing Shi, Lei Yang, Jian-long Wang, et al. A b3lyp and mp2 (full) theoretical investigation into explosive sensitivity upon the formation of the intermolecular hydrogen-bonding interaction between the nitro group of rno₂ (r=–ch₃,–nh₂,–och₃) and hf, hcl or hbr. *Computational and Theoretical Chemistry*, 994:73–80, 2012.
- [36] Miroslav Pospíšil, Pavel Vávra, Monica C Concha, Jane S Murray, and Peter Politzer. A possible crystal volume factor in the impact sensitivities of some energetic compounds. *Journal of molecular modeling*, 16:895–901, 2010.
- [37] Rupeng Bu, Ying Xiong, and Chaoyang Zhang. π – π stacking contributing to the low or reduced impact sensitivity of energetic materials. *Crystal Growth & Design*, 20(5):2824–2841, 2020.

- [38] AK Sikder and Nirmala Sikder. A review of advanced high performance, insensitive and thermally stable energetic materials emerging for military and space applications. *Journal of hazardous materials*, 112(1-2):1–15, 2004.
- [39] Chaoyang Zhang, Fangbao Jiao, and Hongzhen Li. Crystal engineering for creating low sensitivity and highly energetic materials. *Crystal Growth & Design*, 18(10):5713–5726, 2018.
- [40] . On the energy & safety contradiction of energetic materials and the strategy for developing low-sensitive high-energetic materials. *Chinese Journal of Energetic Materials*, 26(1):2–10, 2018.
- [41] U Teipel. Energetic materials—particle processing and characterization, wile, 2005.
- [42] Jerzy Leszczynski. *Computational chemistry: reviews of current trends*, volume 8. World Scientific, 2003.
- [43] Peter Politzer and Jane S Murray. *Energetic materials: part 2. Detonation, combustion*. Elsevier, 2003.
- [44] Philip F Pagoria, Gregory S Lee, Alexander R Mitchell, and Robert D Schmidt. A review of energetic materials synthesis. *Thermochimica acta*, 384(1-2):187–204, 2002.
- [45] Fangbao Jiao, Ying Xiong, Hongzhen Li, and Chaoyang Zhang. Alleviating the energy & safety contradiction to construct new low sensitivity and highly energetic materials through crystal engineering. *CrystEngComm*, 20(13):1757–1768, 2018.
- [46] Peter Politzer and Jane S Murray. Detonation performance and sensitivity: a quest for balance. In *Advances in quantum chemistry*, volume 69, pages 1–30. Elsevier, 2014.
- [47] Peter Politzer and Jane S Murray. Some chemical and structural factors related to the metastabilities of energetic compounds. In *Theoretical and Computational Chemistry*, volume 6, pages 347–363. Elsevier, 1999.
- [48] Yanfei Cheng, Xiang Chen, Na Yang, Yazhou Zhang, Haixia Ma, and Zhaoqi Guo. Sandwich-like low-sensitive nitroamine explosives stabilized by hydrogen bonds and π - π stacking interactions. *CrystEngComm*, 23(9):1953–1960, 2021.
- [49] LQ Xiao, Y Zhao, XL Fu, WX Xie, and XZ Fan. Mechanical sensitivity reduction of energetic materials by using carbon nanomaterials. In *Journal of Physics: Conference Series*, volume 2478, page 032010. IOP Publishing, 2023.

- [50] Christer B Aakeröy, Tharanga K Wijethunga, and John Desper. Crystal engineering of energetic materials: Co-crystals of ethylenedinitramine (edna) with modified performance and improved chemical stability. *Chemistry–A European Journal*, 21(31):11029–11037, 2015.
- [51] Zhen Xu, Guangbin Cheng, Shunguan Zhu, Qiuhan Lin, and Hongwei Yang. Nitrogen-rich salts based on the combination of 1, 2, 4-triazole and 1, 2, 3-triazole rings: a facile strategy for fine tuning energetic properties. *Journal of Materials Chemistry A*, 6(5):2239–2248, 2018.
- [52] Guo-Ying Zhang, Ji-Min Han, Li Yang, and Tong-Lai Zhang. Theoretical study of the reduction in sensitivity of copper azide following encapsulation in carbon nanotubes. *Journal of Molecular Modeling*, 26:1–8, 2020.
- [53] Venugopal Thottempudi, Haixiang Gao, and Jean’ne M Shreeve. Trinitromethyl-substituted 5-nitro-or 3-azo-1, 2, 4-triazoles: synthesis, characterization, and energetic properties. *Journal of the American Chemical Society*, 133(16):6464–6471, 2011.
- [54] Xinyu Nie, Caijin Lei, Hualin Xiong, Guangbin Cheng, and Hongwei Yang. Methylation of a triazole-fused framework to create novel insensitive energetic materials. *Energetic Materials Frontiers*, 1(3-4):165–171, 2020.
- [55] Yongxing Tang, Wei Huang, Gregory H Imler, Damon A Parrish, and Jean’ne M Shreeve. Enforced planar fox-7-like molecules: a strategy for thermally stable and insensitive π -conjugated energetic materials. *Journal of the American Chemical Society*, 142(15):7153–7160, 2020.
- [56] Roman Tsyshevsky, Philip Pagoria, Maoxi Zhang, Ana Racoveanu, Damon A Parrish, Aleksandr S Smirnov, and Maija M Kuklja. Comprehensive end-to-end design of novel high energy density materials: I. synthesis and characterization of oxadiazole based heterocycles. *The Journal of Physical Chemistry C*, 121(43):23853–23864, 2017.
- [57] Davin G Piercey, David E Chavez, Brian L Scott, Greg H Imler, and Damon A Parrish. An energetic triazolo-1, 2, 4-triazine and its n-oxide. *Angewandte Chemie*, 128(49):15541–15544, 2016.
- [58] Jie Li, Yubing Liu, Wenqi Ma, Teng Fei, Chunlin He, and Siping Pang. Tri-explosophoric groups driven fused energetic heterocycles featuring superior energetic and safety performances outperforms hmx. *Nature Communications*, 13(1):5697, 2022.

- [59] Alexander A Dippold, Dániel Izsák, and Thomas M Klapötke. A study of 5-(1, 2, 4-triazol-5-yl) tetrazol-1-ols: Combining the benefits of different heterocycles for the design of energetic materials. *Chemistry—A European Journal*, 19(36):12042–12051, 2013.
- [60] Hao Wei, Chunlin He, Jiaheng Zhang, and Jean’ne M Shreeve. Combination of 1, 2, 4-oxadiazole and 1, 2, 5-oxadiazole moieties for the generation of high-performance energetic materials. *Angewandte Chemie International Edition*, 54(32):9367–9371, 2015.
- [61] Jai Prakash Agrawal. Recent trends in high-energy materials. *Progress in energy and combustion science*, 24(1):1–30, 1998.
- [62] Jai Prakash Agrawal. Some new high energy materials and their formulations for specialized applications. *Propellants, Explosives, Pyrotechnics: An International Journal Dealing with Scientific and Technological Aspects of Energetic Materials*, 30(5):316–328, 2005.
- [63] Jai Prakash Agrawal. Past, present & future of thermally stable explosives. *Central European Journal of Energetic Materials*, 9(3):273–290, 2012.
- [64] Qi-Long Yan, Michael Gozin, Feng-Qi Zhao, Adva Cohen, and Si-Ping Pang. Highly energetic compositions based on functionalized carbon nanomaterials. *Nanoscale*, 8(9):4799–4851, 2016.
- [65] F Farhad, JV Bellito, WM Koppes, et al. The adsorption of hydrazoic acid on single-walled carbon nanotubes. *Mater Chem Phys*, 112:427–431, 2008.
- [66] Qianyou Wang, Xiao Feng, Shan Wang, Naimeng Song, Yifa Chen, Wenchao Tong, Yuzhen Han, Li Yang, and Bo Wang. Metal-organic framework templated synthesis of copper azide as the primary explosive with low electrostatic sensitivity and excellent initiation ability. *Advanced Materials*, 28(28):5837–5843, 2016.
- [67] Xin-lei Jia, Cong-hua Hou, Jing-yu Wang, Ying-xin Tan, Yuan-ping Zhang, and Chao Li. Research progress on the desensitization technology of nitramine explosives. *Chin. J. Explos. Propellants*, 41:326–333, 2018.
- [68] Ekaterina K Kosareva, Mikhail N Zharkov, Dmitry B Meerov, Radmir V Gainutdinov, Igor V Fomenkov, Sergei G Zlotin, Alla N Pivkina, Ilya V Kuchurov, and Nikita V Muravyev. Hmx surface modification with polymers via sc-co₂ antisolvent process: A way to safe and easy-to-handle energetic materials. *Chemical Engineering Journal*, 428:131363, 2022.

- [69] Arthur Provatas. *Energetic polymers and plasticisers for explosive formulations: a review of recent advances*. DSTO Aeronautical and Maritime Research Laboratory Melbourne, 2000.
- [70] Yi Tong, Rui Liu, and Tonglai Zhang. The effect of a detonation nanodiamond coating on the thermal decomposition properties of rdx explosives. *Physical Chemistry Chemical Physics*, 16(33):17648–17657, 2014.
- [71] Trevor A Feagin, Eric M Heatwole, David S Eastwood, Ian Lopez-Pulliam, Thomas Connolley, Neil K Bourne, and Gary R Parker. Mechanistic insights into the initial explosion in the deflagration-to-detonation transition. *Combustion and Flame*, 242:112175, 2022.
- [72] Dimitris Kyprianou, Grzegorz Rarata, Giovanni Emma, Gabriela Diaconu, Mitja Vahcic, David Anderson, et al. Flow chemistry and the synthesis of energetic materials. *1831*, 9424, 2022.
- [73] Shawna F Gallegos, Edgar O Aviles-Rosa, Mallory T DeChant, Nathaniel J Hall, and Paola A Prada-Tiedemann. Explosive odor signature profiling: a review of recent advances in technical analysis and detection. *Forensic science international*, 347:111652, 2023.
- [74] Christopher McFadden. What are the world’s most powerful non-nuclear explosives?, 2021.
- [75] Giorgia Guglielmi. Why beirut’s ammonium nitrate blast was so devastating. *Nature*, 2020.
- [76] T Qiblawi, G Balkiz, S Paget, A Dewan, and H Regan. Emotional rollercoaster in beirut as rescuers end search for possible blast survivor.
- [77] Xiaodong Yang, Yongzhao Li, Yangqing Chen, Yuqi Li, Libo Dai, Ren Feng, and Yih-Shing Duh. Case study on the catastrophic explosion of a chemical plant for production of m-phenylenediamine. *Journal of Loss Prevention in the Process Industries*, 67:104232, 2020.
- [78] John E Field. Hot spot ignition mechanisms for explosives. *Accounts of chemical Research*, 25(11):489–496, 1992.
- [79] Tomas L Jensen, John F Moxnes, Erik Unneberg, and Dennis Christensen. Models for predicting impact sensitivity of energetic materials based on the trigger linkage hypothesis and arrhenius kinetics. *Journal of Molecular Modeling*, 26:1–14, 2020.

- [80] MJ Kamlet and HG Adolph. The relationship of impact sensitivity with structure of organic high explosives. ii. polynitroaromatic explosives. *Propellants, Explosives, Pyrotechnics*, 4(2):30–34, 1979.
- [81] Ying Xiong, Kai Zhong, and Chao-yang Zhang. Trigger linkage mechanism: Two or multiple steps initiate the spontaneous decay of energetic materials. *Energetic Materials Frontiers*, 3(1):38–46, 2022.
- [82] Didier Mathieu. Modeling sensitivities of energetic materials using the python language and libraries. *Propellants, Explosives, Pyrotechnics*, 45(6):966–973, 2020.
- [83] Bao-Hui Li, Wen-jing Shi, Fu-de Ren, and Yong Wang. A b3lyp and mp2 (full) theoretical investigation into the strength of the c–no 2 bond upon the formation of the intermolecular hydrogen-bonding interaction between hf and the nitro group of nitrotriazole or its methyl derivatives. *Journal of molecular modeling*, 19:511–519, 2013.
- [84] Jinshan Li. Relationships for the impact sensitivities of energetic c-nitro compounds based on bond dissociation energy. *The Journal of Physical Chemistry B*, 114(6):2198–2202, 2010.
- [85] Bao-guo Wang, Fu-de Ren, and Wen-jing Shi. A theoretical investigation into the strength of n–no 2 bonds, ring strain and electrostatic potential upon formation of intermolecular h-bonds between hf and the nitro group in nitrogen heterocyclic rings c n h 2 n n–no 2 (n= 2–5), rdx and hmx. *Journal of molecular modeling*, 21:1–11, 2015.
- [86] Wei Qiu, Fu-de Ren, Wen-jing Shi, and Yan-hong Wang. A theoretical study on the strength of the c–no 2 bond and ring strain upon the formation of the intermolecular h-bonding interaction between hf and nitro group in nitrocyclopropane, nitrocyclobutane, nitrocyclopentane or nitrocyclohexane. *Journal of Molecular Modeling*, 21:1–9, 2015.
- [87] Jinshan Li. A multivariate relationship for the impact sensitivities of energetic n-nitrocompounds based on bond dissociation energy. *Journal of hazardous materials*, 174(1-3):728–733, 2010.
- [88] Frank J Owens, Keerthi Jayasuriya, Lars Abrahmsen, and Peter Politzer. Computational analysis of some properties associated with the nitro groups in polynitroaromatic molecules. *Chemical physics letters*, 116(5):434–438, 1985.

- [89] Mohammad Hossein Keshavarz. Simple relationship for predicting impact sensitivity of nitroaromatics, nitramines, and nitroaliphatics. *Propellants, Explosives, Pyrotechnics*, 35(2):175–181, 2010.
- [90] Anna V Kimmel, Peter V Sushko, Alexander L Shluger, and Maija M Kuklja. Effect of charged and excited states on the decomposition of 1, 1-diamino-2, 2-dinitroethylene molecules. *The Journal of chemical physics*, 126(23), 2007.
- [91] Jun Tao and Xiaofeng Wang. Theoretical investigation on the interaction mechanism of fox-7/ap mixed crystals. *Molecular Simulation*, 46(2):155–161, 2020.
- [92] Jorge M Del Campo and Jorge Ignacio Martínez-Araya. Possible use of group 4 metallocene methyl cations as potential neutralizers for fox-7. *Propellants, Explosives, Pyrotechnics*, 39(6):890–896, 2014.
- [93] P. Cossee. Ziegler-natta catalysis i. mechanism of polymerization of α -olefins with ziegler-natta catalysts. *Journal of Catalysis*, 3(1):80–88, 1964.
- [94] EJ Arlman. Ziegler-natta catalysis ii. surface structure of layer-lattice transition metal chlorides. *Journal of Catalysis*, 3(1):89–98, 1964.
- [95] Ambarish Kulkarni, Samira Siahrostami, Anjali Patel, and Jens K Nørskov. Understanding catalytic activity trends in the oxygen reduction reaction. *Chemical Reviews*, 118(5):2302–2312, 2018.
- [96] Qing Liang, Xiaodong Wu, Duan Weng, and Haibo Xu. Oxygen activation on cu/mn-ce mixed oxides and the role in diesel soot oxidation. *Catalysis Today*, 139(1-2):113–118, 2008.
- [97] Lichen Liu and Avelino Corma. Metal catalysts for heterogeneous catalysis: from single atoms to nanoclusters and nanoparticles. *Chemical reviews*, 118(10):4981–5079, 2018.
- [98] Roy A Periana, Douglas J Taube, Scott Gamble, Henry Taube, Takashi Satoh, and Hiroshi Fujii. Platinum catalysts for the high-yield oxidation of methane to a methanol derivative. *Science*, 280(5363):560–564, 1998.
- [99] Bjørk Hammer and Jens Kehlet Nørskov. Theoretical surface science and catalysis—calculations and concepts. In *Advances in catalysis*, volume 45, pages 71–129. Elsevier, 2000.
- [100] Danijela S Kretić, Jelena I Radovanović, and Dušan Ž Veljković. Can the sensitivity of energetic materials be tuned by using hydrogen bonds? another look at the role of hydrogen bonding in the design of high energetic compounds. *Physical Chemistry Chemical Physics*, 23(12):7472–7479, 2021.

- [101] Jiaheng Zhang, Qinghua Zhang, Thao T Vo, Damon A Parrish, and Jean'ne M Shreeve. Energetic salts with π -stacking and hydrogen-bonding interactions lead the way to future energetic materials. *Journal of the American Chemical Society*, 137(4):1697–1704, 2015.
- [102] A Luna, B Amekraz, J-P Morizur, J Tortajada, O M3, and M Yanez. Reactions between guanidine and Cu^+ in the gas phase. an experimental and theoretical study. *The Journal of Physical Chemistry A*, 101(33):5931–5941, 1997.
- [103] J-LM Abboud, I Alkorta, JZ Davalos, J-F Gal, M Herreros, P-C Maria, O M3, MT Molina, R Notario, and M Y3ñez. The $\text{p}^4 \text{Li}^+$ ion in the gas phase: A planetary system. *Journal of the American Chemical Society*, 122(18):4451–4454, 2000.
- [104] Manuel Alcam3, Alberto Luna, Otilia M3, Manuel Y3ñez, Jeanine Tortajada, and Badia Amekraz. Unimolecular reactivity of strong metal–cation complexes in the gas phase: ethylenediamine– Cu^+ . *Chemistry–A European Journal*, 10(12):2927–2934, 2004.

Chapter II

Quantum chemical methods

II.1 The Schrödinger equation

Fundamentally, quantum chemical methods focus on solving the Schrödinger equation to find the wave function, which provides the most comprehensive description of the molecular system. In the case of a stationary state of a given system, this equation is expressed as the following eigenvalue equation:

$$\hat{H}\Psi = E\Psi \quad (\text{II.1})$$

Where \hat{H} is the Hamiltonian operator associated with the sum of the kinetic and potential energies of the system, Ψ is the wave function that depends on the coordinates of electrons and nuclei, and E is the energy of the stationary state (also known as eigenvalue).

The exact solution of the Schrödinger equation is only achievable for extremely simple systems, such as the hydrogen atom, the molecular ion H_2^+ and the hydrogen-like ions (He^+ , Li_2^+ , ... etc), primarily because of the electron-electron repulsion term within the Hamiltonian. Thus, in most situations, it is necessary to employ approximate solutions due to the inherent complexity.

According to the Born-Oppenheimer approximation, due to the significant disparity in mass between nuclei and electrons ($m_p \approx 1800m_e$), it is assumed that electrons can rapidly adjust their positions in response to any nuclear movement. Subsequently, the total wave function is expressed as a product of two components: an electronic function $\Psi_e(\vec{R}, \vec{r})$ and a nuclear function $\Psi_n(\vec{R})$ describing the behavior of the electrons and the nuclei, respectively.

$$\Psi(\vec{R}, \vec{r}) = \Psi_e(\vec{R}, \vec{r})\Psi_n(\vec{R}) \quad (\text{II.2})$$

Where \vec{r} and \vec{R} denote the electron and nuclear coordinates, respectively. For a system composed of N electrons and M nuclei, the electronic equation takes the following form:

$$\hat{H}_e(\vec{r}, \vec{R})\Psi_e(\vec{r}, \vec{R}) = E(\vec{R})\Psi_e(\vec{r}, \vec{R}) \quad (\text{II.3})$$

The electronic Hamiltonian \hat{H}_e is given by:

$$\hat{H}_e(\vec{r}, \vec{R}) = \underbrace{-\sum_{i=1}^N \frac{\hbar^2}{8\pi^2 m_e} \nabla_i^2}_{\hat{T}_e} - \underbrace{\sum_{i=1}^N \sum_{A=1}^M \frac{1}{4\pi\epsilon_0} \frac{Z_A e^2}{|\mathbf{r}_{iA}|}}_{\hat{V}_{eN}} + \underbrace{\sum_{j>i}^N \frac{1}{4\pi\epsilon_0} \frac{e^2}{|\mathbf{r}_{ij}|}}_{\hat{V}_{ee}} \quad (\text{II.4})$$

Where ∇_i^2 is the Laplacian operator involving the coordinates of electron i , $\mathbf{r}_{iA} = |\vec{r}_i - \vec{R}_A|$ represents the distance between nucleus A and electron i , Z_A denotes the nuclear

charge of nucleus A , \mathbf{r}_{ij} is the distance between electrons i and j , m_e denotes The electron's mass = $9,1093.10^{-31}$ kg, ϵ_0 represents the vacuum permittivity = $8,854.10^{-12}$ $F.m^{-1}$ and h is the Planck constant = $6,62606.10^{-34}$ $J.s$.

In atomic units: ($m_e = e = h/2\pi = 1/4\pi\epsilon_0 = 1$)

$$\hat{H}_e(\vec{r}, \vec{R}) = - \sum_{i=1}^N \frac{1}{2} \nabla_i^2 - \sum_{i=1}^N \sum_{A=1}^M \frac{Z_A}{\mathbf{r}_{iA}} + \sum_{j>i}^N \frac{1}{\mathbf{r}_{ij}} \quad (\text{II.5})$$

The terms \hat{T}_e , \hat{V}_{eN} , and \hat{V}_{ee} in expression (II.3) represent, respectively, the operators associated with the kinetic energy of electrons, the nucleus-electron potential energy, and the electron-electron potential energy. The latter term, describing the interelectronic repulsion energy, is typically subject to approximations. The inability to decompose this term into a sum of individual one-electron contributions signifies that it is not possible to precisely define one-electron functions in a polyelectronic system. [1, 2]

Solving the electronic equation (II.3) provides both the energy and the wave function of the system, specific to a given nuclear configuration. This is typically accomplished either by employing the Hartree-Fock (HF) theory, which is founded on a model of independent particles. Alternatively, for a more accurate treatment, the analysis takes into account the instantaneous correlations between electron movements, which the HF theory partially ignores. Incorporating electronic correlation, particularly through post-HF methods, is crucial to achieve results that are accurate enough for direct comparison with experimental results. However, there are often technical challenges to contend with, notably the long computational cost, especially when dealing with large molecules. In such cases, theorists often opt for less computationally demanding and cost-effective approaches, primarily which utilize density functional theory (DFT) [1, 2, 3, 4, 5].

II.2 Hartree-Fock theory

Equations defined in this section and more theoretical details can be found in [6, 2, 7, 8]. The HF theory is predicated on the assumption that it could be appropriate to begin by assuming that electrons do not interact with one another. In this theory, the total wave function $\Psi(\vec{r}_1, \vec{r}_2, \dots, \vec{r}_N)$ is written as a product of spin orbitals $\chi_i(\vec{r}_i)$, which is known as a Hartree Product:

$$\Psi_{HP}(\vec{r}_1, \vec{r}_2, \dots, \vec{r}_N) = \prod_{i=1}^N \chi_i(\vec{r}_i) = \chi_1(\vec{r}_1) \chi_2(\vec{r}_2) \dots \chi_N(\vec{r}_N) \quad (\text{II.6})$$

The spin orbital is simply the product of a space function with a spin function, i.e., $\chi(r) = \phi(r)\alpha$ or $\chi(r) = \phi(r)\beta$.

This form of wavefunction does not satisfy the antisymmetry principle, that implies that a wavefunction defining fermions must be antisymmetric with respect to any interchange of space-spin coordinates. These coordinates denote that fermions have an inherent spin coordinate, either α or β , in addition to three spatial degrees of freedom. Consequently, the Hartree Product does not fulfill the anticipated properties. To address this issue, John Slater proposed the use of the Slater determinant (II.7), which is a determinant of spin orbitals.

$$\Psi = \Psi_{SD} = \frac{1}{\sqrt{N!}} \begin{vmatrix} \chi_1(\vec{r}_1) & \chi_2(\vec{r}_1) & \chi_3(\vec{r}_1) & \dots & \chi_N(\vec{r}_1) \\ \chi_1(\vec{r}_2) & \chi_2(\vec{r}_2) & \chi_3(\vec{r}_2) & \dots & \chi_N(\vec{r}_2) \\ \vdots & \vdots & \vdots & \vdots & \vdots \\ \chi_1(\vec{r}_N) & \chi_2(\vec{r}_N) & \chi_3(\vec{r}_N) & \dots & \chi_N(\vec{r}_N) \end{vmatrix} \quad (\text{II.7})$$

Where $\frac{1}{\sqrt{N!}}$ is the normalization factor.

This selected form of Ψ adheres to the Pauli exclusion principle, it equals zero when two electrons with the same spin occupy the same point in space, and all electrons are indistinguishable, which aligns with the conclusions of quantum mechanics. The previous determinant can be abbreviated in a ket symbol as: $|\chi_i\chi_j\dots\chi_k\rangle$ or even more concisely as $|ij\dots k\rangle$.

HF theory is also known as the independent particle model or mean field theory since it accepts the assumption that each electron moves independently of the others, except for experiencing Coulomb repulsion based on the average positions of all electrons and an exchange interaction arising from antisymmetrization.

Consider \hat{h} , the one-electron operator defined as follows:

$$\hat{h}(i) = -\frac{1}{2}\nabla_i^2 - \sum_A \frac{Z_A}{\mathbf{r}_{iA}} \quad (\text{II.8})$$

And $\hat{h}(i, j)$, a two-electron operator as:

$$\hat{h}(i, j) = \frac{1}{\mathbf{r}_{ij}} \quad (\text{II.9})$$

The electronic Hamiltonian can thus be simplified as:

$$\hat{H}_e = \sum_i \hat{h}(i) + \sum_{j>i} \hat{h}(i, j) \quad (\text{II.10})$$

Assuming that Ψ is normalized, the energy expression will be given by:

$$E_e = \langle \Psi | \hat{H}_e | \Psi \rangle \quad (\text{II.11})$$

The variational theorem, which asserts that the energy of the studied system always represents an upper bound to the exact energy ($E_e \geq E_0$), can be used to symmetric energy expressions. Therefore, by adjusting their parameters until we minimise the energy within the specified spatial function, we can generate better approximate wavefunctions, Ψ . The molecular orbitals that minimise the E_e are, therefore, the proper ones. These orbitals can be generated numerically by integrating over a grid or, more frequently, by linearly combining a set of given basis functions, often referred to as "atomic orbital" basis functions, which are typically Gaussian-type or Slater-type functions centered on the atom.

The HF energy is defined in terms of the one- and two-electron integrals as follows:

$$E_{HF} = \sum_i \langle i | \hat{h} | i \rangle + \frac{1}{2} \sum_{ij} ([ii|jj] - [ij|ji]) \quad (\text{II.12})$$

Where

$$\langle i | \hat{h} | i \rangle = \int dr_1 \chi_i^*(r_1) \hat{h}(r_1) \chi_i(r_1) \quad (\text{II.13})$$

And

$$[ij|kl] = \int dr_1 dr_2 \chi_i^*(r_1) \chi_j(r_1) \frac{1}{r_{12}} \chi_k^*(r_2) \chi_l(r_2) \quad (\text{II.14})$$

II.2.1 The Hartree-Fock equations

We have to minimise the E_{HF} expression while considering changes in the orbitals $\chi_i \rightarrow \chi_i + \delta\chi_i$. Additionally, we have been supposing that the orbitals χ are orthonormal. Therefore, we aim to make sure that the variational procedure maintains their orthonormality. This can be achieved by employing Lagrange's method of undetermined multipliers. In this approach, a functional \mathcal{L} is used.

$$\mathcal{L}[\{\chi_i\}] = E_{HF}[\{\chi_i\}] - \sum_{ij} \epsilon_{ij} (\langle i | j \rangle - \delta_{ij}) \quad (\text{II.15})$$

Where ϵ_{ij} are the undetermined Lagrange multipliers and $\langle i | j \rangle$ is the i and j spin orbitals overlap.

$$\langle i | j \rangle = \int \chi_i^*(r) \chi_j(r) dr \quad (\text{II.16})$$

Putting $\delta\mathcal{L} = 0$, we arrive at the HF equations that characterize the orbitals:

$$\hat{h}(r_1)\chi_i(r_1) + \underbrace{\sum_{i \neq j} \left[\int dr_2 |\chi_j(r_2)|^2 \frac{1}{r_{12}} \right]}_{I_1} \chi_i(r_1) - \underbrace{\sum_{i \neq j} \left[\int dr_2 \chi_j^*(r_2) \chi_i(r_2) \frac{1}{r_{12}} \right]}_{I_2} \chi_j(r_1) = \epsilon_i \chi_i(r_1) \quad (\text{II.17})$$

ϵ_i represents the energy eigenvalue associated with χ_i .

The HF equations can be solved in one of two ways: numerically (exact HF) or within the space defined by a set of basis functions (HF-Roothan equations). In both cases, it's important to note that the solutions depend on the orbitals. Therefore, we must guess initial orbitals and subsequently improve them through an iterative process. This is why, HF is referred to as a self-consistent-field (SCF) approach. The I_1 term (Coulomb term) in equation (II.17), denotes the Coulomb interaction of an electron in χ_i with the average charge distribution of the (N-1) other electrons. The Coulomb operator defined as:

$$\hat{\mathcal{J}}_j(r_1) = \int dr_2 |\chi_j(r_2)|^2 \frac{1}{r_{12}} \quad (\text{II.18})$$

Providing the average local potential at point r_1 as a result of the charge distribution from the electron in χ_j . The I_2 term is more challenging to elucidate and lacks a classical analogue and it emerges due to the wavefunction's antisymmetry property. It appears similar to the Coulomb term, but it involves the exchanging of spin orbitals χ_i and χ_j . For that, it is referred to as the exchange term. The exchange operator is defined as:

$$\hat{\mathcal{K}}_j(r_1)\chi_i(r_1) = \left[\int dr_2 \chi_j^*(r_2) \frac{1}{r_{12}} \chi_i(r_2) \right] \chi_j(r_1) \quad (\text{II.19})$$

So, the HF equations become:

$$\left[\hat{h}(r_1) + \sum_{i \neq j} \hat{\mathcal{J}}_j(r_1) - \sum_{i \neq j} \hat{\mathcal{K}}_j(r_1) \right] \chi_i(r_1) = \epsilon_i \chi_i(r_1) \quad (\text{II.20})$$

Now, it's clearer that the HF equations are eigenvalue equations. If we know that

$$\left[\hat{\mathcal{J}}_i(r_1) - \hat{\mathcal{K}}_i(r_1) \right] \chi_i(r_1) = 0 \quad (\text{II.21})$$

We can eliminate the restrictions $i \neq j$ in the summations, and we introduce the Fock operator, as

$$\hat{f}(r_1) = \hat{h}(r_1) + \sum_j \left[\hat{\mathcal{J}}_j(r_1) - \hat{\mathcal{K}}_j(r_1) \right] \quad (\text{II.22})$$

The HF equations are simply:

$$\hat{f}(r_1)\chi_i(r_1) = \epsilon_i\chi_i(r_1) \quad (\text{II.23})$$

The introduction of a basis set converts the HF equations into the Roothaan equations. For each χ_i , we have :

$$\chi_i = \sum_{\mu=1}^K C_{\mu i} \tilde{\chi}_\mu \quad (\text{II.24})$$

$\tilde{\chi}$ denotes the atomic orbital basis functions.

$$\hat{f}(x_1) \sum_{\nu} C_{\nu i} \tilde{\chi}_\nu(\chi_1) = \epsilon_i \sum_{\nu} C_{\nu i} \tilde{\chi}_\nu(\chi_1) \quad (\text{II.25})$$

When multiplying by $\tilde{\chi}_\mu^*(r_1)$ and integrating, we obtain a matrix equation.

$$\sum_{\nu} C_{\nu i} \int dr_1 \tilde{\chi}_\mu^*(r_1) f(r_1) \tilde{\chi}_\nu(\chi_1) = \epsilon_i \sum_{\nu} C_{\nu i} \int dr_1 \tilde{\chi}_\mu^*(r_1) \tilde{\chi}_\nu(\chi_1) \quad (\text{II.26})$$

For simplicity, we introduce matrix element notation.

$$\mathcal{S}_{\mu\nu} = \int dr_1 \tilde{\chi}_\mu^*(r_1) \tilde{\chi}_\nu(\chi_1) \quad (\text{II.27})$$

$$\mathcal{F}_{\mu\nu} = \int dr_1 \tilde{\chi}_\mu^*(r_1) f(r_1) \tilde{\chi}_\nu(\chi_1) \quad (\text{II.28})$$

The HF-Roothaan equations could be written as a matrix form :

$$\sum_{\nu} \mathcal{F}_{\mu\nu} C_{\nu i} = \epsilon_i \sum_{\nu} \mathcal{S}_{\mu\nu} C_{\nu i} \quad (\text{II.29})$$

Or simply as:

$$\mathcal{F}C = \mathcal{S}C\epsilon \quad (\text{II.30})$$

Where ϵ represents a diagonal matrix containing the orbital energies ϵ_i . This situation resembles an eigenvalue equation, except for the presence of the overlap matrix \mathcal{S} . One undergoes a change of basis to shift to an orthogonal basis, ensuring that \mathcal{S} becomes zero. After this transformation, it becomes a matter of solving an eigenvalue equation (diagonalizing \mathcal{F}). However, because \mathcal{F} relies on its own solution via the orbitals, the process requires iteration. This iterative nature is why the solution to the HF-Roothaan equations is often referred to as SCF procedure.

II.3 Post Hartree-Fock methods

Electrons demonstrate correlation through two ways: first, due to their negative charge, they experience mutual repulsion, and second, as fermions, they exhibit repulsion when their spins are the same. Using the independent particle model, the HF approach produces a wave function and an energy that are somewhat unsatisfactory. The term "correlation energy" denotes the difference between the exact energy and the energy calculated using the HF method ($E_{correlation} = E_{exact} - E_{HF}$). This discrepancy arises from the nature of the total wave function, which does not approach zero when two electrons with different spins are situated at the same point. Consequently, electronic repulsions are overevaluated. Better results can be achieved by taking into account electron correlation. Several post HF methods are available for this purpose, such as [1, 9]:

1. The Møller-Plesset (MP) method.
2. The Configuration Interaction (CI) method.
3. The Multi-Configuration Self-Consistent Field (MCSCF) method.
4. The Multireference Configuration Interaction (MRCI) method.
5. The Many-Body Perturbation Theory (MBPT) method.
6. The Coupled-Cluster (CC) method.

II.4 Density Functional Theory (DFT)

To accurately account for electronic correlation, it becomes extremely challenging to employ advanced post HF computations when dealing with significantly large systems. An alternative to address these challenges is through the use of DFT. L.H.Thomas and E.Fermi were the first to propose the idea of representing the total energy of a molecular system as a function of the total electron density. Nonetheless, the precise formulation of this model, which is now known as density functional theory (DFT), was not presented until 1964 by Hohenberg and Kohn. Mathematically, a functional is an application that associates a scalar with a function [10, 11, 12, 13, 14, 15]. DFT is based on two theorems established by Hohenberg and Kohn that confirm the following principles:

1. The ground state of a system, along with all its observable characteristics, is completely defined by knowing the total electron density $\rho(x, y, z)$ at every spatial point. Specifically, energy is a functional of density: $E = F(\rho)$. However, this functional is unknown.

2. The ground state is characterized by $\rho(x, y, z)$ being the density that minimizes the energy, analogous to the variational theorem for wavefunctions but applied to density. More details about these two theorems can be found at [16, 17, 18].

The DFT approach seems especially beneficial because the electron density $\rho(x, y, z)$ relies just on three variables (four if we include spin), and is also considered an observable, can be measured experimentally, e. g. through X-ray diffraction. Nevertheless, the wave function Ψ , which is not an observable, encompasses $3N$ spatial variables, where N denotes the total number of electrons within the system. Moreover, DFT is currently crucial for computing molecular properties due to the accuracy of the obtained results and the computational efficiency of all approaches based on it. The electron density $\rho(\vec{r})$ is given by the following expression [10]:

$$\rho(\vec{r}) = \sum_{i=1}^N |\phi_i(\vec{r})|^2 \quad (\text{II.31})$$

In precise terms, $\rho(\vec{r})$ (e/Bohr^3) represents the probability of finding an electron at a specific point in space. However, it's usual to refer to it as electron density. Certainly, $\rho(\vec{r})$ is a non-negative function that approaches zero at infinity, and it is normalized to N , the total number of electrons.

$$\rho(\vec{r} \rightarrow \infty) = 0 \quad (\text{II.32})$$

$$\int \rho(\vec{r}) d\vec{r} = N \quad (\text{II.33})$$

II.4.1 Kohn-Sham equations

Equations defined in this section and more theoretical details can be found in [10, 11, 12, 13, 14, 15]. The energy is divided into three components, all functionals of ρ : kinetic energy T , nucleus-electron potential energy E_{eN} , and electron-electron potential energy E_{ee} :

$$E[\rho] = T[\rho] + E_{eN}[\rho] + E_{ee}[\rho] \quad (\text{II.34})$$

Only the E_{eN} term can be readily expressed, the other two terms are unknown. The charge contained within an infinitesimal volume element at the coordinate \vec{r} is given by $\rho(\vec{r})d\vec{r}$, so:

$$E_{eN}[\rho] = \sum_A \int \frac{Z_A \rho(\vec{r})}{|\vec{R}_A - \vec{r}|} d\vec{r} \quad (\text{II.35})$$

A portion of the electron-electron energy can be represented as the repulsion between two charges $\rho(\vec{r})d\vec{r}$ situated at two points separated by a distance of \mathbf{r}_{12} , as described

by:

$$J[\rho] = \frac{1}{2} \int \int \frac{\rho(\vec{r}_1)\rho(\vec{r}_2)}{\mathbf{r}_{12}} d\vec{r}_1 d\vec{r}_2 \quad (\text{II.36})$$

However, this term lacks correlation since the product of probability densities should be subject to the modulation by \mathbf{r}_{12} . Also, exchange energy (Fermi hole) is not addressed. Furthermore, because all electrons contribute to the overall density, a single electron exhibits a particular density at both r_1 and r_2 , resulting in self-interaction in this term.

Based on the KS method, the density is typically represented in the form of a Slater determinant composed of molecular orbitals. The KS orbitals, indicated as ϕ_i , are distinct from the HF orbitals. These orbitals are associated with a model system of non-interacting electrons while maintaining an identical electron density as the real system. This method permits the precise representation of the terms E_{eN} and J . Given that the system's corresponding operator is a one electron, the kinetic energy for this system is calculated as follows:

$$T_s[\rho] = \sum_{i=1}^N \langle \phi_i | -\frac{1}{2} \nabla_i^2 | \phi_i \rangle \quad (\text{II.37})$$

Nonetheless, it does not equal to the kinetic energy of the actual system. The entirety of the remaining energy is combined into an exchange-correlation term, E_{xc} . Thus, the expression of energy in terms of KS orbitals is:

$$E = -\frac{1}{2} \sum_i \langle \phi_i | \nabla_i^2 | \phi_i \rangle + \sum_i \int_{\infty}^N \sum_{i,A} \frac{Z_A |\phi_i(\vec{r}_1)|^2 dr_1}{\mathbf{r}_{iA}} \quad (\text{II.38})$$

$$+ \sum_{i,j>i} \int \int_{\infty}^N |\phi_i(\vec{r}_1)|^2 \frac{1}{\mathbf{r}_{12}} |\phi_j(\vec{r}_2)|^2 dr_1 dr_2 + E_{xc}[\rho(\vec{r})]$$

$$E_{KS-DFT}[\rho] = T_s[\rho] + E_{eN}[\rho] + J[\rho] + E_{xc}[\rho] \quad (\text{II.39})$$

The expression of the exchange-correlation energy is given by:

$$E_{xc}[\rho] = (T[\rho] - T_s[\rho]) + (E_{ee}[\rho] - J[\rho]) \quad (\text{II.40})$$

Frequently, E_{xc} is divided into exchange and correlation components and expressed with respect to the energy per particle (ϵ_x and ϵ_c).

$$E_{xc}[\rho] = E_x[\rho] + E_c[\rho] = \int \rho(\vec{r}) \epsilon_x[\rho(\vec{r})] d\vec{r} + \int \rho(\vec{r}) \epsilon_c[\rho(\vec{r})] d\vec{r} \quad (\text{II.41})$$

The E_{xc} term must explicitly rely on r_1 and r_2 . Its formulation constitutes the primary difficulty of the method, and various solutions have been suggested to address it. An

energy that needs to be minimized is formulated based on the KS orbitals, which are also not initially known. Consequently, an iterative process (SCF) is employed, beginning with trial functions to directly determine the correlated energy.

II.4.2 The main exchange-correlation density functionals of DFT

There exists a multiple of approximations for the E_{xc} functional, In Gaussian, these approximations are designated by a group of letters, frequently representing the initials of the authors associated with the method. The initial part typically signifies the method used to calculate the exchange, while the second part indicates the method for calculating the correlation [10, 11, 12, 13, 14, 15].

II.4.2.1 Local Density Approximation

In the uniform electron gas model, we possess highly accurate approximations for the E_{xc} term. In the LDA Approximation, the electron density is considered to exhibit local uniformity, and the expression for E_{xc} is as follows:

$$E_{xc}^{LDA}[\rho] = \int \rho(\vec{r}) \epsilon_{xc} \rho(\vec{r}) d\vec{r} \quad (\text{II.42})$$

For unrestricted spin systems, its expansion is referred to as Local Spin Density (LSD)

$$E_{xc}^{LSD}[\rho_\alpha, \rho_\beta] = \int \rho(\vec{r}) \epsilon_{xc}[\rho_\alpha(\vec{r}), \rho_\beta(\vec{r})] d\vec{r} \quad (\text{II.43})$$

II.4.2.2 Generalized Gradient Approximation (GGA) and Hybrid Functionals

The GGA approximation takes into account exchange-correlation functionals that depends on local density and its gradient following a general form :

$$E_{xc}^{GGA}[\rho_\alpha, \rho_\beta] = \int f(\rho_\alpha, \rho_\beta, \nabla \rho_\alpha, \nabla \rho_\beta) d\vec{r} \quad (\text{II.44})$$

The exchange portion is commonly represented by the Becke functional (B), while the correlation can be either the Lee-Yang-Parr (LYP) functional or the Perdew-Wang (PW) functional, with variants such as 86 or 91. This results in keywords like BLYP, BPW86, and BPW91. Hybrid methods merge empirical combinations of energies from LDA and the HF approaches with the GGA energy. The "Becke three-parameter" method (B3) is the most commonly employed, B3LYP functional, for instance, incorporating the LYP functional for the GGA component. Additionally, the GGA component can be defined using the PW91 and PW86 functionals.

II.5 Molecular Electrostatic Potential (MEP)

The electrostatic potential on the molecular surface (MEP) represents the electrostatic interaction energy between a positive point charge (proton) placed at a distance r and the electrons and nuclei of the studied molecule. These electrons and nuclei create an electrostatic potential $V(\mathbf{r})$, expressed as follows through the equation [19] :

$$V(\mathbf{r}) = \underbrace{\sum_{A=1}^{N_{atoms}} \frac{Z_A}{|\mathbf{R}_A - \mathbf{r}|}}_{I_1} - \underbrace{\int \frac{\rho(\mathbf{r}') d\mathbf{r}'}{|\mathbf{r}' - \mathbf{r}|}}_{I_2} \quad (\text{II.45})$$

In this equation, \mathbf{R}_A and Z_A represent position vector and nuclear charge of atom A, respectively. The term I_1 denotes the positive electrostatic potential contribution resulting from nuclear charges. The second component, denoted as I_2 , corresponds to a negative contribution referred to as the Hartree potential, representing the classical Coulomb potential at point \mathbf{r} generated by the electron density located at point \mathbf{r}' . The integral symbol represents a continuous electron density and is simplified from a triple integral to a single integral for ease of notation [20]. The atomic unit (a.u.) for the electrostatic potential is defined as Hartree per elementary charge (*Hartree/e*). It can also be expressed in other common units such as *eV/e* and *kcal/(mol.e)*. Nevertheless, for simplicity, these units are often presented as "eV" and "kcal/mol", respectively [21].

The electrostatic potential is a fundamental tool in revealing and predicting chemical reactivity [22]. The sign of $V(r)$ at each point on the MEP surface is determined by one of the two dominant charge distributions (electrons and nuclei). A high electrostatic potential reflects the regions of low electron density, capable of undergoing a nucleophilic attack, and a low electrostatic potential indicates regions of high electron concentration justifying their nucleophilic character. The electrostatic potential is close to zero in the regions where the molecule is non-polar primarily. These regions are poor in chemical reactivity and reflect the transition areas between the positive and negative charge distributions. The global maximum reflects the most electron-deficient site, susceptible to readily undergoing a nucleophilic attack, while the global minimum refers to the most electron-rich site, which preferentially attracts an electrophilic reagent.

To obtain precise quantitative information, Politzer et al.[23] have introduced a series of statistically-based molecular descriptors derived from the ESP on vdW surface. Among these descriptors, the following quantities: positive surface area (A_+), negative surface area (A_-), positive variance (σ_+^2), negative variance (σ_-^2) have been investigated in this work.

A_+ and A_- represent the regions of the surface where the ESP is positive and negative, respectively. The overall surface area, denoted as A , is the sum of A_+ and A_- areas.)

$$A_{tot} = A_+ + A_- \quad (\text{II.46})$$

The variance illustrates the ESP's fluctuation. When σ_+^2 and σ_-^2 are larger, the molecule is more prone to interact through its positive and negative ESP regions, respectively. The total variance σ_{tot}^2 is expressed as the sum of σ_+^2 and σ_-^2 components.

$$\sigma_{tot}^2 = \sigma_+^2 + \sigma_-^2 = (1/m) \sum_{i=1}^m [V(\mathbf{r}_i) - \bar{V}_s^+]^2 + (1/n) \sum_{j=1}^n [V(\mathbf{r}_j) - \bar{V}_s^-]^2 \quad (\text{II.47})$$

\bar{V}_s^+ and \bar{V}_s^- represents respectively, the average of positive and negative ESP on vdW surface which are expressed by the following equations:

$$\bar{V}_s^+ = (1/m) \sum_{i=1}^m V(\mathbf{r}_i) \quad (\text{II.48})$$

$$\bar{V}_s^- = (1/n) \sum_{j=1}^n V(\mathbf{r}_j) \quad (\text{II.49})$$

The total variance is also positively correlates to the positive and negative extrema and is particularly sensitive to maximum magnitudes. The A_+ and A_- parameters have been essential in predicting the density of molecular and ionic crystals [24, 25].

II.6 Energy Decomposition Analysis-Natural Orbitals for Chemical Valence (EDA-NOCV)

The EDA-NOCV is a very popular method used to analyse in depth qualitatively and quantitatively the nature of chemical bonds between interacting molecular fragments [26, 27, 28, 29]. This method combines the energy decomposition analysis proposed by Ziegler and Rauk [30, 31], with the NOCV concept described by Mitoraj and Michalak [32, 33]. In this approach, the interaction energy (ΔE_{int}) is primarily divided into three physically meaningful terms. The dispersion interaction (ΔE_{disp}) arises from an explicit correction associated with D3BJ functional. In this way, a fourth extra contribution is added to the interaction energy equation according to:

$$\Delta E_{int} = \Delta E_{Pauli} + \Delta E_{orb} + \Delta E_{elstat} + \Delta E_{disp} \quad (\text{II.50})$$

The orbital interaction (ΔE_{orb}) accounts for charge, polarisation, and electron-pair bonding [34]. This term reflects the energy involved in the bond formation, which yields

a relevant description of the bonding situation in the equilibrium geometry [35, 36].

ΔE_{Pauli} represents the repulsive interaction between electrons with the same spin due to Pauli principle, which is also called exchange-repulsion term. ΔE_{elstat} is the classical electrostatic interaction between the molecular fragments. Within the theoretical framework of EDA-NOCV, the ΔE_{orb} may be separated into contributions associated with the NOCV pairs according to:

$$\Delta E_{orb} = \sum_{i=1}^N \Delta E_{orb}^{(i)} = \sum_{i=1}^{N/2} \nu_i [F_{i,i}^{TS} - F_{-i,-i}^{TS}] \quad (\text{II.51})$$

Where i is an index of NOCV, $F_{i,i}^{TS}$ and $F_{-i,-i}^{TS}$ are the i^{th} diagonal terms of transition-state Kohn-Sham matrix elements corresponding to NOCV with the eigenvalues ν_i and ν_{-i} , respectively. The key feature of this analysis is its ability to deconvolute variation of electron density due to orbital interaction to a set of NOCV pairs $\{\phi_i(\mathbf{r}), \phi_{-i}(\mathbf{r})\}$ of complementary orbitals with the same eigenvalue and opposite sign as shown by:

$$\Delta\rho(\mathbf{r}) = \sum_{i=1}^{N/2} \Delta\rho_{(i)}^{orb}(\mathbf{r}) = \sum_{i=1}^{N/2} [\nu_i \phi_i^2(\mathbf{r}) + \nu_{-i} \phi_{-i}^2(\mathbf{r})] \quad (\text{II.52})$$

Each two NOCV orbitals with opposite eigenvalues constitute a NOCV pair. The Equation (II.52) allows us to quantify the amount of electron density transferred between fragments. There are frequently many NOCV orbitals, among which only a few pairs have significant effect on the deformation density, $\Delta\rho(\mathbf{r})$. NOCV pairs with a larger eigenvalue magnitude show a more significant effect on the deformation density caused by the orbital interaction. For this reason, usually only the first two NOCV pairs are considered.

II.7 Quantum Theory of Atoms In Molecules (QTAIM)

Bader's topology analysis was initially employed to examine electron density within the framework of "Atoms in Molecules" (AIM) theory, also recognized as "the quantum theory of atoms in molecules" (QTAIM) [37, 38]. In the context of topology analysis, the term "critical points" (CPs) refers to regions where the gradient norm of a function is equal to zero ($\nabla\rho(\mathbf{r}_c) = 0$). CPs can be categorized into four distinct types based on the number of negative eigenvalues in the Hessian matrix of the real space function. In this theory, the number of these coexisting CPs within a molecule validates the Poincaré-Hopf equation [39]. The CPs are labeled as (ω, σ) , where ω represents the

critical point's rank, and σ stands for its signature. ω is determined by the count of non-zero eigenvalues within the Hessian matrix of $\rho(r_c)$. σ is calculated as the algebraic sum of the signs of the eigenvalues within this matrix. Thus, the four types of CPs are: (3, -3) nuclear critical points (NCP), (3, +1) ring critical points (RCP), (3, +3) cage critical points (CCP) and (3, -1) bond critical points (BCP) [40]. The latter type plays a primordial role in this analysis. There are three curvatures of $\rho(\mathbf{r}_c)$ established based on three Hessian eigenvalues, which are represented as λ_1 , λ_2 and λ_3 . Furthermore, these curvatures are associated with three mutually orthogonal eigenvectors that are aligned with the principal curvatures [41]. The distribution of the electron density observed at the BCP results from a direct interplay between two opposing factors. One is the perpendicular compression, which leads to a local accumulation of $\rho(\mathbf{r}_B)$ towards the bonding path, represented by the two negative curvatures (λ_1 and λ_2). The other factor is the expansion, causing a local depletion of $\rho(\mathbf{r}_B)$ along the bonding path, as indicated by the positive curvature λ_3 [42].

In the framework of QTAIM, the electron density at the BCPs is commonly employed to measure the strength of chemical bonds [43, 44]. The sign of the Laplacian of the electron density, $\nabla^2\rho(\mathbf{r}_B) = \lambda_1 + \lambda_2 + \lambda_3$, characterizes the accumulation ($\nabla^2\rho(\mathbf{r}_B) < 0$) and depletion ($\nabla^2\rho(\mathbf{r}_B) > 0$) of electron density in interatomic regions. Further, the $\nabla^2\rho(\mathbf{r}_B)$ is related to energetic topological properties through the Virial theorem [45]: $(1/4)\nabla^2\rho(\mathbf{r}_B) = 2G(\mathbf{r}_B) + V(\mathbf{r}_B)$, where $G(\mathbf{r}_B)$ and $V(\mathbf{r}_B)$ stand for the kinetic energy density and the potential energy density, respectively. The total energy density $H(\mathbf{r}_B) = G(\mathbf{r}_B) + V(\mathbf{r}_B)$ is another helpful parameter allowing to explore the nature of chemical bonding. A negative value of $H(\mathbf{r}_B)$, indicate a stabilising electron concentration. In this study, the classification of the different chemical bonding is established according to the criterion defined by Cremer *et al.*[46, 47, 48]: (a) $\nabla^2\rho(\mathbf{r}_B) < 0$ and $H(\mathbf{r}_B) < 0$ for shared-shell interactions including nonpolar and weakly polar covalent bonds. (b) $\nabla^2\rho(\mathbf{r}_B) > 0$ and $H(\mathbf{r}_B) < 0$ for the mixed type interactions such as polar covalent bonds, strong hydrogen and coordination bonds [47]. (c) $\nabla^2\rho(\mathbf{r}_B) > 0$ and $H(\mathbf{r}_B) > 0$ for the closed-shell interactions including ionic bonds, weak hydrogen and van der Waals bonds.

Additionally, a ratio of $|V(\mathbf{r}_B)|/G(\mathbf{r}_B) > 2$, means a shared-shell interaction, in such a situation the potential electron energy $V(\mathbf{r}_B)$ becomes locally predominant. In contrast, for $|V(\mathbf{r}_B)|/G(\mathbf{r}_B) < 1$, the kinetic electron energy $G(\mathbf{r}_B)$ is locally predominant, implying a closed-shell interaction. In cases where $|V(\mathbf{r}_B)|/G(\mathbf{r}_B)$ falls between these two thresholds, the interaction is considered as mixed or intermediate [47]. The balance between $V(\mathbf{r}_B)$ and $G(\mathbf{r}_B)$ values determines the kind of interaction. This criterion is particularly helpful in revealing the bonding nature in the investigated chemical

systems.

II.8 Interaction Region Indicator (IRI)

This descriptor is a new scalar field based on electron density and its derivatives, which was developed to detect covalent and non-covalent interactions in a single map [49]. Non-covalent interactions can be of electronic (interference) or electrostatic (due to permanent or fluctuating charges) origin [50]. The QTAIM approach does not distinguish the attractive and repulsive nature of non-covalent interactions because the sign of $\nabla^2\rho(\mathbf{r})$ does not provide this information. Through the IRI descriptor, this information is achieved by the decomposition of $\nabla^2\rho(\mathbf{r})$ into the sum of Hessian eigenvalues: $\nabla^2\rho(\mathbf{r}) = \lambda_1 + \lambda_2 + \lambda_3$. In this context, the λ_2 eigenvalue is essential in distinguishing the attractive and repulsive effects of non-covalent interactions. Therefore, the combination of QTAIM and IRI methods provides a complete picture of the interactions involved in the studied chemical systems. More details of the theoretical aspect of IRI can be found at [49].

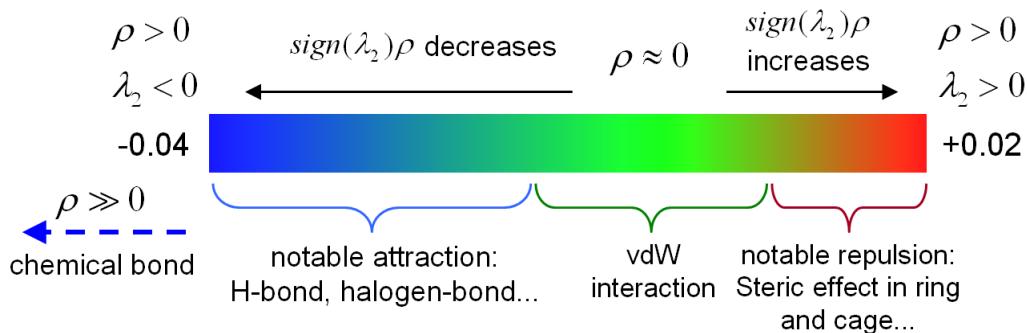


Figure II.1: IRI colorbar

The isosurface maps of IRI are coloured based on the corresponding values of $\Omega(\mathbf{r}) = \text{sign}(\lambda_2)\rho(\mathbf{r})$ (Figure II.1), providing a varied graphical visualization of electronic effects including steric repulsion, hydrogen bonds, and van der Waals interactions. The λ_2 eigenvalue results from the diagonalisation of the Hessian matrix of $\rho(\mathbf{r})$. Therefore, the sign of λ_2 helps to distinguish bonded ($\lambda_2 < 0$) from non-bonded ($\lambda_2 > 0$) interactions. In this way, the sign of this eigenvalue allows classifying non-covalent interactions. The attractive and repulsive (mainly steric effects) interactions are based on negative and positive values of $\Omega(\mathbf{r})$, respectively. The van der Waals interactions occur when the $\Omega(\mathbf{r})$ values approach zero. The regions between the blue and green colours denote progressively weaker attractive interactions. The regions between the green and red colours denote progressively weaker repulsive effects.

Bibliography

- [1] Ghania Boucekkine. *Méthodes de la chimie quantique*. Ed. Techniques Ingénieur, 2007.
- [2] R KI, G Deepa, and DK Namboori. Computational chemistry and molecular modeling: principles and applications, 2008.
- [3] Hervé TOULHOAT. Modélisation moléculaire-bases théoriques (partie 2). 2007.
- [4] Bin Guan, Han Jiang, Yanfei Wei, Ziqian Liu, Xingze Wu, He Lin, and Zhen Huang. Density functional theory researches for atomic structure, properties prediction, and rational design of selective catalytic reduction catalysts: Current progresses and future perspectives. *Molecular Catalysis*, 510:111704, 2021.
- [5] Jorge M Seminario. An introduction to density functional theory in chemistry. In *Theoretical and computational chemistry*, volume 2, pages 1–27. Elsevier, 1995.
- [6] C David Sherrill. An introduction to hartree-fock molecular orbital theory. *School of Chemistry and Biochemistry Georgia Institute of Technology*, 2000.
- [7] M Ya Amusia, AZ Msezane, and VR Shaginyan. Density functional theory versus the hartree-fock method: Comparative assessment. *Physica Scripta*, 68(6):C133, 2003.
- [8] Errol Lewars. Computational chemistry: introduction to the theory and applications of molecular and quantum mechanics., 2016.
- [9] Jacob Townsend, Justin K Kirkland, and Konstantinos D Vogiatzis. Post-hartree-fock methods: configuration interaction, many-body perturbation theory, coupled-cluster theory. In *Mathematical Physics in Theoretical Chemistry*, pages 63–117. Elsevier, 2019.
- [10] Wolfram Koch and Max C Holthausen. *A chemist's guide to density functional theory*. John Wiley & Sons, 2015.
- [11] Patrick Chaquin. Pratique de la chimie théorique.

- [12] John P Perdew, Adrienn Ruzsinszky, Lucian A Constantin, Jianwei Sun, and Gábor I Csonka. Some fundamental issues in ground-state density functional theory: A guide for the perplexed. *Journal of chemical theory and computation*, 5(4):902–908, 2009.
- [13] Walter Kohn and Lu Jeu Sham. Self-consistent equations including exchange and correlation effects. *Physical review*, 140(4A):A1133, 1965.
- [14] Pierre Hohenberg and Walter Kohn. Inhomogeneous electron gas. *Physical review*, 136(3B):B864, 1964.
- [15] Norman Henry March. Electron density theory of atoms and molecules. *The Journal of Physical Chemistry*, 86(12):2262–2267, 1982.
- [16] Walter Kohn, Axel D Becke, and Robert G Parr. Density functional theory of electronic structure. *The journal of physical chemistry*, 100(31):12974–12980, 1996.
- [17] Eugene S Kryachko and Eduardo V Ludeña. *Energy density functional theory of many-electron systems*, volume 4. Springer Science & Business Media, 2012.
- [18] Helmut Eschrig. *The fundamentals of density functional theory*, volume 32. Springer, 1996.
- [19] Peter Politzer and Jane S Murray. Detonation performance and sensitivity: a quest for balance. In *Advances in quantum chemistry*, volume 69, pages 1–30. Elsevier, 2014.
- [20] Samir Kenouche, Claudia Sandoval-Yañez, and Jorge I Martínez-Araya. The antioxidant capacity of myricetin. a molecular electrostatic potential analysis based on dft calculations. *Chemical Physics Letters*, 801:139708, 2022.
- [21] Tian Lu and Qinxue Chen. Realization of conceptual density functional theory and information-theoretic approach in multiwfn program. *Conceptual Density Functional Theory: Towards a New Chemical Reactivity Theory*, 2:631–647, 2022.
- [22] Jane S Murray and Peter Politzer. The electrostatic potential: an overview. *Wiley Interdisciplinary Reviews: Computational Molecular Science*, 1(2):153–163, 2011.
- [23] Jane S Murray, Tore Brinck, Pat Lane, Kirn Paulsen, and Peter Politzer. Statistically-based interaction indices derived from molecular surface electrostatic potentials: a general interaction properties function (gipf). *Journal of Molecular Structure: THEOCHEM*, 307:55–64, 1994.

- [24] Peter Politzer, Jorge Martinez, Jane S Murray, Monica C Concha, and Alejandro Toro-Labbe. An electrostatic interaction correction for improved crystal density prediction. *Molecular Physics*, 107(19):2095–2101, 2009.
- [25] Peter Politzer, Jorge Martinez, Jane S Murray, and Monica C Concha. An electrostatic correction for improved crystal density predictions of energetic ionic compounds. *Molecular Physics*, 108(10):1391–1396, 2010.
- [26] Sai Manoj NVT Gorantla and Kartik Chandra Mondal. Uncovering the hidden reactivity of benzyne/aryne precursors utilized under milder condition: Bonding and stability studies by eda-nocv analyses. *Journal of Computational Chemistry*, 43(23):1543–1560, 2022.
- [27] Kavita Devi, Sai Manoj NVT Gorantla, and Kartik Chandra Mondal. Eda-nocv analysis of carbene-borylene bonded dinitrogen complexes for deeper bonding insight: A fair comparison with a metal-dinitrogen system. *Journal of Computational Chemistry*, 43(11):757–777, 2022.
- [28] Samir Kenouche, Nassima Bachir, and Jorge I Martínez-Araya. Explaining the high catalytic activity in bis (indenyl) methyl zirconium cation using combined eda-nocv/qtam approach. *ChemPhysChem*, 24(2):e202200488, 2023.
- [29] Sai Manoj NVT Gorantla and Kartik Chandra Mondal. Eda-nocv calculation for efficient n₂ binding to the reduced ni₃s₈ complex: Estimation of ni-n₂ intrinsic interaction energies. *ACS omega*, 6(49):33389–33397, 2021.
- [30] Tom Ziegler and Arvi Rauk. Carbon monoxide, carbon monosulfide, molecular nitrogen, phosphorus trifluoride, and methyl isocyanide as. sigma. donors and. pi. acceptors. a theoretical study by the hartree-fock-slater transition-state method. *Inorganic Chemistry*, 18(7):1755–1759, 1979.
- [31] Tom Ziegler and Arvi Rauk. A theoretical study of the ethylene-metal bond in complexes between copper (1+), silver (1+), gold (1+), platinum (0) or platinum (2+) and ethylene, based on the hartree-fock-slater transition-state method. *Inorganic Chemistry*, 18(6):1558–1565, 1979.
- [32] Mariusz Mitoraj and Artur Michalak. Donor-acceptor properties of ligands from the natural orbitals for chemical valence. *Organometallics*, 26(26):6576–6580, 2007.
- [33] Mariusz Mitoraj and Artur Michalak. Applications of natural orbitals for chemical valence in a description of bonding in conjugated molecules. *Journal of molecular modeling*, 14:681–687, 2008.

- [34] Gernot Frenking and Sason Shaik. *The chemical bond: fundamental aspects of chemical bonding*, volume 1. John Wiley & Sons, 2014.
- [35] Lili Zhao, Markus Hermann, WH Eugen Schwarz, and Gernot Frenking. The lewis electron-pair bonding model: modern energy decomposition analysis. *Nature Reviews Chemistry*, 3(1):48–63, 2019.
- [36] Moritz von Hopffgarten and Gernot Frenking. Energy decomposition analysis. *Wiley Interdisciplinary Reviews: Computational Molecular Science*, 2(1):43–62, 2012.
- [37] Richard FW Bader and Hanno Essén. The characterization of atomic interactions. *The Journal of chemical physics*, 80(5):1943–1960, 1984.
- [38] Richard FW Bader and Preston J MacDougall. Toward a theory of chemical reactivity based on the charge density. *Journal of the American Chemical Society*, 107(24):6788–6795, 1985.
- [39] Heinz Hopf. Vektorfelder in n-dimensionalen mannigfaltigkeiten. *Mathematische Annalen*, 96:225–249, 1927.
- [40] P Shyam Vinod Kumar, V Raghavendra, and V Subramanian. Bader’s theory of atoms in molecules (aim) and its applications to chemical bonding. *Journal of Chemical Sciences*, 128:1527–1536, 2016.
- [41] Vladimir G Tsirelson. Topological analysis of the experimental electron density. *Canadian journal of chemistry*, 74(6):1171–1179, 1996.
- [42] Samir Kenouche and Jorge I Martínez-Araya. A combined qtai/iri topological analysis of the effect of axial/equatorial positions of nh₂ and cn substituents in the [(py₅me₂) moo]⁺ complex. *Journal of Molecular Graphics and Modelling*, 116:108273, 2022.
- [43] RFW Bader et al. A quantum theory. *Clarendon: Oxford, UK*, 1990.
- [44] PL Popelier. A.; aicken, fm; o’brien, se atoms in molecules, 2000.
- [45] Richard FW Bader and PM Beddall. Virial field relationship for molecular charge distributions and the spatial partitioning of molecular properties. *The Journal of Chemical Physics*, 56(7):3320–3329, 1972.
- [46] Dieter Cremer and Elfi Kraka. A description of the chemical bond in terms of local properties of electron density and energy. *Croatica Chemica Acta*, 57(6):1259–1281, 1984.

- [47] Enrique Espinosa, Ibon Alkorta, José Elguero, and Elies Molins. From weak to strong interactions: A comprehensive analysis of the topological and energetic properties of the electron density distribution involving x–h f–y systems. *The Journal of chemical physics*, 117(12):5529–5542, 2002.
- [48] Elfi Kraka and Dieter Cremer. Description of chemical reactions in terms of the properties of the electron density. *Journal of Molecular Structure: THEOCHEM*, 255:189–206, 1992.
- [49] Tian Lu and Qinxue Chen. Interaction region indicator: A simple real space function clearly revealing both chemical bonds and weak interactions. *Chemistry-Methods*, 1(5):231–239, 2021.
- [50] Julia Contreras-García, Mónica Calatayud, Jean-Philip Piquemal, and JM Reico. Ionic interactions: Comparative topological approach. *Computational and Theoretical Chemistry*, 998:193–201, 2012.

Chapter III

Theoretical Investigation of the Effect of $O \cdots M = \{Ti, Zr, Hf\}$ Interactions on the Sensitivity of RDX and HMX

exploration of the potential energy hyper-surface [5]. The energy decomposition analysis based on the EDA-NOCV scheme was used for a detailed theoretical description of the $O \cdots M = \{Ti, Zr, Hf\}$ bonding. Based on the QTAIM formalism, some topological parameters have been calculated and analyzed to quantify the chemical nature of bonding. The N-NO₂ trigger bond properties were quantified before and after interactions between the metal atom of MMCs and the oxygen atom of RDX and HMX. The IRI-based analysis was carried out to further investigate the electronic properties of group 4 transition metals in coordination environments.

III.2 Computational details

All molecular geometries (isolated molecules and complexes) have been optimised using Gaussian16 Revision B.01 [32]. We considered the CAM-B3LYP [33] exchange-correlation functionals along with the effective core potentials MDF10/MWB28/MWB60 with a basis set for Ti, Zr, and Hf, respectively [34]. The 6-31+G(d,p) basis set was used for O, N, C, and H atoms. The EDA-NOCV analysis has been performed by single-point calculation based on the optimized geometries obtained by Gaussian 16 using the Amsterdam Density Functional (ADF 2013.01) [35]. The revised Perdew-Burke-Ernzerhof exchange-correlation functional (revPBE) [36, 37] was used in combination with the D3BJ [38] dispersion correction (revPBE-D3BJ). By investigating 83 dispersion corrected density functionals [39], the revPBE-D3BJ functional has been recommended in the case of intra- and intermolecular non-covalent interactions. According to the same authors [39], the dispersion correction D3(BJ) should be the preferred in most cases due to its physically more correct behavior for short- and medium-range distances in non-covalently bound complexes. Triple-zeta with two polarization functions (TZ2P) basis set of Slater-type orbitals [40] has been applied to represent all the elements along with a Becke integration grid of "very good" precision [41]. Relativistic effects were incorporated using the ZORA approximation [42, 43] as implemented in ADF 2013.01 software. The calculation of topological properties from QTAIM/IRI methods were performed using the multifunctional wavefunction analyser code, Multiwfn 3.8 [44]. Quantitative MEP analysis was performed using the same code in combination with the Cubegen utility of Gaussian software. The isosurfaces of deformation densities were plotted based on the cube files generated by ADF software. All the isosurface maps were rendered by Visual Molecular Dynamics (VMD) program [45].

III.3 Results and discussion

III.3.1 MEP analysis

MEP-mapped van der Waals surfaces with $0.001 e/\text{bohr}^3$ isosurface of electron density and their surface extrema for the studied energetic compounds are shown in Figure III.2. The positive and negative electrostatic potential values are displayed in blue and red colours, respectively. Orange and cyan spheres correspond to the positions of maxima and minima, respectively. Some of the statistically-based molecular descriptors defined by Politzer *et al.* [46] were investigated to quantitatively analyse the positive and negative charges distribution on the whole molecular surface.

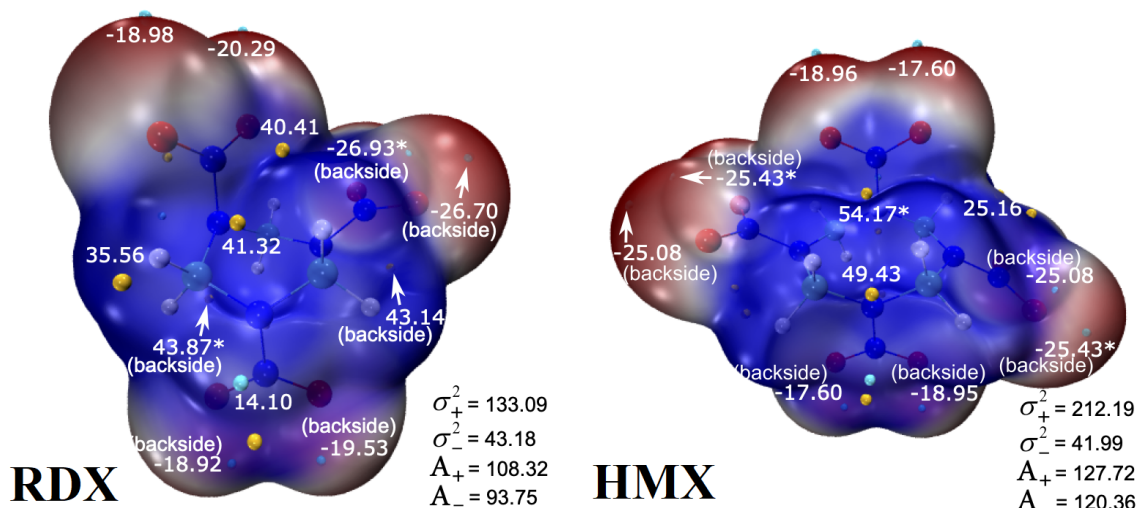


Figure III.2: MEP-mapped van der Waals surfaces ($kcal/mol$) using a colour scale ranging from red (negative MEP), through white (neutral MEP) to blue (positive MEP). The blue regions are prone to nucleophilic attack, and the red regions are sites for electrophilic attack. The grid spacings were set to 0.2 bohr and the van der Waals surface denotes the isosurface of $\rho = 0.001 e/\text{bohr}^3 \equiv a.u.$ Values with a star indicate global surface extrema. The bold numbers in the bottom right-hand corner are the positive MEP variance (σ_+^2), negative MEP variance (σ_-^2), positive surface area (A_+) and negative surface area (A_-) whose units are $(kcal/mol)^2$, \AA^2 , respectively.

From Figure III.2, we observe a marked positive central region and negative peripheral regions around the nitro groups. The electron deficiency in the central region is typical of energetic molecules since the nitro groups simultaneously exert a strong electron-withdrawing effect. The electron-rich sites are around the nitro groups for the two compounds and primarily arise from the lone pairs of oxygen atoms. As expected, the molecular symmetry of the two molecules leads to surface extrema with the same value. For RDX and HMX, the global maximums are observed in the central region of both molecules, and the most negative values are achieved around the nitro groups. In

addition, there is a strong link between electron density depletion in the central regions of energetic molecules and sensitivity to detonation [47, 48, 49], but this correlation does not necessarily imply a causal relationship [19]. A possible explanation of this depletion is related to the attractive mesomeric effect of NO₂ groups, which weaken the trigger bonds [50, 51]. Furthermore, the regions around the N-NO₂ trigger bonds are also deficient in electron density. This finding reflects a weakening of these bonds and constitutes a fundamental feature of such molecules [52].

The total variance with a value of 254.12 (*kcal/mol*)² shows a large charge fluctuation for HMX. The weakest fluctuations with a value of 176.28 (*kcal/mol*)² are obtained for RDX. Besides, the negative and positive variances reflect the trends for electrophilic and nucleophilic electrostatic interactions, respectively. The σ_-^2 and σ_+^2 values obtained for these molecules covers a range from 41.99 to 43.18 (*kcal/mol*)² and from 133.09 to 212.19 (*kcal/mol*)², respectively. We found $\sigma_+^2 > \sigma_-^2$ revealing a more prominent trend for nucleophilic non-covalent interactions in each case. This propensity is more marked for HMX, with a contribution of 80.21 % compared to the total variance. We found $A_+ > A_-$, and therefore, positive surface areas cover larger zones for the studied compounds. The largest value is observed for RDX, with a contribution of 13.45% compared to the total surface area. These results confirm what is known in the literature [51], since a larger positive surface potential characterized by a high variability is a common feature of ECs. This behavior is unusual since, for most organic molecules, the most positive electrostatic potential arises mainly from the hydrogen atoms, and the positive regions are generally less marked and less variable than the negative ($\sigma_+^2 < \sigma_-^2$).

Moreover, MMCs is highly reactive due to its transition metal atom, which can form shared electron bonds with non-metal atoms. A shared interaction between the transition metal and the oxygen atom belonging to nitro is only possible at short range. Indeed, the ability of MMCs to neutralise these ECs (models of interactions between MMCs and RDX/HMX are depicted in Figure III.3) must be demonstrated through detailed topological analyses to verify a possible charge transfer between the interacting molecules. This aspect is addressed in the following sections.

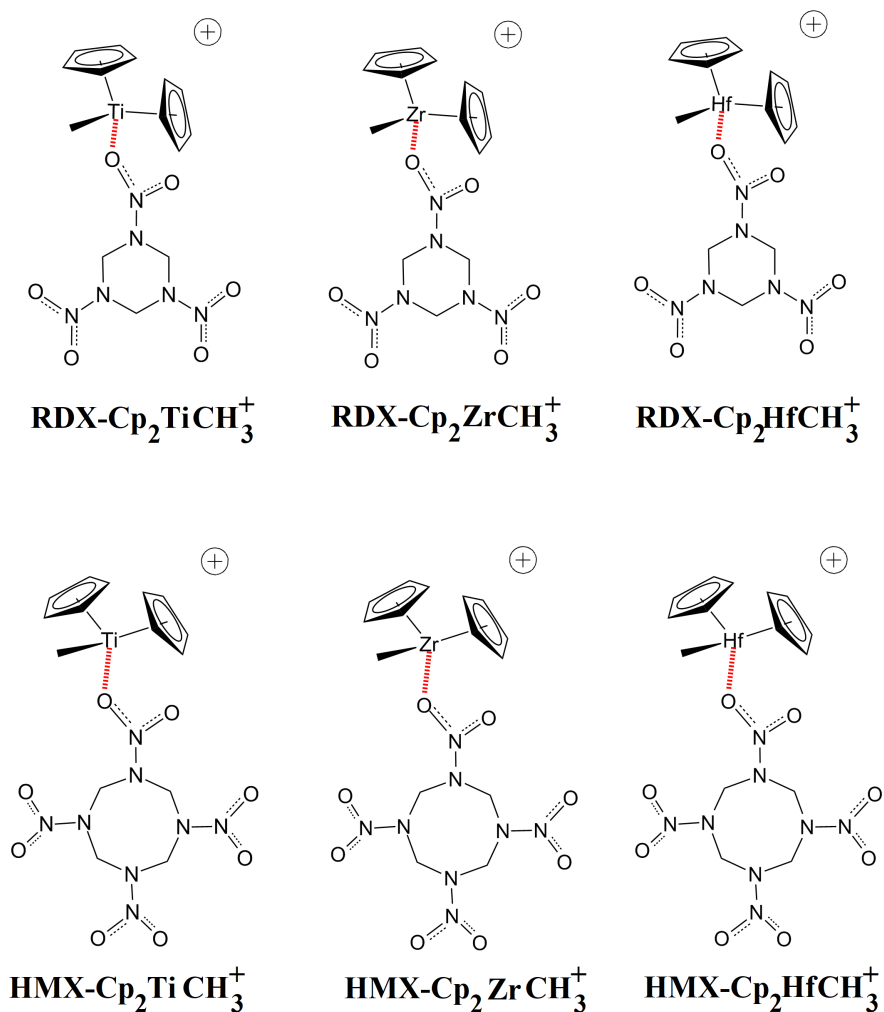


Figure III.3: Models of interactions between methyl metallocene cations (MMCs) and RDX/HMX

III.3.2 EDA-NOCV

The EDA-NOCV approach combines Energy Decomposition Analysis [53, 54] with Natural Orbitals for Chemical Valence [55, 56]. This approach allow to theoretically investigate the chemical trend in oxygen's ability to bind to group 4 transition metals. The obtained N-nitro distances (in Å), as well as the chemical structures of all the compounds are depicted in Figure (III.4).

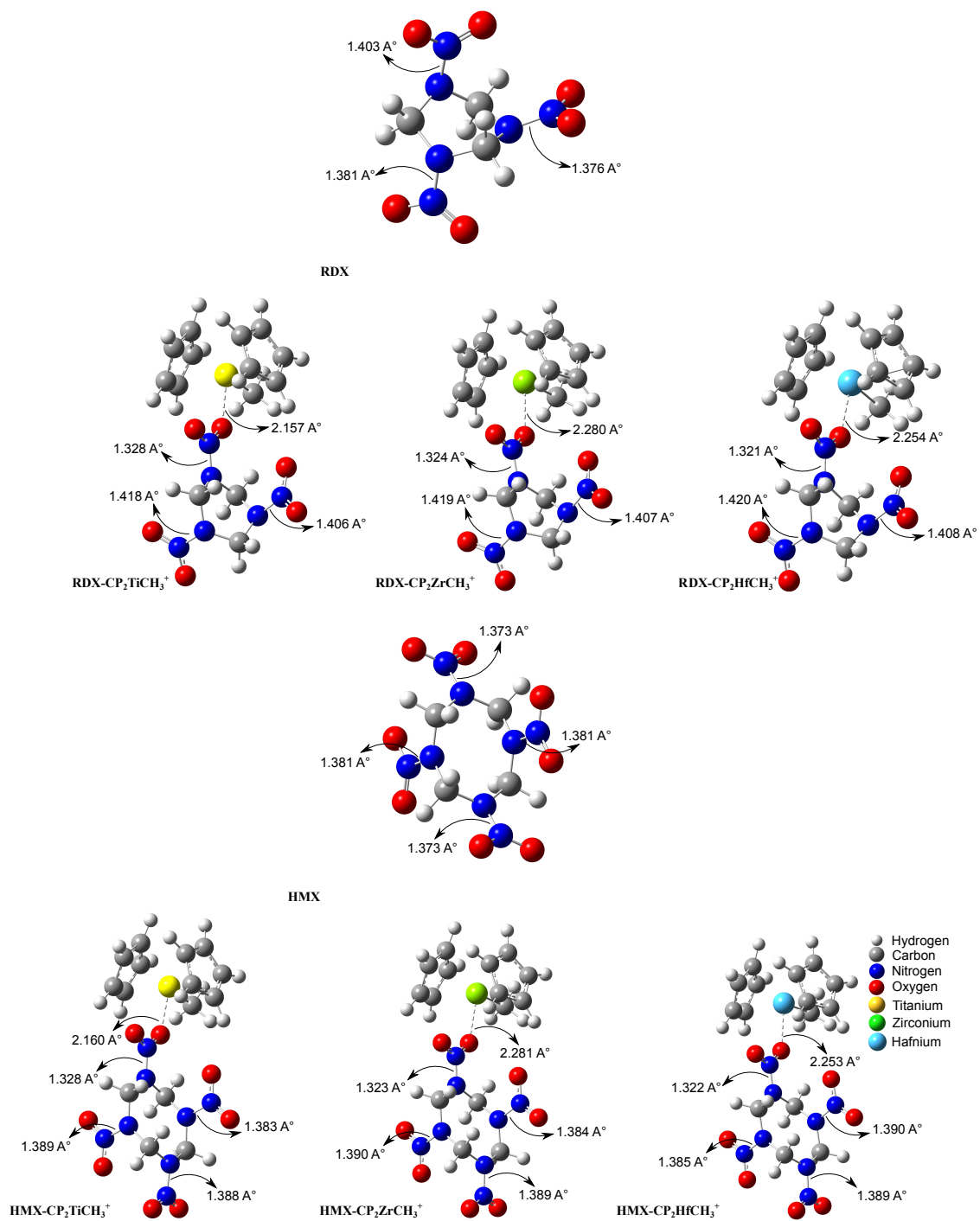


Figure III.4: Bond distances (Å) for trigger bonds in RDX-Cp₂M(CH₃)⁺ and HMX-Cp₂M(CH₃)⁺.

Distances between interacting O and M= {*Ti, Zr, Hf*} atoms vary from 2.16 to 2.28 Å. The bond length of N-NO₂ interacting with the metal centers decreased by about 6.0%. This result suggests a strengthening of these bonds due to a negative charge redistribution after interaction with MMCs. However, the length of some adjacent N-NO₂ bonds also increased after the formation of the complexes, especially for RDX. These lengths increased by about 2.1 % for RDX and 0.7 % for HMX, causing a slight increase in sensitivity. The activation of isolated N-NO₂ trigger bonds can be attributed to several factors. As shown by Shoaf et al. [57], the steric effects, the electron withdrawing effect exerted by NO₂ groups, as well as the repulsion between adjacent functional groups inducing twists (enlargement of dihedral angles) activate the trigger bonds. In our case, the hypothesis of activation of adjacent N-NO₂ bonds caused by an increase in the dihedral angle seems to be conclusive.

The results of EDA-NOCV calculation are listed in Table (III.1). The percentages in parentheses indicate the contribution to the stabilizing interactions (attractive terms), and the numbers in bold highlight the largest values for each complex. The destabilization energy arising from Pauli repulsion interaction (ΔE_{Pauli}) is largely offset by the electrostatic (ΔE_{elstat}) and orbital (ΔE_{orb}) contributions, providing a large negative interaction energy (ΔE_{int}). In RDX...Cp₂M(CH₃)⁺ complexes, the interaction energy of RDX-Cp₂Hf(CH₃)⁺ is more stabilizing ($-44.12 kcal/mol$), followed by RDX-Cp₂Zr(CH₃)⁺ ($-40.82 kcal/mol$) and RDX-Cp₂Ti(CH₃)⁺ ($-34.91 kcal/mol$). The same pattern with slightly lower values is obtained with HMX...-Cp₂M(CH₃)⁺ complexes. The low values of ΔE_{int} observed in the Ti-based complexes is due to a strong contribution from destabilising repulsive interactions, with percentages of 35.95% and 36.21% in RDX-Cp₂Ti(CH₃)⁺ and HMX-Cp₂Ti(CH₃)⁺, respectively. The electrostatic contribution is dominant and seems to be the driving force behind the stabilization of the studied complexes. The strongest electrostatic contributions are obtained with the Hf-based complexes. By considering only the attractive terms, the percentages obtained are 51.1% and 49.9% for RDX-Cp₂Hf(CH₃)⁺ and HMX-Cp₂Hf(CH₃)⁺, respectively.

The strong contribution of the electrostatic component to the bonding energy can be attributed to the difference in electronegativity between the interacting atoms. Indeed, the oxygen atom being the second-most electronegative element of the periodic table, enhances the ionic character of its bonding with electron density deficient elements, making the electrostatic contribution strongly dominant. Conversely, as the metal's electronegativity increases, its bond with the oxygen atom becomes less polar and therefore the influence of electrostatic effects also decreases. Therefore, the transition metal with the lowest electronegativity (the group 4 transition metals become

more electropositive down the column) develops the strongest interaction with oxygen, this result is in agreement with those obtained by Moltved et al. [58]. The dispersive component also contributes to the bonding, but its magnitude is much smaller. This component show nearly similar magnitudes for all complexes with a tight range from -9.21 to -10.15 *kcal/mol* in $\text{RDX}\cdots\text{Cp}_2\text{M}(\text{CH}_3)^+$ and from -9.48 to -11.21 *kcal/mol* in $\text{HMX}\cdots\text{Cp}_2\text{M}(\text{CH}_3)^+$.

Table III.1: Results of the EDA-NOCV calculations of the studied complexes at the DFT/revPBE-D3(BJ)/TZ2P level of theory. All the values are in *kcal/mol*.

Comp	ΔE_{Pauli}	ΔE_{orb}	ΔE_{elstat}	ΔE_{disp}	ΔE_{int}^*
$\text{RDX-Cp}_2\text{Ti}(\text{CH}_3)^+$	46.39	-30.10 (37.02%)	-41.05 (50.49%)	-10.15 (12.48%)	-34.91
$\text{RDX-Cp}_2\text{Zr}(\text{CH}_3)^+$	40.38	-30.96 (38.12%)	-40.93 (50.40%)	-9.31 (11.46%)	-40.82
$\text{RDX-Cp}_2\text{Hf}(\text{CH}_3)^+$	46.22	-34.96 (38.69%)	-46.17 (51.10%)	-9.21 (10.19%)	-44.12
$\text{HMX-Cp}_2\text{Ti}(\text{CH}_3)^+$	46.50	-30.79 (37.59%)	-39.89 (48.71%)	-11.21 (13.68%)	-35.39
$\text{HMX-Cp}_2\text{Zr}(\text{CH}_3)^+$	40.59	-31.42 (38.93%)	-39.72 (49.21%)	-9.56 (11.84%)	-40.11
$\text{HMX-Cp}_2\text{Hf}(\text{CH}_3)^+$	46.42	-35.47 (39.46%)	-44.92 (49.98%)	-9.48 (10.54%)	-43.45

- *The interaction energy is calculated according to: $\Delta E_{\text{int}} = \Delta E_{\text{orb}} + \Delta E_{\text{Pauli}} + \Delta E_{\text{elstat}} + \Delta E_{\text{disp}}$.
- The percentages in parentheses indicate the contribution to the stabilizing interactions (attractive terms).
- The numbers in bold highlight the largest values for each energetic term.

Moreover, the ΔE_{int} value appears to be positively correlated with the atomic radius of the transition metal. Let us recall that the electronegativity is negatively correlated to the atomic radius. Thus, as the difference in electronegativity between the two interacting atoms increases and more ΔE_{int} increases, since the electrostatic component is dominant. Another salient point is related to the difference in ΔE_{int} values between Ti and Zr-based complexes, which is systematically higher than between Zr and Hf-based complexes. Electron configurations of the three transition metals are: Ti ($[\text{Ar}] 3d^2 4s^2$), Zr ($[\text{Kr}] 4d^2 5s^2$) and Hf ($[\text{Xe}] 4f^{14} 5d^2 6s^2$). It is well known that the atomic radius increases down a group in the periodic table, although nuclear charge increases down a group, shielding effect more than counters its effect. However, the increase in atomic radius between the 3d and 4d metals exceeds that between the 4d and 5d metals due to the lanthanide contraction [59]. This phenomenon occurs because the metals characterized by the filling of the *f*-orbitals screen the atomic nucleus less efficiently than the other orbitals. In decreasing order of screening efficiency, the atomic orbitals rank according to $s > p > d > f$. Therefore, because of this imperfect shielding, the nuclear charge acts more on the peripheral electrons as the atomic number increases [60]. This contraction effect may explain the observed differences in ΔE_{int} values between the three transition metals, which are slightly more important between (RDX,HMX)- $\text{Cp}_2\text{Ti}(\text{CH}_3)^+$ and (RDX,HMX)- $\text{Cp}_2\text{Zr}(\text{CH}_3)^+$ than between (RDX,HMX)- $\text{Cp}_2\text{Zr}(\text{CH}_3)^+$ and (RDX,HMX)- $\text{Cp}_2\text{Hf}(\text{CH}_3)^+$.

Besides, the orbital interaction although less prominent than the electrostatic term contributes strongly to the stabilization energy. This may suggest that the $O \cdots M = \{Ti, Zr, Hf\}$ bonding exhibits a partially covalent character. The largest orbital contributions to the total attractive interactions are reached for RDX-Cp₂Hf(CH₃)⁺ and HMX-Cp₂Hf(CH₃)⁺ with percentages of 38.6% and 39.4%, respectively. In addition, the orbital interaction comprises both σ -donation (σ -donor character, EM \rightarrow MMCs) and π -backdonation (π -acceptor character, EM \leftarrow MMCs). Therefore, to compare their respective charge transfers, it would be appropriate to separate the two contributions. The numerical values of the orbital interaction energies (in *kcal/mol*) of σ -donation $\Delta E_{orb}^{(1)}$ and π -backdonation $\Delta E_{orb}^{(2)}$ with the respective charge transfer are summarized in Table III.2. The deformation densities $\Delta\rho(r)^{(1)}$ and $\Delta\rho(r)^{(2)}$ corresponding to the σ -donation and π -backdonation of the first two NOCV pairs are shown in Figure III.5 and Figure III.6. The $\Delta E_{orb}^{(2)}$ combined with its deformation density map $\Delta\rho(r)^{(2)}$ yield information about secondary interactions that may arise between the two molecular fragments. Indeed, the π -backdonation is specifically present in organometallic transition metal complexes where the metal binds to the ligand by releasing its excess of negative charges [61, 62].

Table III.2: Orbital interaction energies of σ -donation ($\Delta E_{orb}^{(1)}$) and π -backdonation ($\Delta E_{orb}^{(2)}$) with the respective charge transfer.

Comp	$\Delta E_{orb}^{(1)}$	$ \nu_1 $	$\Delta E_{orb}^{(2)}$	$ \nu_2 $
RDX-Cp ₂ Ti(CH ₃) ⁺	-14.767	0.355	-5.252	0.259
RDX-Cp ₂ Zr(CH ₃) ⁺	-14.249	0.330	-6.119	0.260
RDX-Cp ₂ Hf(CH ₃) ⁺	-16.516	0.341	-6.688	0.284
HMX-Cp ₂ Ti(CH ₃) ⁺	-14.697	0.355	-5.263	0.257
HMX-Cp ₂ Zr(CH ₃) ⁺	-14.233	0.330	-6.130	0.258
HMX-Cp ₂ Hf(CH ₃) ⁺	-16.500	0.341	-6.728	0.283

By looking at the largest pairwise contributions to orbital interaction, the σ -donation appears to be stronger than the π -backdonation. Intuitively, one would expect that the more excess charge the metal atom has from σ -donation, the more the metal compensates by yielding electrons from d-orbitals to a π -acceptor ligand. From Table III.2, the σ -donor and π -acceptor characters of the studied complexes seem not to be correlated. This type of behaviour has already been identified by Mitoraj et al. [55]. However, the π -acceptor character is positively correlated to the atomic radius of the transition metals. The magnitude of the charge transfer ranges from $|0.33|$ to $|0.35|$ for σ -donation and from $|0.25|$ to $|0.28|$ for π -backdonation. In all complexes, the charge transfer is more pronounced for σ -donation. Indeed, the π -electrons delocalized in NO₂ tend to strongly move towards $M = \{Ti, Zr, Hf\}$ which are an electron-deficient

species because of the unoccupied d-orbitals. The $O \cdots M = \{Ti, Zr, Hf\}$ bonding is based on a simultaneous charge transfer from the occupied oxygen orbitals to the empty transition metal orbitals, and from the filled metal d-orbitals to the π^* anti-bonding orbitals of oxygen. The backdonation decreases the electron density on the metal, and the two charge transfer processes mentioned previously reinforce each other.

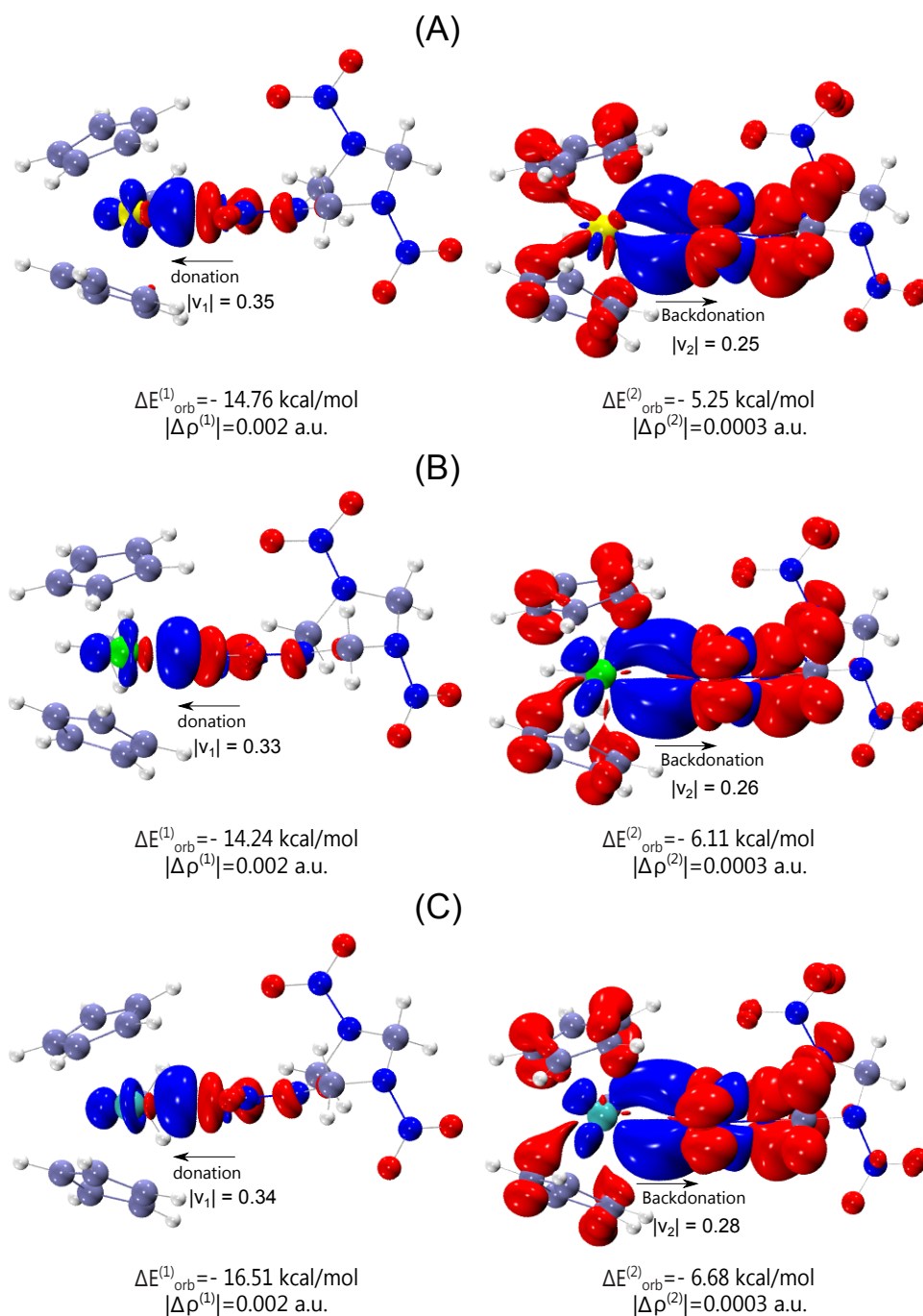


Figure III.5: EDA-NOCV deformation densities of RDX- $\text{Cp}_2\text{M}(\text{CH}_3)^+$ complexes. A: RDX- $\text{Cp}_2\text{Ti}(\text{CH}_3)^+$, B: RDX- $\text{Cp}_2\text{Zr}(\text{CH}_3)^+$ and C: RDX- $\text{Cp}_2\text{Hf}(\text{CH}_3)^+$. The direction of the negative charge flow is from the red to the blue region.

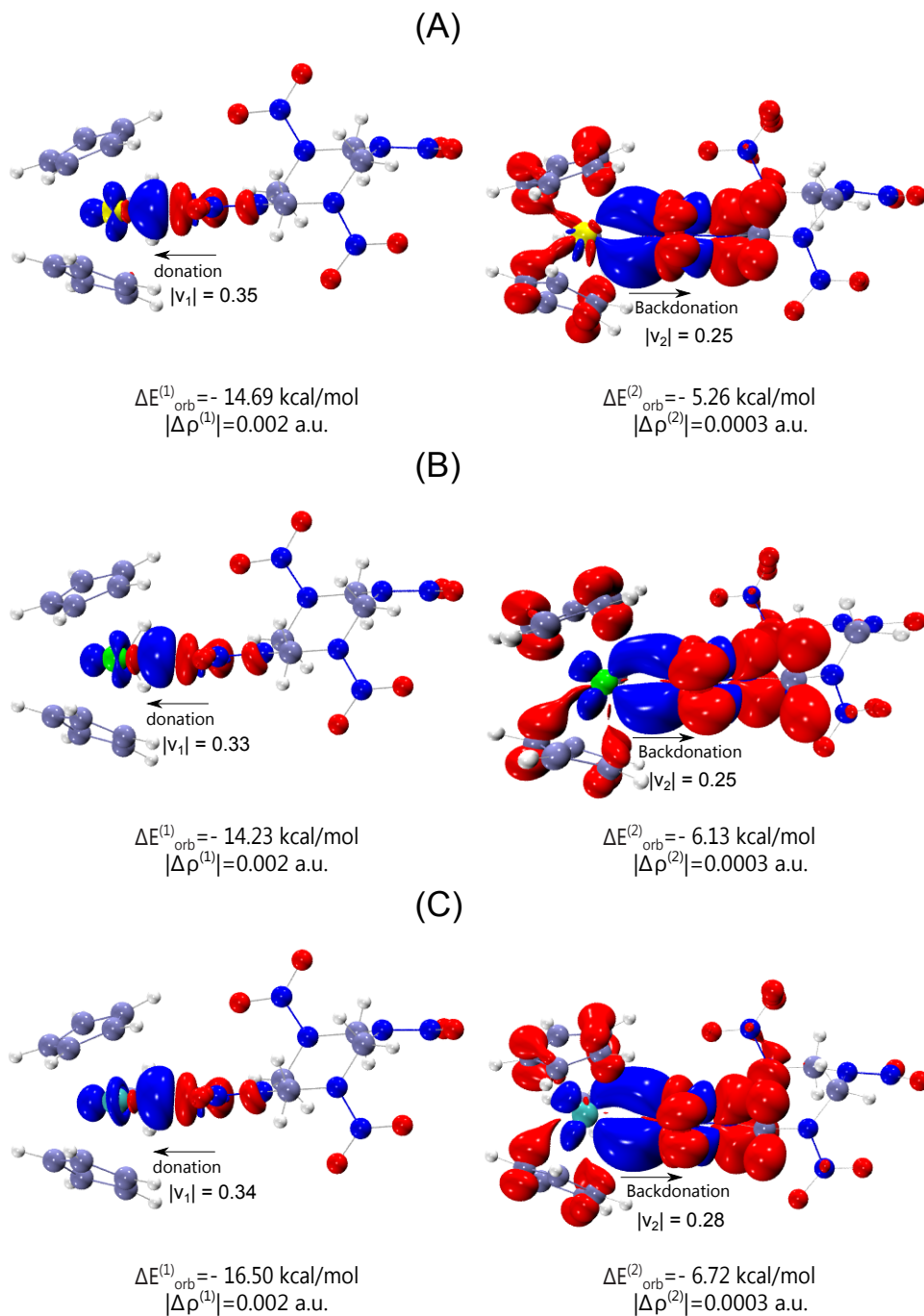


Figure III.6: EDA-NOCV deformation densities of HMX-Cp₂M(CH₃)⁺ complexes. A: HMX-Cp₂Ti(CH₃)⁺, B: HMX-Cp₂Zr(CH₃)⁺ and C: HMX-Cp₂Hf(CH₃)⁺. The direction of the negative charge flow is from the red to the blue region.

By summarizing, the EDA-NOCV analysis revealed that the $O \cdots M = \{Ti, Zr, Hf\}$ bonding is mainly electrostatic and its ionic character increase with an increasing difference in electronegativity between the interacting atoms. Furthermore, this interaction may exhibit a partially covalent character due to the relatively high contribution of orbital interactions and therefore this aspect deserves to be studied in detail. In this regard, the chemical nature of this bonding is examined based on the QTAIM formal-

ism.

III.3.3 QTAIM analysis

In this section, the topological information in the bonding region has been established from the QTAIM theory [63, 64]. The molecular graphs of RDX-MMCs and HMX-MMCs obtained by QTAIM topological analysis are shown in Figure III.7. The numerical values calculated at the bond critical points (BCPs) are grouped in Table III.3 and Table III.4.

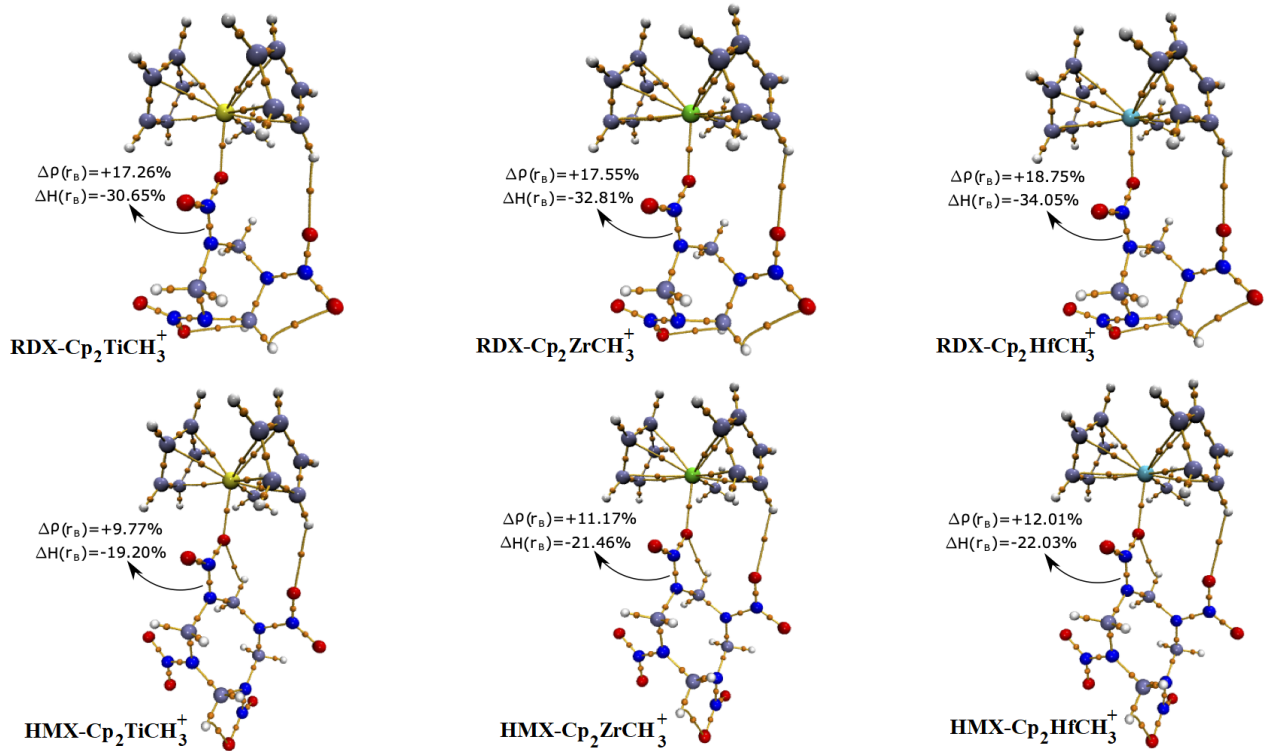


Figure III.7: Molecular graph obtained by QTAIM topological analysis. Brown lines denote bond paths and the bond critical points (BCPs) are represented by orange circles. Only the (3,-1) critical points have been displayed. Percentage changes in electron density ($\Delta\rho(\mathbf{r}_B)\%$) and total electron energy ($\Delta H(\mathbf{r}_B)\%$) are shown at BCPs of $O \cdots M = \{Ti, Zr, Hf\}$. Colour-coded by element: C = iceblue, H = white, O = red, N = blue, Ti = yellow, Zr = green, Hf = cyan.

From Figure III.7, we observe the formation of a BCP associated with its bonding path between the interacting molecular fragments. The presence of such topological features in the $O \cdots M = \{Ti, Zr, Hf\}$ interatomic region reveals the establishment of a new interaction between the two attractors (the oxygen atom and the metallic center). In the theoretical framework of QTAIM, the presence of the (3,-1) saddle point associated with the bonding path satisfies both necessary and sufficient conditions of charge density accumulation in the interatomic region [65, 66].

Table III.3: Topological properties of the electron density calculated at the (3,-1) bond critical point for the $O \cdots M = \{Ti, Zr, Hf\}$ bonding.

Atoms involved	dist. ^a	$\rho(\mathbf{r}_B)^b$	$\nabla^2\rho(\mathbf{r}_B)^c$	$H(\mathbf{r}_B)^d$	$V(\mathbf{r}_B)^e$	$G(\mathbf{r}_B)^f$	$-V(\mathbf{r}_B)/G(\mathbf{r}_B)$
(RDX) $O \cdots M = \{Ti, Zr, Hf\}$							
Ti \cdots O31	2.157	0.0544	0.2533	0.0007	-0.06141	0.06212	0.9885
Zr \cdots O31	2.280	0.0516	0.2584	0.0042	-0.05597	0.06026	0.9288
Hf \cdots O31	2.254	0.0555	0.2931	0.0045	-0.05742	0.06195	0.9268
(HMX) $O \cdots M = \{Ti, Zr, Hf\}$							
Ti \cdots O31	2.158	0.0541	0.2503	0.0007	-0.06111	0.06184	0.9881
Zr \cdots O31	2.281	0.0516	0.2580	0.0042	-0.05593	0.06019	0.9292
Hf \cdots O31	2.254	0.0556	0.2933	0.0045	-0.05750	0.06201	0.9272

^aBond distance (\AA), ^bElectron density ($e \text{\AA}^{-3}$), ^cLaplacian of the electron density ($e \text{\AA}^{-5}$), ^dTotal electron energy density (*hartree* \AA^{-3}), ^ePotential electron energy density ($V(\mathbf{r}_B)$, *hartree* \AA^{-3}), ^fKinetic electron energy density ($G(\mathbf{r}_B)$, *hartree* \AA^{-3}). The vector \mathbf{r}_B locates the position of the critical point.

Table III.4: Topological properties of the electron density calculated at the (3,-1) bond critical point of the N-NO₂ bonds.

Compound	Bonds	dist. ^a	$\rho(\mathbf{r}_B)^b$	$\nabla^2\rho(\mathbf{r}_B)^c$	$H(\mathbf{r}_B)^d$	$V(\mathbf{r}_B)^e$	$G(\mathbf{r}_B)^f$	$-V(\mathbf{r}_B)/G(\mathbf{r}_B)$
RDX	N7-N10	1.403	0.3363	-0.6040	-0.3205	-0.49001	0.16950	2.8909
RDX-Cp ₂ Ti(CH ₃) ⁺	N28-N32	1.328	0.3938	-0.8294	-0.4222	-0.63721	0.21492	2.9648
RDX-Cp ₂ Zr(CH ₃) ⁺	N28-N32	1.323	0.3977	-0.8440	-0.4299	-0.64890	0.21893	2.9639
RDX-Cp ₂ Hf(CH ₃) ⁺	N28-N32	1.321	0.3993	-0.8497	-0.4329	-0.65338	0.22048	2.9634
HMX	N14-N27	1.374	0.3581	-0.6868	-0.3549	-0.53828	0.18328	2.9369
HMX-Cp ₂ Ti(CH ₃) ⁺	N28-N32	1.328	0.3938	-0.8272	-0.4223	-0.63778	0.21548	2.9598
HMX-Cp ₂ Zr(CH ₃) ⁺	N28-N32	1.323	0.3978	-0.8422	-0.4301	-0.64976	0.21960	2.9588
HMX-Cp ₂ Hf(CH ₃) ⁺	N28-N32	1.322	0.3989	-0.8462	-0.4323	-0.65312	0.22078	2.9582

^aBond distance (\AA), ^bElectron density ($e \text{\AA}^{-3}$), ^cLaplacian of the electron density ($e \text{\AA}^{-5}$), ^dTotal electron energy density (*hartree* \AA^{-3}), ^ePotential electron energy density ($V(\mathbf{r}_B)$, *hartree* \AA^{-3}), ^fKinetic electron energy density ($G(\mathbf{r}_B)$, *hartree* \AA^{-3}). The vector \mathbf{r}_B locates the position of the critical point.

The electron density at the BCP is the most specific topological parameter helping to characterize the nature and strength of chemical bonding. For instance, in a typical ionic bond, which is identified as a closed-shell interaction, the electron density at the BCP is of the order of $0.01 e \text{\AA}^{-3}$ whereas for a shared-shell interaction it is typically about $0.10 e \text{\AA}^{-3}$ (an order of magnitude larger) [67]. Moreover, it has been evidenced that the electron density at BCP can be reliably employed to predict the hydrogen bonding energies[68]. Surveying all the numerical values summarized in Table III.3, the electron densities at the BCP of $O \cdots M = \{Ti, Zr, Hf\}$ are in a very narrow range from 0.051 to $0.055 e \text{\AA}^{-3}$, and the values of $\nabla^2\rho(\mathbf{r}_B)$ are small and all positive, in a range of $0.2503 - 0.2933 e \text{\AA}^{-5}$. The positive values of $\nabla^2\rho(\mathbf{r}_B)$ reflect the depletion of electron density in the interatomic region and denotes a closed-shell character of $O \cdots M = \{Ti, Zr, Hf\}$. Beside, the values of $H(\mathbf{r}_B)$ are close to zero and the $-V(\mathbf{r}_B)/G(\mathbf{r}_B)$ ratio are close to unity. This result suggests that locally both $V(\mathbf{r}_B)$ and $G(\mathbf{r}_B)$ contribute equally, which also allows recovering of the conventional concept of a coordination bond where a donor atom (here Oxygen) shares a pair of electrons with

the transition metal. These findings suggest that the $O \cdots M = \{Ti, Zr, Hf\}$ bonding are predominantly ionic with a weak covalent character. The relationship between the sensitivity of N-NO₂ bond and the strength of $O \cdots M = \{Ti, Zr, Hf\}$ bonding, was examined by calculating some topological properties at N-NO₂ BCPs before and after the formation of the complexes. In this way, the strengthening or weakening of N-NO₂ bonds is established by comparing the difference of the electron density (and other topological properties) for the same bond in the complexes ($X(\mathbf{r}_B)^\#$) and the isolated molecule ($X(\mathbf{r}_B)^0$) according to:

$$\Delta X(\mathbf{r}_B) = \frac{X(\mathbf{r}_B)^\# - X(\mathbf{r}_B)^0}{X(\mathbf{r}_B)^0} \times 100 \quad (\text{III.1})$$

The bond topological properties of N-NO₂ calculated at the (3,-1) BCPs are reported in Table III.4. These results concern the N-NO₂ bonds before and after the formation of the complexes. As expected, the N-NO₂ bonds in RDX and HMX are characterized by a high value of $\rho(\mathbf{r}_B)$ (from 0.33 to 0.35 $e \text{ \AA}^{-3}$) and negative values of $H(\mathbf{r}_B)$ (from -0.32 to -0.35 Hartree \AA^{-3}), confirming the purely covalent character of this bond.

Based on the average of the computed topological properties in Table III.4, for the RDX-Cp₂M(CH₃)⁺ complexes, we observe an enhancement of $\rho(\mathbf{r}_B)$ by 18.1% and $|\nabla^2\rho(\mathbf{r}_B)|$ by 38.3%. This result indicates an increase of the electronic density in the interatomic region, leading to a strengthening of the N-NO₂ bond during the complex formation. The $|V(\mathbf{r}_B)|/G(\mathbf{r}_B)$ ratio also increases by about 2.4%. Further, the magnitude of $H(\mathbf{r}_B)$ increases by 31.2% after interaction with the metal centers, confirming the N-NO₂ trigger bond stabilization from the intermolecular interaction. Indeed, a more negative value of $H(\mathbf{r}_B)$ stands for stronger interaction between the interacting atoms. The most significant increases in $\rho(\mathbf{r}_B)$ (18.7%) and $|H(\mathbf{r}_B)|$ (34%) have been obtained with RDX-Cp₂Hf(CH₃)⁺.

Overall, a similar trend is observed for the HMX-Cp₂M(CH₃)⁺ complexes. The N-NO₂ bond strengthens after the formation of the complexes, since $\rho(\mathbf{r}_B)$ and $|H(\mathbf{r}_B)|$ increase by 11.4% and 20%, respectively. This points to a redistribution of negative charges after interaction with $M = \{Ti, Zr, Hf\}$. The largest increases in $\rho(\mathbf{r}_B)$ (12%) and $|H(\mathbf{r}_B)|$ (22%) have been observed with HMX-Cp₂Hf(CH₃)⁺. All topological parameter values point to a strengthening of the N-NO₂ bond due to the intermolecular $O \cdots M = \{Ti, Zr, Hf\}$ interaction. From this analysis, it emerges that the strengthening of N-NO₂ trigger bonds is clearly influenced by the $O \cdots M = \{Ti, Zr, Hf\}$ bonding. Furthermore, the strengthening of N-NO₂ bonds depends on the chemical

nature of the interacting transition metal. In each case, the best performances in terms of decreased sensitivity to decomposition are obtained with the Hf-based complexes.

III.3.4 IRI analysis

The IRI-based analysis [69] was conducted to further investigate the nature of $O \cdots M = \{Ti, Zr, Hf\}$ intermolecular interactions in each complex. This analysis enables to quantify the N-NO₂ bond strength variation before and after the formation of the complexes. The 3D spatial visualization of IRI isosurface and the corresponding scatter map between IRI and $\Omega(\mathbf{r})$ are shown in Figure III.8 and Figure III.9, respectively.

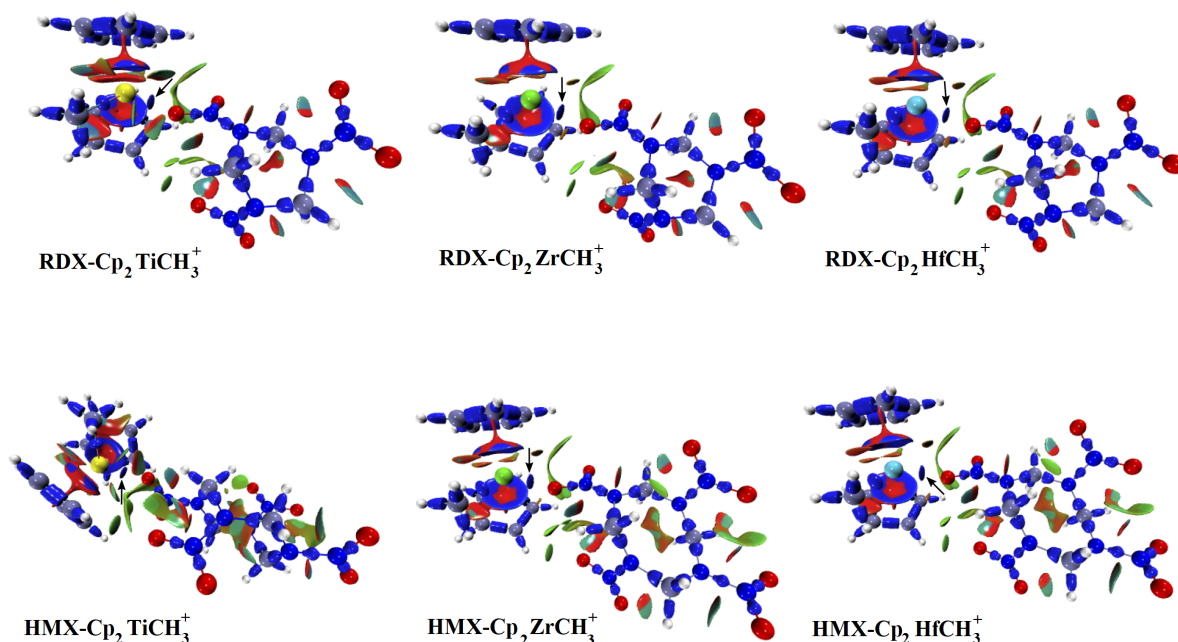


Figure III.8: Isosurface map of IRI = 1.0 for the studied complexes. Colour-coded by element: C = iceblue, H = white, O = red, N = blue, Ti = yellow, Zr = green, Hf = cyan. The black arrow refers to the $O \cdots M = \{Ti, Zr, Hf\}$ bonding.

From Figure III.8, the IRI scalar field highlights all interactions (covalent bonds, van der Waals and repulsive interactions) present in each complex. The apparition of spikes (points nearly approaching bottom) in the negative regions of $\Omega(\mathbf{r}) < 0$, means that the studied complexes contain attractive intermolecular interactions. From a qualitative point of view, the differences in the strength of attractive interactions can be distinguished based on the depth of the blue colour. Surveying these interactions, it appears that the $O \cdots M = \{Ti, Zr, Hf\}$ bonding should be strong enough since the corresponding IRI isosurface is characterized by a deep blue (stabilising interaction). The $\Omega(\mathbf{r})$ values obtained for $O \cdots M = \{Ti, Zr, Hf\}$ range from -0.050 to -0.060 *a.u.*

(Figure III.9). The spikes located in the central region around $\Omega(\mathbf{r}) \approx 0$ correspond to van der Waals interactions.

By comparing the isolated energetic molecule with its corresponding complex, we clearly distinguish the appearance of a new peak ($0.04 - 0.06 a.u.$) attributed to $O \cdots M = \{Ti, Zr, Hf\}$. As highlighted in Figure III.9, the spike located at the middle ($0.09 - 0.12 a.u.$) is a signature of the bonding between the transition metal and the methyl carbon. In RDX and HMX, the electron density values of the N-NO₂ bonds range from 0.32 to 0.35 *a.u.* and increases in a range of 0.39 – 0.41 *a.u.* after the formation of the complexes. This shift to higher values (to the left) reflects a strengthening of the N-NO₂ bonds after intercalation with the metal centers. Some spikes also appear at $\Omega(\mathbf{r}) > 0$, therefore repulsive steric interactions should exist in RDX-Cp₂M(CH₃)⁺ and HMX-Cp₂M(CH₃)⁺. The IRI isosurfaces with a red colour are mainly visible within the rings as well as in the region between the methyl group and cyclopentadienyl rings.

The regions between the transition metals and cyclopentadienyl rings are featured as large blue discs surrounded by a red ring of depletion, this red ring is interpreted as repulsion caused by steric crowding. This large electrostatic repulsion strongly points at a strained coordination sphere around the central metal [70]. These destabilising repulsive interactions are significantly more pronounced in Cp₂Ti(CH₃)⁺ compared to Cp₂Hf(CH₃)⁺ and Cp₂Zr(CH₃)⁺. It seems that the Ti-based complexes presents an excess of repulsive interaction due to the small size of atomic radius of Ti that induces a more closeness between cyclopentadienyl rings. These findings are in agreement with those obtained from EDA-NOCV, where the repulsive component was found to be more pronounced for the Ti-based complexes.

On the other hand, the IRI isosurfaces do not exhibit any evidence that the interatomic regions of $O \cdots M = \{Ti, Zr, Hf\}$ are strained, since no destabilising repulsive interaction was detected or as being van der Waals type of interaction. Only a blue isosurface is present between the interacting atoms, proving a stabilising electronic charge accumulation. An IRI isosurface is also detected from the IRI map due to the close contact between the energetic molecules and MMCs. Since its colour is green, it should be regarded as van der Waals interaction (mainly from dispersion effects). Steric and van der Waals interactions (attractive dispersion effect) are also present between the N-NO₂ groups. These two kinds of interactions are specifically observed between the oxygen atoms of nitro groups and the neighboring hydrogen atoms as well.

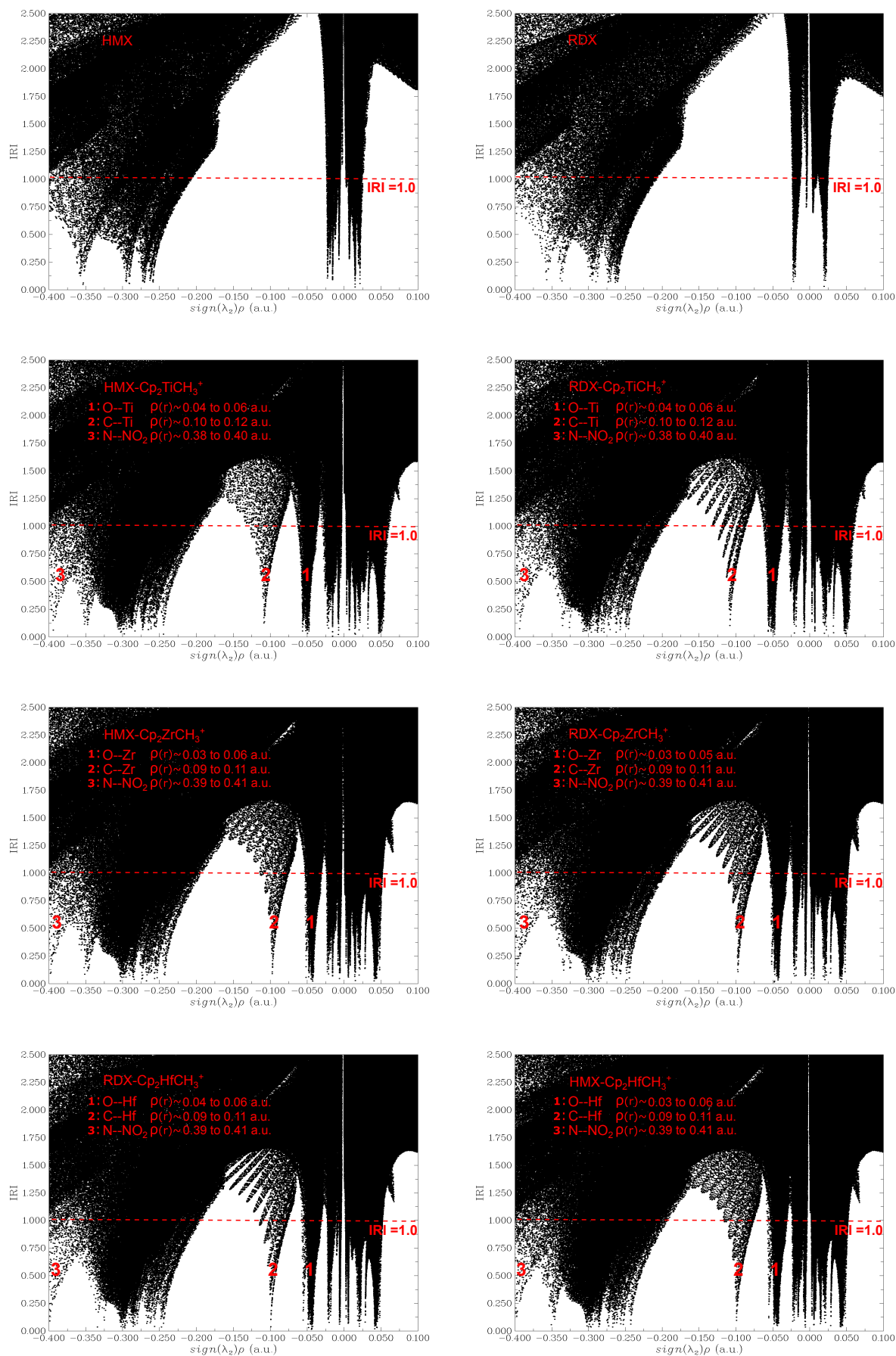


Figure III.9: Scatter plot of $\text{IRI} = 1.0$ for the studied complexes using a grid spacing of 0.08 bohr . The points intersecting with the red line at $\text{IRI} = 1.0$ visualized on the scatter plots correspond to the grid points forming the isosurfaces.

According to these results, the IRI-based results are consistent with the conclusions derived from the QTAIM results. In addition, it does not supply any proof of steric constraint in the interatomic region of $O \cdots M = \{Ti, Zr, Hf\}$ bonding or as being a van der Waals type interaction.

III.4 Conclusion

The present work focuses on the roles of intermolecular interactions involving group 4 transition metals in stabilising the N-NO₂ trigger bonds of RDX and HMX. Qualitative and quantitative analysis of MEP have been conducted to reveal sites preferably for non-covalent interactions. From the MEP-mapped van der Waals surfaces, the anomalies arising from the substantial depletion of negative charge distribution in the central regions of RDX and HMX have been evidenced. The EDA-NOCV analysis reveals that the electrostatic and orbital interactions are the major contributors to the stabilizing interactions in each complex. In addition, the $O \cdots M = \{Ti, Zr, Hf\}$ bonds strengthen as the electronegativity difference through the bond increases.

In this study, a detailed QTAIM analysis has been conducted to quantify the N-NO₂ bonds strength before and after interactions with the transition metal in the MMCs. It clearly appears that the intermolecular $O \cdots M = \{Ti, Zr, Hf\}$ interactions strengthens and deactivates the N-NO₂ bonds. Energetic molecules with such interactions are expected to be less sensitive to decomposition. Further, the strengthening of N-NO₂ bonds depends on the chemical nature of the interacting transition metal. In each case, the best performances in terms of increased stability to decomposition are obtained for the Hf- and Zr-based complexes. Overall, it emerges that the $O \cdots M = \{Ti, Zr, Hf\}$ bonding are characterized as a closed-shell interaction with a partially covalent character. As highlighted by the IRI analysis, it does not supply any proof of steric constraint in the interatomic region of $O \cdots M = \{Ti, Zr, Hf\}$ bonding or as being a van der Waals type interaction. Therefore, we can conclude that the $O \cdots M = \{Ti, Zr, Hf\}$ bonding are of mixed nature, mainly electrostatic with a partially covalent character. These results are in agreement with the conclusions derived from the QTAIM analysis.

Our study provides additional support for understanding the role of intermolecular interactions involving group 4 transition metals in stabilising the N-NO₂ trigger bonds.

Bibliography

- [1] https://treaties.un.org/Pages/ViewDetails.aspx?src=IND&mtdsg_no=XXVI-5&chapter=26&clang=_en.
- [2] <https://www.refworld.org/docid/3ae6b3ad0.html>.
- [3] <https://www.icrc.org/en/doc/resources/documents/legal-fact-sheet/landmines-factsheet-150807.htm>.
- [4] Peter Politzer, Jane S. Murray, Jorge M. Seminario, Pat Lane, M. Edward Grice, and Monica C. Concha. Computational characterization of energetic materials. *Journal of Molecular Structure: THEOCHEM*, 573(1):1–10, 2001.
- [5] Jorge M. del Campo and Jorge Ignacio Martínez-Araya. Possible use of group 4 metallocene methyl cations as potential neutralizers for fox-7. *Propellants, Explosives, Pyrotechnics*, 39(6):890–896, 2014.
- [6] Ambarish Kulkarni, Samira Siahrostami, Anjali Patel, and Jens K Nørskov. Understanding catalytic activity trends in the oxygen reduction reaction. *Chemical Reviews*, 118(5):2302–2312, 2018.
- [7] Qing Liang, Xiaodong Wu, Duan Weng, and Haibo Xu. Oxygen activation on Cu/Mn–Ce mixed oxides and the role in diesel soot oxidation. *Catalysis Today*, 139(1-2):113–118, 2008.
- [8] Lichen Liu and Avelino Corma. Metal catalysts for heterogeneous catalysis: from single atoms to nanoclusters and nanoparticles. *Chemical Reviews*, 118(10):4981–5079, 2018.
- [9] Roy A Periana, Douglas J Taube, Scott Gamble, Henry Taube, Takashi Satoh, and Hiroshi Fujii. Platinum catalysts for the high-yield oxidation of methane to a methanol derivative. *Science*, 280(5363):560–564, 1998.
- [10] Bjørk Hammer and Jens Kehlet Nørskov. Theoretical surface science and catalysis—calculations and concepts. *Advances in Catalysis*, 45:71–129, 2000.

- [11] Peter Politzer and Jane S Murray. Some molecular/crystalline factors that affect the sensitivities of energetic materials: molecular surface electrostatic potentials, lattice free space and maximum heat of detonation per unit volume. *Journal of Molecular Modeling*, 21(2):1–11, 2015.
- [12] Peter Politzer and Jane S Murray. High performance, low sensitivity: conflicting or compatible? *Propellants, Explosives, Pyrotechnics*, 41(3):414–425, 2016.
- [13] Jane S Murray, Pat Lane, and Peter Politzer. Relationships between impact sensitivities and molecular surface electrostatic potentials of nitroaromatic and nitroheterocyclic molecules. *Molecular Physics*, 85(1):1–8, 1995.
- [14] Peter Politzer and Jane S Murray. C–NO₂ dissociation energies and surface electrostatic potential maxima in relation to the impact sensitivities of some nitroheterocyclic molecules. *Molecular Physics*, 86(2):251–255, 1995.
- [15] Peter Politzer and Jane S Murray. Relationships between dissociation energies and electrostatic potentials of C–NO₂ bonds: applications to impact sensitivities. *Journal of Molecular Structure*, 376(1-3):419–424, 1996.
- [16] Peter Politzer and Jane S Murray. *Energetic Materials: part 1. Decomposition, Crystal and Molecular Properties*. Elsevier, 2003.
- [17] Svatopluk Zeman. Sensitivities of high energy compounds. *High Energy Density Materials*, pages 195–271, 2007.
- [18] Peter Politzer and Sylke Boyd. Molecular dynamics simulations of energetic solids. *Structural Chemistry*, 13(2):105–113, 2002.
- [19] Jane S Murray, Monica C Concha, and Peter Politzer. Links between surface electrostatic potentials of energetic molecules, impact sensitivities and C–NO₂/N–NO₂ bond dissociation energies. *Molecular Physics*, 107(1):89–97, 2009.
- [20] Maija M Kuklja, Eugene V Stefanovich, and A Barry Kunz. An excitonic mechanism of detonation initiation in explosives. *The Journal of Chemical Physics*, 112(7):3417–3423, 2000.
- [21] Danijela S Kretić, Jelena I Radovanović, and Dušan Ž Veljković. Can the sensitivity of energetic materials be tuned by using hydrogen bonds? another look at the role of hydrogen bonding in the design of high energetic compounds. *Physical Chemistry Chemical Physics*, 23(12):7472–7479, 2021.
- [22] Jiaheng Zhang, Qinghua Zhang, Thao T Vo, Damon A Parrish, and Jean’ne M Shreeve. Energetic salts with π -stacking and hydrogen-bonding interactions lead

- the way to future energetic materials. *Journal of the American Chemical Society*, 137(4):1697–1704, 2015.
- [23] MJ Kamlet and HG Adolph. The relationship of impact sensitivity with structure of organic high explosives. ii. polynitroaromatic explosives. *Propellants, Explosives, Pyrotechnics*, 4(2):30–34, 1979.
- [24] Chaoyang Zhang. Review of the establishment of nitro group charge method and its applications. *Journal of Hazardous Materials*, 161(1):21–28, 2009.
- [25] Gilberto Anders and Itamar Borges Jr. Topological analysis of the molecular charge density and impact sensitivity models of energetic molecules. *The Journal of Physical Chemistry A*, 115(32):9055–9068, 2011.
- [26] Miroslav Pospíšil, Pavel Vávra, Monica C Concha, Jane S Murray, and Peter Politzer. A possible crystal volume factor in the impact sensitivities of some energetic compounds. *Journal of Molecular Modeling*, 16(5):895–901, 2010.
- [27] Yu Ma, Anbang Zhang, Xianggui Xue, Daojian Jiang, Yuanqiang Zhu, and Chaoyang Zhang. Crystal packing of impact-sensitive high-energy explosives. *Crystal Growth & Design*, 14(11):6101–6114, 2014.
- [28] A. Luna, B. Amekraz, J.-P. Morizur, J. Tortajada, O. Mó, and M. Yáñez. Reactions between guanidine and Cu^+ in the gas phase. an experimental and theoretical study. *The Journal of Physical Chemistry A*, 101(33):5931–5941, 1997.
- [29] Manuel Alcamí, Alberto Luna, Otilia Mó, Manuel Yáñez, Jeanine Tortajada, and Badia Amekraz. Unimolecular reactivity of strong metal–cation complexes in the gas phase: Ethylenediamine– Cu^+ . *Chemistry–A European Journal*, 10(12):2927–2934, 2004.
- [30] J.-L. M. Abboud, I. Alkorta, J. Z. Dávalos, J.-F. Gal, M. Herreros, P.-C. Maria, O. Mó, M. T. Molina, R. Notario, and M. Yáñez. The $\text{P}_4 \cdots \text{Li}^+$ ion in the gas phase: A planetary system. *Journal of the American Chemical Society*, 122(18):4451–4454, 2000.
- [31] Tian Lu and Qinxue Chen. Interaction region indicator: A simple real space function clearly revealing both chemical bonds and weak interactions. *Chemistry–Methods*, 1(5):231–239, 2021.
- [32] M. J. Frisch, G. W. Trucks, H. B. Schlegel, G. E. Scuseria, M. A. Robb, J. R. Cheeseman, G. Scalmani, V. Barone, G. A. Petersson, H. Nakatsuji, X. Li, M. Caricato, A. V. Marenich, J. Bloino, B. G. Janesko, R. Gomperts,

- B. Mennucci, H. P. Hratchian, J. V. Ortiz, A. F. Izmaylov, J. L. Sonnenberg, D. Williams-Young, F. Ding, F. Lipparini, F. Egidi, J. Goings, B. Peng, A. Petrone, T. Henderson, D. Ranasinghe, V. G. Zakrzewski, J. Gao, N. Rega, G. Zheng, W. Liang, M. Hada, M. Ehara, K. Toyota, R. Fukuda, J. Hasegawa, M. Ishida, T. Nakajima, Y. Honda, O. Kitao, H. Nakai, T. Vreven, K. Throssell, J. A. Montgomery, Jr., J. E. Peralta, F. Ogliaro, M. J. Bearpark, J. J. Heyd, E. N. Brothers, K. N. Kudin, V. N. Staroverov, T. A. Keith, R. Kobayashi, J. Normand, K. Raghavachari, A. P. Rendell, J. C. Burant, S. S. Iyengar, J. Tomasi, M. Cossi, J. M. Millam, M. Klene, C. Adamo, R. Cammi, J. W. Ochterski, R. L. Martin, K. Morokuma, O. Farkas, J. B. Foresman, and D. J. Fox. Gaussian 16 Revision B.01, 2016. Gaussian Inc. Wallingford CT.
- [33] Takeshi Yanai, David P. Tew, and Nicholas C. Handy. A new hybrid exchange-correlation functional using the coulomb-attenuating method (cam-b3lyp). *Chemical Physics Letters*, 393:51–57, 2004.
- [34] Patricio Fuentealba, Heinz Werner Preuss, Hermann Stoll, and László Von Szentpály. A proper account of core-polarization with pseudopotentials: single valence-electron alkali compounds. *Chemical Physics Letters*, 89(5):418–422, 1982.
- [35] G t Te Velde, F Matthias Bickelhaupt, Evert Jan Baerends, C Fonseca Guerra, Stan JA van Gisbergen, Jaap G Snijders, and Tom Ziegler. Chemistry with adf. *Journal of Computational Chemistry*, 22(9):931–967, 2001.
- [36] John P Perdew, Kieron Burke, and Matthias Ernzerhof. Generalized gradient approximation made simple. *Physical review letters*, 77(18):3865, 1996.
- [37] Yingkai Zhang and Weitao Yang. Comment on "generalized gradient approximation made simple". *Physical Review Letters*, 80(4):890, 1998.
- [38] Stefan Grimme, Stephan Ehrlich, and Lars Goerigk. Effect of the damping function in dispersion corrected density functional theory. *Journal of computational chemistry*, 32(7):1456–1465, 2011.
- [39] Lars Goerigk, Andreas Hansen, Christoph Bauer, Stephan Ehrlich, Asim Najibi, and Stefan Grimme. A look at the density functional theory zoo with the advanced gmtkn55 database for general main group thermochemistry, kinetics and noncovalent interactions. *Physical Chemistry Chemical Physics*, 19(48):32184–32215, 2017.
- [40] Erik Van Lenthe and Evert Jan Baerends. Optimized slater-type basis sets for the elements 1–118. *Journal of computational chemistry*, 24(9):1142–1156, 2003.

- [41] Mirko Franchini, Pierre Herman Theodoor Philipsen, and Lucas Visscher. The becke fuzzy cells integration scheme in the amsterdam density functional program suite. *Journal of computational chemistry*, 34(21):1819–1827, 2013.
- [42] E van Lenthe, Evert-Jan Baerends, and Jaap G Snijders. Relativistic regular two-component hamiltonians. *The Journal of chemical physics*, 99(6):4597–4610, 1993.
- [43] E Van Lenthe, R Van Leeuwen, EJ Baerends, and JG Snijders. Relativistic regular two-component hamiltonians. *International Journal of Quantum Chemistry*, 57(3):281–293, 1996.
- [44] Tian Lu and Feiwu Chen. Multiwfn: a multifunctional wavefunction analyzer. *Journal of Computational Chemistry*, 33(5):580–592, 2012.
- [45] William Humphrey, Andrew Dalke, and Klaus Schulten. VMD: visual molecular dynamics. *Journal of Molecular Graphics*, 14(1):33–38, 1996.
- [46] Jane S Murray, Tore Brinck, Pat Lane, Kim Paulsen, and Peter Politzer. Statistically-based interaction indices derived from molecular surface electrostatic potentials: a general interaction properties function (GIPF). *Journal of Molecular Structure: THEOCHEM*, 307:55–64, 1994.
- [47] Peter Politzer, Pat Lane, and Jane S Murray. Tricyclic polyazine n-oxides as proposed energetic compounds. *Central European Journal of Energetic Materials*, 10(3), 2013.
- [48] Thomas M Klapötke, Andreas Nordheider, and Jörg Stierstorfer. Synthesis and reactivity of an unexpected highly sensitive 1-carboxymethyl-3-diazonio-5-nitrimino-1, 2, 4-triazole. *New Journal of Chemistry*, 36(7):1463–1468, 2012.
- [49] Elif Gökçınar, Thomas M Klapötke, and Anthony J Bellamy. Computational study on 2, 6-diamino-3, 5-dinitropyrazine and its 1-oxide and 1, 4-dioxide derivatives. *Journal of Molecular Structure: THEOCHEM*, 953(1-3):18–23, 2010.
- [50] Peter Politzer, Jane S Murray, and Timothy Clark. Mathematical modeling and physical reality in noncovalent interactions. *Journal of Molecular Modeling*, 21(3):1–10, 2015.
- [51] Peter Politzer, Jane S Murray, Jorge M Seminario, Pat Lane, M Edward Grice, and Monica C Concha. Computational characterization of energetic materials. *Journal of Molecular Structure: THEOCHEM*, 573(1-3):1–10, 2001.

- [52] Zhiyong Su, Xiangyu Liu, Qi Yang, Sheng Zhang, Qing Wei, Gang Xie, Sanping Chen, and Shengli Gao. Intermolecular interaction influenced energy and sensitivity of highly energetic salts: structure and physicochemical properties. *CrystEngComm*, 16(20):4245–4253, 2014.
- [53] Ziegler Tom and Rauk Arvi. Carbon monoxide, carbon monosulfide, molecular nitrogen, phosphorus trifluoride, and methyl isocyanide as. sigma. donors and. pi. acceptors. A theoretical study by the Hartree-Fock-Slater transition-state method. *Inorganic Chemistry*, 18(7):1755–1759, 1979.
- [54] Ziegler Tom and Rauk Arvi. A theoretical study of the ethylene-metal bond in complexes between copper (1+), silver (1+), gold (1+), platinum (0) or platinum (2+) and ethylene, based on the Hartree-Fock-Slater transition-state method. *Inorganic Chemistry*, 18(6):1558–1565, 1979.
- [55] Mitoraj Mariusz and Michalak Artur. Donor–acceptor properties of ligands from the natural orbitals for chemical valence. *Organometallics*, 26(26):6576–6580, 2007.
- [56] Mitoraj Mariusz and Michalak Artur. Applications of natural orbitals for chemical valence in a description of bonding in conjugated molecules. *Journal of molecular modeling*, 14(8):681–687, 2008.
- [57] Ashley L Shoaf and Craig A Bayse. Trigger bond analysis of nitroaromatic energetic materials using wiberg bond indices. *Journal of Computational Chemistry*, 39(19):1236–1248, 2018.
- [58] Moltved Klaus A. and Kasper P. Kepp. The chemical bond between transition metals and oxygen: electronegativity, d-orbital effects, and oxophilicity as descriptors of metal-oxygen interactions. *The Journal of Physical Chemistry C*, 123(30):18432–18444, 2019.
- [59] Emsley John. Nature’s building blocks: an AZ guide to the elements. *Oxford University Press*, 2011.
- [60] Cotton Simon A. and Raithby Paul R. Systematics and surprises in lanthanide coordination chemistry. *Coord. Chem. Rev.*, 340:220–231, 2017.
- [61] Peter Margl, Liqun Deng, and Tom Ziegler. A unified view of ethylene polymerization by d^0 and $d^0 f^n$ transition metals. 1. precursor compounds and olefin uptake energetics. *Organometallics*, 17(5):933–946, 1998.

- [62] Peter Margl, Liqun Deng, and Tom Ziegler. A unified view of ethylene polymerization by d^0 and $d^0 f^n$ transition metals. part 2: Chain propagation. *Journal of the American Chemical Society*, 120(22):5517–5525, 1998.
- [63] Richard FW Bader and Hanno Essén. The characterization of atomic interactions. *The Journal of chemical physics*, 80(5):1943–1960, 1984.
- [64] Richard FW Bader and Preston J MacDougall. Toward a theory of chemical reactivity based on the charge density. *Journal of the American Chemical Society*, 107(24):6788–6795, 1985.
- [65] Richard FW Bader. A bond path: a universal indicator of bonded interactions. *The Journal of Physical Chemistry A*, 102(37):7314–7323, 1998.
- [66] Richard FW Bader. Pauli repulsions exist only in the eye of the beholder. *Chemistry—A European Journal*, 12(10):2896–2901, 2006.
- [67] Gernot Frenking and Sason Shaik. *The Chemical Bond: Fundamental Aspects of Chemical bonding*. John Wiley & Sons, 2014.
- [68] Saeedreza Emamian, Tian Lu, Holger Kruse, and Hamidreza Emamian. Exploring nature and predicting strength of hydrogen bonds: A correlation analysis between atoms-in-molecules descriptors, binding energies, and energy components of symmetry-adapted perturbation theory. *Journal of Computational Chemistry*, 40(32):2868–2881, 2019.
- [69] Chen Q. Lu T. Interaction region indicator: A simple real space function clearly revealing both chemical bonds and weak interactions. *Chemistry-Methods*, 1(5):231–239, 2021.
- [70] Mitoraj M. Cukrowski I., de Lange J. H. Physical nature of interactions in zni complexes with 2, 2-bipyridyl: Quantum theory of atoms in molecules (QTAIM), interacting quantum atoms (IQA), noncovalent interactions (NCI), and extended transition state coupled with natural orbitals for chemical valence (ETS–NOCV) comparative studies. *The Journal of Physical Chemistry A*, 118(3):623–637, 2014.

Chapter IV

The effect of



interactions on the sensitivity of
C-NO₂ trigger bonds in FOX-7.

IV.1 Introduction

In this study, we are looking to stabilize the C-NO₂ trigger bond in FOX-7 (1,1-diamino-2,2-nitroethylene, Figure IV.1) through intermolecular interactions involving group IV transition metals (M = {Ti, Zr, Hf}) in metallocene methyl cations (MMCs).

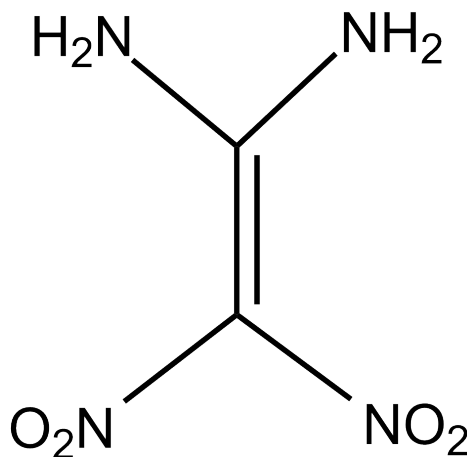


Figure IV.1: Structural formula of FOX-7, also known as DADNE.

FOX-7 is an energetic molecule first synthesised in 1998 by Latypov et al. [22]. Despite its simple composition and structure, its chemical reactivity is extremely rich [23]. This molecule has attracted an increasing interest in many theoretical and experimental investigations [24, 25, 26, 27, 28, 29]. More precisely, many studies have highlighted the decomposition mechanism of FOX-7 using different experimental and theoretical methods, and there is evidence that breaking C-NO₂ bonds is a crucial step in the initiation of decomposition [30, 31, 32, 33, 34]. The aim of this work is to use the coordination capability of the MMCs to prevent the explosion channel. FOX-7 can interact with MMCs through its nucleophilic regions (lone pair electrons of NO₂) according to an electrophilic addition reaction. The nitrogen atom of NO₂ can interact with a nucleophilic moiety from MMCs because this atom is positively charged. The formation of such complexes can enhance the trigger bond strength. Therefore, the sensitivity of the EC decreases.

In the previous chapter, we have already shown the effectiveness of MMCs in reducing the sensitivity of the N-NO₂ trigger bonds in cyclic energetic compounds, where the only type of interplay between HMX/RDX and MMCs involves Oxygen···metal interaction. At the present work, we detected two possible interactions which deserved a more detailed analysis: Oxygen···metal and Nitrogen···metal. The former is the expected one and the latter is the non expected one. We needed to address both types of interactions in order to discard the weakest one and use the strongest one

thus providing a support for the FOX-7 and MMCs interplay. We had the preliminary hypothesis that Nitrogen...metal interaction was as important as Oxygen...metal interaction found when HMX (or RDX) and MMCs interplays one each other. Moreover, reducing the sensitivity of FOX-7 is challenging, as this molecule is known for its low sensitivity compared to the cyclic compounds [38, 39]. Besides, the FOX-7 molecule is interesting because it also contains two C-NH₂ bonds that are not trigger bonds and, hence, are not directly involved in the explosion process. Indeed, the bond dissociation energies have been evaluated by 293 *kJ/mol* for C-NO₂ and by 466 *kJ/mol* for C-NH₂, therefore the former is more unstable and breaks more easily in detonation initiation [40]. These dissociation energy values change with the number of NO₂ linked to the carbon [41]. The NH₂ group generates both inductive and resonance effects. The nitrogen atom being more electronegative than the carbon, tends to pull out electrons from the carbon-carbon double bond by inductive effect, and it can also provide its lone pair through a resonance effect. The aim is to study the influence of these effects on the C-NO₂ bonds before and after forming the complexes.

In this study, we examined three types of interactions: oxygen and nitrogen from a nitro group interacting with the metal atom, as well as nitrogen from an amino group interacting with the metal atom. Furthermore, we also analysed the effect of NH₂ groups on the sensitivity of the C-NO₂ trigger bond in FOX-7.

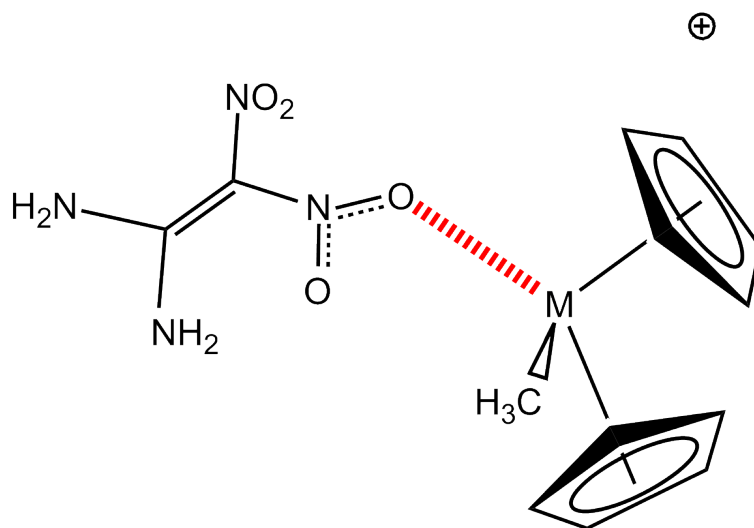


Figure IV.2: Interaction O...M leading to the complex of type (H₂N)₂C=C(NO₂)-(O)NO...Cp₂MCH₃⁺.

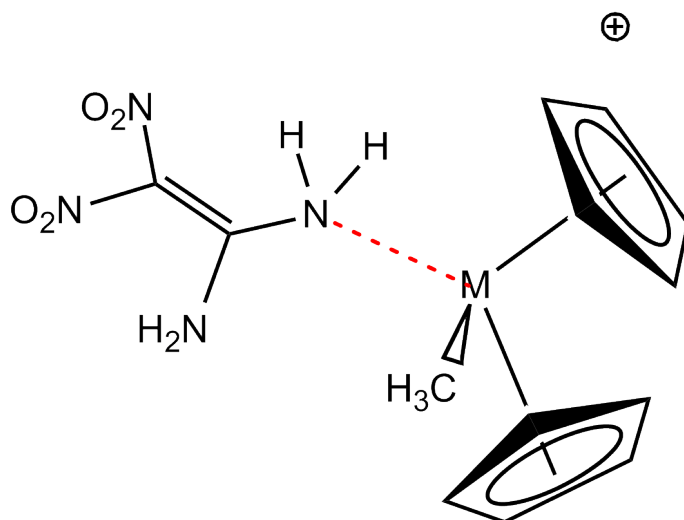


Figure IV.3: Interaction $\text{N}\cdots\text{M}$ leading to the complex of type $(\text{O}_2\text{N})_2\text{C}=\text{C}(\text{NH}_2)\text{-H}_2\text{N}\cdots\text{Cp}_2\text{MCH}_3^+$.

The topological analysis and the decomposition of intermolecular interaction energies between the two molecular fragments were conducted using QTAIM and EDA-NOCV methods, respectively. The EDA-NOCV approach unlike most other energy decomposition methods focuses on the mechanism of bond formation between the interacting molecular fragments and not just only on the analysis of the finally formed bonding [44]. This method also provides an effective way through the study of deformation densities to quantitatively assess the σ -donor and π -acceptor properties of MMCs. The QTAIM topological approach was performed to elucidate the nature of the different interactions involved in complexes $(\text{H}_2\text{N})_2\text{C}=\text{C}(\text{NO}_2)\text{-(O)NO}\cdots\text{Cp}_2\text{MCH}_3^+$ (Figure IV.2) and $(\text{O}_2\text{N})_2\text{C}=\text{C}(\text{NH}_2)\text{-H}_2\text{N}\cdots\text{Cp}_2\text{MCH}_3^+$ (Figure IV.3), in which the interacting atoms are highlighted in bold. The chemical reactivity of FOX-7 towards nucleophilic and electrophilic reagents was elucidated through the electrostatic potential on the molecular surface [45, 46, 47, 48]. This scalar field is regularly employed to assess the sensitivity of ECs to detonation, especially concerning the electron density depletion in the central regions of the molecular surface [49, 50, 51, 52]. In addition, some of statistically-based indices [53, 54, 55] derived from molecular surface electrostatic potentials were discussed.

IV.2 Computational details

All molecular structures were fully optimised using Gaussian16 Revision B.01 [70]. We employed the CAM-B3LYP [71] and ω B97X-D [72] exchange-correlation functionals along with the following effective core potentials: MDF10, MWB28, MWB60 for Ti, Zr, and Hf, respectively [73]. The O, N, C, and H atoms were represented using the 6-31+G(d,p) basis set. The atomic coordinates of the six complexes obtained with the

CAM-B3LYP and ω B97X-D density functionals are included in Appendix-B. The EDA-NOCV method was carried out by single-point calculations on the optimised structures employing the Amsterdam Density Functional software (ADF 2013.01)[74] using the revPBE-D3BJ functional. This density functional combines the revised Perdew-Burke-Ernzerhof exchange-correlation (revPBE) [75] with the D3BJ dispersion correction [76]. Goerigk et al. [77] recommend the use of revPBE-D3BJ for its ability to efficiently describe non-covalent interactions. A Slater type orbital (STO) basis set [78] of triple zeta quality with two polarisation functions (TZ2P) was considered for all atoms using Becke integration grid [79] of "very good" precision and without a frozen core. Scalar relativistic effects were included through the zero-order regular approximation (ZORA) [80]. The cube files produced by ADF software were used to visualise the deformation densities isosurfaces by using Visual Molecular Dynamics (VMD) program [81]. The electrostatic potential on the molecular surface as well as the topological analysis were conducted using the Multiwfn 3.8 code [82] based on the formatted Gaussian checkpoint file. To ensure the reproducibility of the results, all the calculations (QTAIM and EDA-NOCV) in this study were performed on the molecular structures optimised by the CAM-B3LYP and ω B97X-D density functionals (see Appendix-B). Further, the interaction energy is also calculated using various density functionals from a single point calculation.

IV.3 Results and discussion

IV.3.1 Electrostatic potential analysis

For predicting the reactivity of a molecule toward an approaching reactant, one typically plots the electrostatic potential (ESP) on a van der Waals surface of the molecule of $\rho(\mathbf{r}) = 0.001 e/Bohr^3 \equiv a.u.$, which covers about 98 % of the negative charge. This isosurface value was proposed by R. Bader [83], which reflects specific electron structure features of a molecule, such as π -electrons and lone pairs of heteroatoms. The ESP measures the electrostatic interaction between a unit point charge placed at \mathbf{r} and the molecule of interest. Negative and positive values indicate that current position is dominated by electronic and nuclear charges, respectively. The reactive site closer to the global ESP maximum (minimum) on van der Waals surface is theoretically the most electrophilic (nucleophilic) site. The mapped-ESP onto a surface of constant electron density surrounding FOX-7 along with the surface extrema are shown in Figure IV.4.

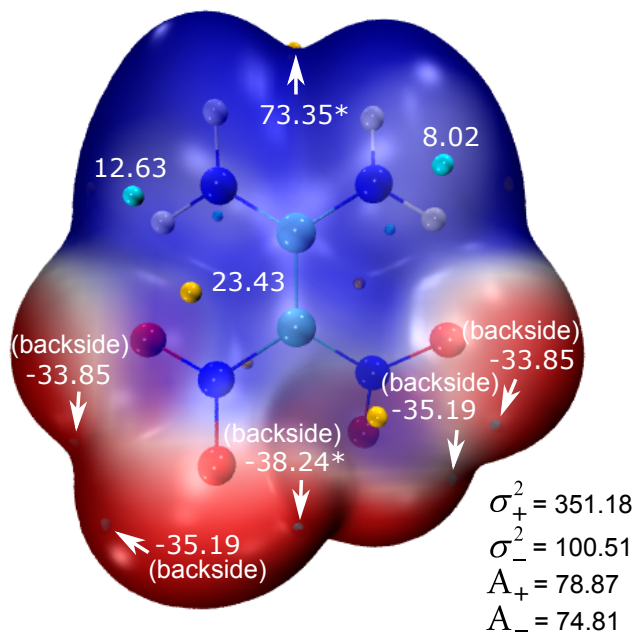


Figure IV.4: ESP-mapped van der Waals surface (kcal/mol) using a colour scale ranging from red (negative ESP), through white (neutral ESP) to blue (positive ESP). The blue regions are prone to nucleophilic attack, and the red regions are sites for electrophilic attack. The grid spacings were set to 0.2 Bohr and the van der Waals surface denotes the iso-surface of $\rho = 0.001 e/\text{Bohr}^3 \equiv 0.001 \text{ a.u.}$ Values with a star indicate global surface extreme. The bold numbers in the bottom right-hand corner are the positive ESP variance (σ_+^2), negative ESP variance (σ_-^2), positive surface area (A_+) and negative surface area (A_-) whose units are $(\text{Kcal/mol})^2 \text{ \AA}^2$, respectively.

As can be seen, the positive ESP values are around the NH_2 groups, reflecting the electrostatic repulsion between the unit charge (a proton) and the atomic nuclei. These regions are characterised by low electron density, where the nuclear charge is partially shielded. The absence of an electron-rich site in NH_2 , proves that the nitrogen lone pair is involved in a resonance structure. As expected, we observe strongly negative peripheral regions around the NO_2 groups. These electron-rich sites are mainly attributable to the lone pairs of oxygen atoms. The positive ESP values above the C-NO_2 bonds indicate a decrease in electron density due to the high electron-withdrawing effect of NO_2 , leading to a weakening of these bonds.

The regions coloured in shades of white, which are electrically neutral, reflect the transition area between positively and negatively charged regions. The global maximum ($V_{s,max}$) on the potential surface with a value of 73.35 kcal/mol is reached in the region between the two amino groups. On the other hand, its global minimum ($V_{s,min}$) with a value of -38.24 kcal/mol is located between the two nitro groups. The global maximum reflects the most electron-deficient site, susceptible to easily undergoing a nucleophilic attack, while the global minimum refers to the most electron-rich site,

which preferentially attracts electrophilic reagents. This charge separation induces a polarisation along the central axis passing through the two carbons. As reported by Zhang et al. [23], the positive end of the carbon-carbon double bond can undergo nucleophilic attack. The pattern of the surface potential reveals an imbalance in the total charge distribution induced by the two electron-donating amino groups and the two electron-accepting nitro groups. Indeed, the nitro groups tend to decrease the electron density over the carbon-carbon double bond. In contrast, the amino groups tend to enhance the electron density above the carbon-carbon double bond.

These two antagonistic effects give rise to the so-called push-pull effect [40]. The depletion of electron density around the carbon-carbon double bond also indicates that electron-withdrawing NO_2 groups predominate over electron-donating NH_2 groups. The positive (A_+) and negative (A_-) surface areas are slightly different, with respective contributions of 51.4% and 48.6% to the total area. The positive (σ_+^2) and negative (σ_-^2) variance contributions are 77.7% and 22.3% compared to the total variance, respectively. The $\sigma_+^2 > \sigma_-^2$ suggests a strong positive charge density fluctuation compared to the negative charge density. This result is typical of energetic molecules characterised by a strong concentrated positive charge in the central regions, in contrast to the negative charges spread in the peripheral regions. FOX-7 shows a tendency to react preferentially as an electrophilic entity. It is worth noting that for most organic molecules $\sigma_-^2 > \sigma_+^2$, since the positive regions come mainly from hydrogen atoms and the negative regions are dominant, such as lone pairs of heteroatoms and π -electrons in aromatic systems and multiple bonds [84].

IV.3.2 Topological analysis of electron density

The Bader's theory [85, 86] was used to quantitatively analyse the chemical nature of the $\{\text{O}, \text{N}\} = \text{X} \cdots \text{M} = \{\text{Ti}, \text{Zr}, \text{Hf}\}$ bonding. The molecular graphs of $(\text{H}_2\text{N})_2\text{C}=\text{C}(\text{NO}_2) - (\text{O})\text{NO} \cdots \text{Cp}_2\text{MCH}_3^+$ and $(\text{O}_2\text{N})_2\text{C}=\text{C}(\text{NH}_2) - \text{H}_2\text{N} \cdots \text{Cp}_2\text{MCH}_3^+$ are depicted in Figures IV.5 and IV.6, respectively. The numerical values calculated at the bond critical points (BCPs) are quoted in Tables IV.1 and IV.2.

As can be seen from Figures IV.5 and IV.6, the presence of a bonding path (line of maximum density) between $\{\text{O}, \text{N}\} = \text{X}$ and $\text{M} = \{\text{Ti}, \text{Zr}, \text{Hf}\}$ means that these atoms are linked by an interaction. From QTAIM's point of view, the formation of a (3,-1) saddle point associated with its bonding path satisfies both necessary and sufficient conditions of negative charges accumulation in the interatomic region [87, 88].

Furthermore, by interacting with MMCs, we also looked into whether the NO_2 group interacts only via its oxygen atom, or whether it is also possible to obtain interactions between the nitrogen atom (positively charged) and a nucleophilic fraction of MMCs. Our chemical intuition was that these transition metals could react through their $(n-1)$ orbitals electrons with the π^* anti-bonding orbitals of nitrogen from NO_2 group to stabilise a positive charge, this is not the case. To this end, during molecular optimization we placed the nitrogen of the NO_2 group in interaction with MMCs. From the molecular graphs obtained in this case, neither a $(3,-1)$ critical point nor a bonding path is found for nitrogen from a nitro group interacting with the metal atom, therefore these two atoms are not bonded. The absence of interaction between the NO_2 group nitrogen atom and the transition metal could be explained by the fact that MMCs reacts mainly with its π -acceptor character. Most likely, charge transfer occurs from the occupied nitrogen (NH_2 group) and oxygen (NO_2 group) orbitals to the vacant d -orbitals of $M = \{\text{Ti}, \text{Zr}, \text{Hf}\}$, since these atoms are electron rich species. Another possible explanation is that since the interaction between $\{\text{O}, \text{N}\} = \text{X}$ and $M = \{\text{Ti}, \text{Zr}, \text{Hf}\}$ is electrostatic in nature (without charge transfer), a repulsive interaction occurs between the two positively charged atoms (nitrogen in NO_2 and M). Anyway, this implies that the metal center reacts systematically with the oxygen of the nitro group. Therefore, the results confirm that the interaction $\text{O} \cdots M$ governs complex formation when a nitro group interacts with MMCs. In this study, only the interactions between the oxygen from NO_2 group and the nitrogen from NH_2 group with $M = \{\text{Ti}, \text{Zr}, \text{Hf}\}$ is considered.

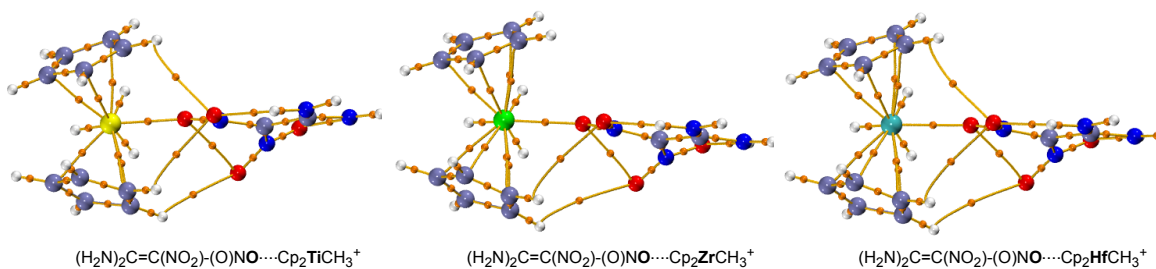


Figure IV.5: Molecular graph of the $(\text{H}_2\text{N})_2\text{C}=\text{C}(\text{NO}_2)-(\text{O})\text{NO} \cdots \text{Cp}_2\text{MCH}_3^+$ complexes obtained by QTAIM topological analysis. Brown lines denote bond paths and the bond critical points (BCPs) are represented by orange circles. Only the $(3,-1)$ critical points have been displayed. Color-coded by element: C = iceblue, H = white, O = red, N = blue, Ti = yellow, Zr = green, Hf = cyan.

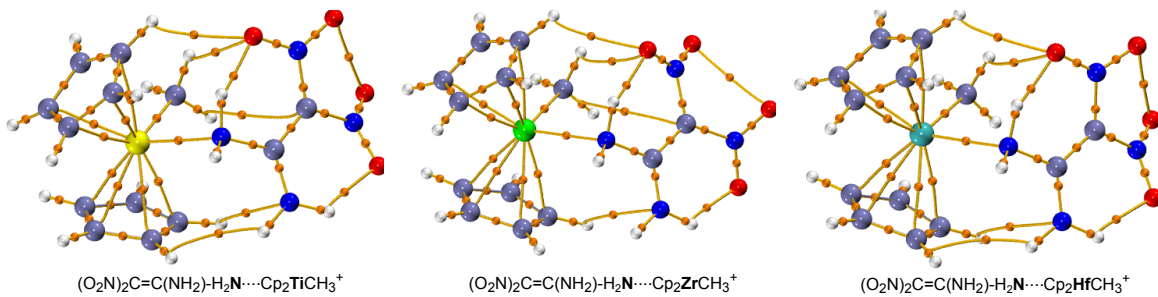


Figure IV.6: Molecular graph of the $(\text{O}_2\text{N})_2\text{C}=\text{C}(\text{NH}_2)\text{-(H)HN}\cdots\text{Cp}_2\text{MCH}_3^+$ complexes obtained by QTAIM topological analysis. Brown lines denote bond paths and the bond critical points (BCPs) are represented by orange circles. Only the (3,-1) critical points have been displayed. Color-coded by element: C = iceblue, H = white, O = red, N = blue, Ti = yellow, Zr = green, Hf = cyan.

The electron density is the first parameter that emerges when investigating the nature and strength of chemical bonds. The more C-NO₂ bonds are deficient in electron density, the weaker these bonds and therefore it becomes easy to break them to initiate the detonation process. From Table IV.1, the electron densities obtained at the BCPs vary from 0.041 to 0.045 $e\text{Å}^{-3}$ for $\text{N}\cdots\text{M} = \{\text{Ti}, \text{Zr}, \text{Hf}\}$ and from 0.058 to 0.062 $e\text{Å}^{-3}$ for $\text{O}\cdots\text{M} = \{\text{Ti}, \text{Zr}, \text{Hf}\}$, indicating that the latter is stronger. The values of $\nabla^2\rho(\mathbf{r}_\mathbf{B})$ are all positive, revealing an electron density depletion in the interatomic region, and therefore the $\{\text{O}, \text{N}\} = \text{X}\cdots\text{M} = \{\text{Ti}, \text{Zr}, \text{Hf}\}$ bonding seems to belong to the closed-shell type. The total energy density $H(\mathbf{r}_\mathbf{B})$ at the BCP is a very meaningful index to characterise the nature of interactions, which is used in many QTAIM investigations involving both strongly and weakly interacting complexes [89, 90, 91]. A negative value of $H(\mathbf{r}_\mathbf{B})$ is evidence of a covalent pairwise atom-atom interaction [92]. The $H(\mathbf{r}_\mathbf{B})$ values are all positive and close to zero, except in the case of $\text{N}\cdots\text{Ti}$, where $H(\mathbf{r}_\mathbf{B})$ is negative which can be considered as an indicator of covalency. This means that $V(\mathbf{r}_\mathbf{B})$ and $G(\mathbf{r}_\mathbf{B})$ contribute locally with similar values in all complexes while $V(\mathbf{r}_\mathbf{B})$ slightly dominates in $(\text{O}_2\text{N})_2\text{C}=\text{C}(\text{NH}_2)\text{-H}_2\text{N}\cdots\text{Cp}_2\text{TiCH}_3^+$. The $|V(\mathbf{r}_\mathbf{B})|/G(\mathbf{r}_\mathbf{B})$ ratio at the BCP may be construed as a measure of covalent character of an interaction [92]. This ratio is very informative in this regard, since some authors [93] point out that $1 < |V(\mathbf{r}_\mathbf{B})|/G(\mathbf{r}_\mathbf{B}) < 1.10$ is typical of an ionic bond with a partially covalent character, and thus the $\text{N}\cdots\text{Ti}$ bonding can be classified in this category.

As expected, in Table IV.2 we can see that the C-NH₂ bond is stronger as compared to C-NO₂. The nitrogen atom is positively charged in NO₂ group and negatively charged in NH₂ group, since the carbons are positively charged in both C-NO₂ and C-NH₂, from a purely electrostatic point of view, the C-NO₂ bond which is repulsive in nature is weaker than the C-NH₂ bond that is attractive.

Therefore, the sensitivity to detonation is higher for the C-NO₂ bond. The sensitivity of the C-NO₂ bond was quantified by calculating some topological parameters at the BCP before and after the complex's formation. The possible deactivation of this bond is determined by evaluating the difference in topological parameters for the same C-NO₂ in the isolated compound ($X(\mathbf{r}_B)^0$) and in the complex ($X(\mathbf{r}_B)^\#$) according to [61]:

$$\Delta X(\mathbf{r}_B) = \frac{X(\mathbf{r}_B)^\# - X(\mathbf{r}_B)^0}{X(\mathbf{r}_B)^0} \quad (\text{IV.1})$$

Where $\Delta X(r_B)$ represents the difference in the topological property ($\rho(r_B)$ or $H(r_B)$), $X(r_B)^\#$ and $X(r_B)^0$ denote the property calculated at the BCP in the complex and the isolated molecule, respectively.

In this way, the influence of $\{\text{O}, \text{N}\} = \text{X} \cdots \text{M} = \{\text{Ti}, \text{Zr}, \text{Hf}\}$ intermolecular interactions on the C-NO₂ bond can be evaluated. In this respect, the Equation IV.1 is applied to $\rho(\mathbf{r}_B)$ and $H(\mathbf{r}_B)$. The numerical values obtained are highlighted in bold in Table IV.2.

Table IV.1: Topological properties of the electron density calculated at the (3,-1) bond critical point for the $\{\text{O}, \text{N}\} = \text{X} \cdots \text{M} = \{\text{Ti}, \text{Zr}, \text{Hf}\}$ bonding at DFT/CAM-B3LYP level of theory. The vector \mathbf{r}_B locates the position of the critical point.

Bond	dist. ^a	$\rho(\mathbf{r}_B)^b$	$\nabla^2 \rho(\mathbf{r}_B)^c$	$H(\mathbf{r}_B)^d$	$V(\mathbf{r}_B)^e$	$G(\mathbf{r}_B)^f$	$-V(\mathbf{r}_B)/G(\mathbf{r}_B)$
(O₂N)₂C=C(NH₂)-H₂N\cdotsCp₂MCH₃⁺							
Ti31 \cdots N30	2.3060	0.0426	0.1292	-0.0027	-0.0378	0.0351	1.0769
Zr31 \cdots N30	2.4512	0.0418	0.1507	0.0008	-0.0359	0.0367	0.9782
Hf31 \cdots N30	2.4055	0.0453	0.1663	0.0002	-0.0369	0.0371	0.9946
(H₂N)₂C=C(NO₂)-(O)NO\cdotsCp₂MCH₃⁺							
Ti39 \cdots O37	2.1002	0.0625	0.2990	0.0001	-0.0744	0.0746	0.9973
Zr39 \cdots O37	2.2255	0.0580	0.3005	0.0041	-0.0667	0.0709	0.9407
Hf39 \cdots O37	2.2050	0.0622	0.3383	0.0042	-0.0680	0.0722	0.9418

^aBond distance (Å), ^bElectron density ($e \text{Å}^{-3}$), ^cLaplacian of the electron density ($e \text{Å}^{-5}$), ^dTotal electron energy density ($\text{Hartree } \text{Å}^{-3}$), ^ePotential electron energy density ($V(\mathbf{r}_B)$, $\text{Hartree } \text{Å}^{-3}$), ^fKinetic electron energy density ($G(\mathbf{r}_B)$, $\text{Hartree } \text{Å}^{-3}$).

Table IV.2: Topological properties of the electron density calculated at the (3,-1) bond critical point of the C-NO₂ and C-NH₂ bonds at the DFT/CAM-B3LYP level of theory. bonding at DFT/CAM-B3LYP level of theory.

Compound	Bond	dist. ^a	$\rho(\mathbf{r}_B)^b$	$\nabla^2\rho(\mathbf{r}_B)^c$	$H(\mathbf{r}_B)^d$	$V(\mathbf{r}_B)^e$	$G(\mathbf{r}_B)^f$	$-V(\mathbf{r}_B)/G(\mathbf{r}_B)$
C-NO ₂ bond								
FOX-7	C2-N10	1.425	0.286	-0.790	-0.409	-0.620	0.211	2.934
(H ₂ N) ₂ C=C(NO ₂)-(O)NO...Cp ₂ TiCH ₃ ⁺	C26-N34	1.373	0.305 (6.6%) ^g	-0.363	-0.488 (19.3%) ^g	-0.886	0.397	2.228
(H ₂ N) ₂ C=C(NO ₂)-(O)NO...Cp ₂ ZrCH ₃ ⁺	C26-N34	1.366	0.309 (8.0%) ^g	-0.326	-0.495 (21.0%) ^g	-0.910	0.414	2.197
(H ₂ N) ₂ C=C(NO ₂)-(O)NO...Cp ₂ HfCH ₃ ⁺	C26-N34	1.364	0.310 (8.4%) ^g	-0.312	-0.497 (21.5%) ^g	-0.917	0.419	2.186
(O ₂ N) ₂ C=C(NH ₂)-H ₂ N...Cp ₂ TiCH ₃ ⁺	C25-N27	1.448	0.280 (-2.1%) ^g	-0.834	-0.360 (-11.9%) ^g	-0.513	0.152	3.369
(O ₂ N) ₂ C=C(NH ₂)-H ₂ N...Cp ₂ ZrCH ₃ ⁺	C25-N27	1.443	0.282 (-1.4%) ^g	-0.842	-0.367 (-10.3%) ^g	-0.524	0.1566	3.3461
(O ₂ N) ₂ C=C(NH ₂)-H ₂ N...Cp ₂ HfCH ₃ ⁺	C25-N27	1.448	0.280 (-2.1%) ^g	-0.835	-0.359 (-12.2%) ^g	-0.509	0.150	3.391
C-NH ₂ bond								
FOX-7	C1-N3	1.339	0.344	-1.185	-0.553	-0.810	0.257	3.152
(H ₂ N) ₂ C=C(NO ₂)-(O)NO...Cp ₂ TiCH ₃ ⁺	C25-N30	1.330	0.349 (1.4%) ^g	-1.090	-0.582 (5.2%) ^g	-0.892	0.310	2.879
(H ₂ N) ₂ C=C(NO ₂)-(O)NO...Cp ₂ ZrCH ₃ ⁺	C25-N30	1.328	0.350 (1.7%) ^g	-1.086	-0.584 (5.6%) ^g	-0.898	0.313	2.867
(H ₂ N) ₂ C=C(NO ₂)-(O)NO...Cp ₂ HfCH ₃ ⁺	C25-N30	1.328	0.350 (1.7%) ^g	-1.085	-0.585 (5.7%) ^g	-0.899	0.314	2.864
(O ₂ N) ₂ C=C(NH ₂)-H ₂ N...Cp ₂ TiCH ₃ ⁺	C26-N30	1.413	0.304 (-11.6%) ^g	-1.024	-0.383 (-30.7%) ^g	-0.511	0.127	4.009
(O ₂ N) ₂ C=C(NH ₂)-H ₂ N...Cp ₂ ZrCH ₃ ⁺	C26-N30	1.421	0.298 (-13.4%) ^g	-0.991	-0.372 (-32.6%) ^g	-0.496	0.124	3.995
(O ₂ N) ₂ C=C(NH ₂)-H ₂ N...Cp ₂ HfCH ₃ ⁺	C26-N30	1.420	0.299 (-13.1%) ^g	-0.994	-0.373 (-32.5%) ^g	-0.497	0.124	3.995

^aBond distance (Å), ^bElectron density ($e\text{Å}^{-3}$), ^cLaplacian of the electron density ($e\text{Å}^{-5}$), ^dTotal electron energy density ($Hartree\text{Å}^{-3}$), ^ePotential electron energy density ($V(\mathbf{r}_B)$, $Hartree\text{Å}^{-3}$), ^fKinetic electron energy density ($G(\mathbf{r}_B)$, $Hartree\text{Å}^{-3}$). The vector \mathbf{r}_B locates the position of the critical point.

In complexes (H₂N)₂C=C(NO₂)-(O)NO...Cp₂MCH₃⁺, the electron density at the BCP of C-NO₂ increases, where the largest percentage (8.4%) was obtained for both (H₂N)₂C=C(NO₂)-(O)NO...Cp₂ZrCH₃⁺ and (H₂N)₂C=C(NO₂)-(O)NO...Cp₂HfCH₃⁺. A similar trend with higher percentages (from 19.3 to 21.5%) is obtained for the property $H(\mathbf{r}_B)$. The C-NO₂ bond is affected by the interaction between the oxygen atom from nitro group and the transition metal. This strengthening enhances the structural stability towards decomposition, especially for the Hf- and Zr-based complexes.

A completely opposite pattern is observed in complexes (O₂N)₂C=C(NH₂)-H₂N...Cp₂MCH₃⁺, for which both $\rho(\mathbf{r}_B)$ and $H(\mathbf{r}_B)$ decrease after their formation. This result is also in agreement with the increase in C-NO₂ bond length by about 1.0%, leading to its weakening. This suggests that the NH₂ group has a stabilising effect on the C-NO₂ bond in the isolated FOX-7 molecule. One possible explanation is that by donating its lone pair to one of the oxygen atoms, the nitrogen atom in NO₂ carries a positive charge. Therefore, the molecule will attempt to stabilise its positive charge through the resonance (lone pair of N) and inductive (electronegativity difference between N and C in C-NH₂) effects caused by NH₂. These two effects lead to an increase in the electron density along the C-NO₂ bond, resulting the increased molecular stability. Moreover, the intermolecular interaction in (O₂N)₂C=C(NH₂)-H₂N...Cp₂MCH₃⁺ significantly weakens the C-NH₂ bond, as evidenced by the decrease in $\rho(\mathbf{r}_B)$ (from 11.1 to 13.4 %) and $H(\mathbf{r}_B)$ (from 30.7 to 32.6 %) after the complexes formation. MMCs seems to act specifically on the C-NO₂ bond by strengthening it, which is expected from a neutraliser.

IV.3.3 Bond length

Figure IV.7 shows the O/N \cdots M interaction distances along with the C-NO₂ and C-NH₂ bond lengths (in Å). The significance of bond length as a crucial geometric parameter for representing molecular stability is widely recognized. While it is acknowledged that relying solely on bond length is insufficient for obtaining precise information, it remains a valuable metric for investigating bond strength. The bond's length serves as an indicator of its strength (with shorter bonds indicating greater strength), thus correlating with the sensitivity of energetic compounds. Our objective is to assess the impact of O/N \cdots M intermolecular interactions on the stability of the C-NO₂ trigger bonds.

As can be seen from Figure IV.7, the distances between interacting O and M = {Ti, Zr, Hf} atoms range from 2.10 to 2.22 Å, while those of N \cdots M = {Ti, Zr, Hf} vary from 2.30 to 2.45 Å. On the other hand, in (H₂N)₂C=C(NO₂)-(O)NO \cdots Cp₂MCH₃⁺, the bond length of C-NO₂ interacting with the metal centers decreased by approximately 4.0%. This result implies a strengthening of these bonds, which can be attributed to the redistribution of the negative charge after interaction with the MMCs. In addition, a slight contraction of about 0.8% was observed in the C-NH₂ bonds in these complexes. However, the length of some adjacent C-NO₂ bonds also increased by about 2% after the formation of the complexes, which may lead to a slight increase in sensitivity. As we demonstrated in the previous chapter, this activation is largely due to the widening of the dihedral angle. In (O₂N)₂C=C(NH₂)-(H)HN \cdots Cp₂MCH₃⁺, the C-NO₂ bond length increased by about 1.0%. Additionally, the bond length of C-NH₂ interacting with metal centers increased by about 6.0%. This result suggests a weakening of these bonds after interaction with MMCs.

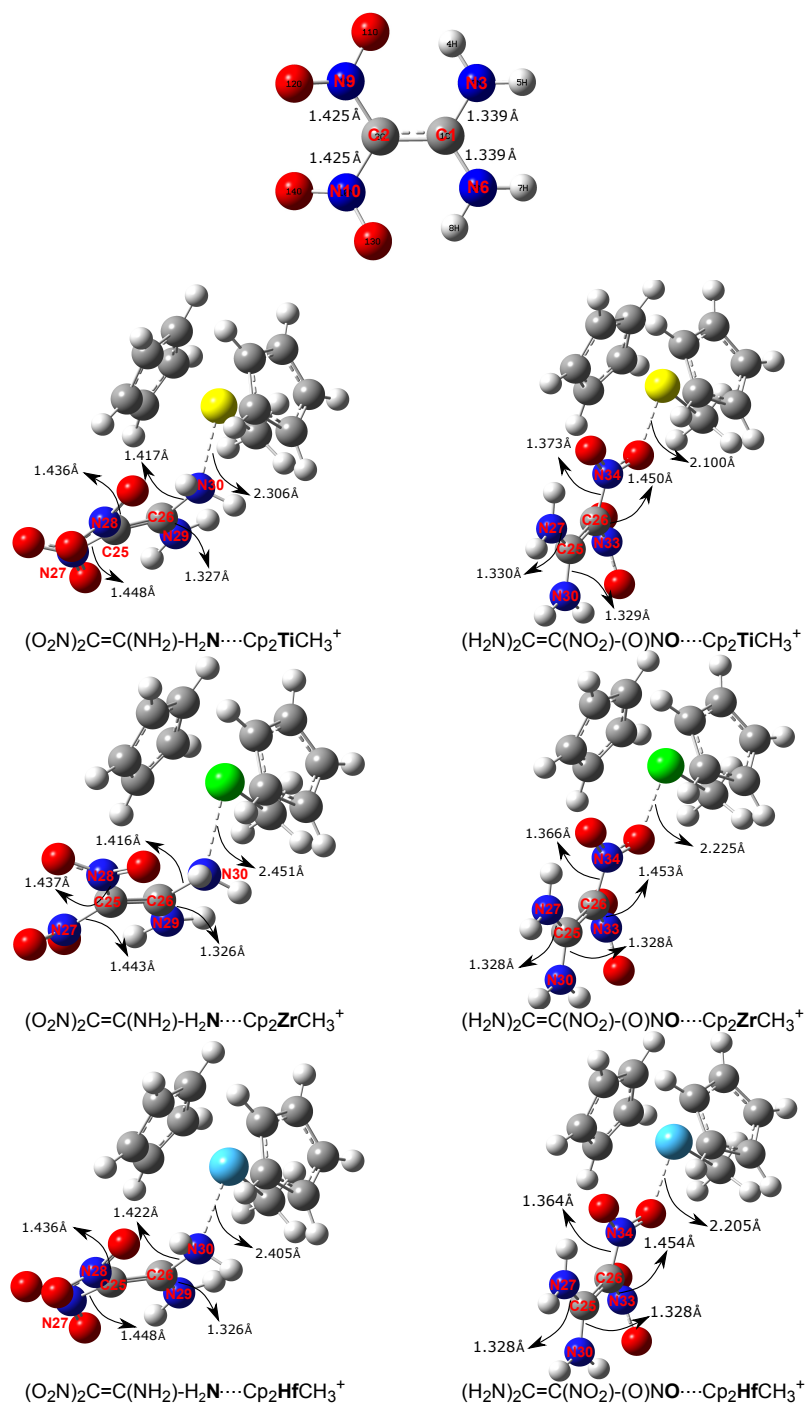


Figure IV.7: Bond lengths (Å) in FOX-7 and the studied complexes. Coloured-coded by element: C=gray, H=white, O=red, N=blue, Ti=yellow, Zr=green, Hf=cyan.

IV.3.4 EDA-NOCV analysis

The EDA-NOCV results are summarised in Table IV.3. All these energy terms are expressed as the difference between the two molecular interacting fragments before and after bond formation. The percentages in parentheses emphasise the contribution to the stabilising interactions (attractive terms), and the numbers in bold indicate the largest values for each complex.

Table IV.3: Results of the EDA-NOCV calculations at the DFT/revPBE-D3(BJ)/TZ2P level of theory^a. All the values are in *kcal/mol*.

Complex	ΔE_{Pauli}	ΔE_{orb}	ΔE_{elstat}	ΔE_{disp}	ΔE_{int} ^b
$(O_2N)_2C=C(NH_2)-H_2N \cdots Cp_2TiCH_3^+$	45.88	-28.44 (40.14%)	-25.67 (36.23%)	-16.73 (23.61%)	-24.96
$(O_2N)_2C=C(NH_2)-H_2N \cdots Cp_2ZrCH_3^+$	40.47	-28.14 (40.85%)	-25.55 (37.09%)	-15.18 (22.04%)	-28.40
$(O_2N)_2C=C(NH_2)-H_2N \cdots Cp_2HfCH_3^+$	46.58	-32.19 (41.38%)	-31.04 (39.90%)	-14.55 (18.70%)	-31.19
$(H_2N)_2C=C(NO_2)-(O)NO \cdots Cp_2TiCH_3^+$	52.06	-36.71 (37.63%)	-50.07 (51.33%)	-10.76 (11.03%)	-45.48
$(H_2N)_2C=C(NO_2)-(O)NO \cdots Cp_2ZrCH_3^+$	45.10	-37.40 (39.13%)	-49.40 (51.68%)	-8.77 (9.17%)	-50.47
$(H_2N)_2C=C(NO_2)-(O)NO \cdots Cp_2HfCH_3^+$	51.12	-41.58 (39.45%)	-55.04 (52.23%)	-8.76 (8.31%)	-54.26

^a The EDA-NOCV method was conducted with a single point calculation at the DFT/revPBE-D3(BJ)/TZ2P level of theory from the fully optimised molecular structures using the CAM-B3LYP density functional. ^b The interaction energy is calculated according to: $\Delta E_{int} = \Delta E_{Pauli} + \Delta E_{orb} + \Delta E_{elstat} + \Delta E_{disp}$. The percentages in parentheses indicate the contribution to the stabilising interactions (attractive terms). The numbers in bold highlight the largest values for each energetic term in $(H_2N)_2C=C(NO_2)-(O)NO \cdots Cp_2MCH_3^+$ and $(O_2N)_2C=C(NH_2)-H_2N \cdots Cp_2MCH_3^+$

From Table IV.3, the interaction energies are significantly more stable in complexes $(H_2N)_2C=C(NO_2)-(O)NO \cdots Cp_2MCH_3^+$ in comparison to $(O_2N)_2C=C(NH_2)-H_2N \cdots Cp_2MCH_3^+$, their difference in interaction energies is about 21.8 *kcal/mol* on average. These findings emphasise that the interaction between the metal center of MMCs and the oxygen atom is more stabilising than the one with the nitrogen atom. Besides, whatever the atom (oxygen or nitrogen) interacting with $M = \{Ti, Zr, Hf\}$, it appears that the Hf-based complexes exhibit the best structural stability. The most stable complex is $(H_2N)_2C=C(NO_2)-(O)NO \cdots Cp_2HfCH_3^+$ with a value of -54.26 *kcal/mol*, and the least stable complex is $(O_2N)_2C=C(NH_2)-H_2N \cdots Cp_2TiCH_3^+$ with a value of -24.96 *kcal/mol*.

In general terms, the magnitudes of the electrostatic (ΔE_{elstat}) and orbital (ΔE_{orb}) interactions are smaller for the complex $(O_2N)_2C=C(NH_2)-H_2N \cdots Cp_2MCH_3^+$ than for $(H_2N)_2C=C(NO_2)-(O)NO \cdots Cp_2MCH_3^+$, in such a way that the covalent interactions and electrostatic attraction in $(H_2N)_2C=C(NO_2)-(O)NO \cdots Cp_2MCH_3^+$ are stronger than they are in the set of complexes $(O_2N)_2C=C(NH_2)-H_2N \cdots Cp_2MCH_3^+$. The orbital (covalent character) terms are predominant and contribute 40.1 – 41.3% to the total attractive interactions in $(O_2N)_2C=C(NH_2)-H_2N \cdots Cp_2MCH_3^+$ complexes, while the electrostatic and dispersion terms contribute 36.2 – 39.9% and 18.7 – 23.6%, respectively. The large orbital contributions denote the covalent character of the $N \cdots M = \{Ti, Zr, Hf\}$ bond since this interaction leads to an accumulation of negative charge in

the bonding region. In contrast, the electrostatic terms are more dominant in complexes of type $(\text{H}_2\text{N})_2\text{C}=\text{C}(\text{NO}_2)-(\text{O})\text{NO}\cdots\text{Cp}_2\text{MCH}_3^+$. The largest electrostatic component (-55.04 kcal/mol) is observed for the $(\text{H}_2\text{N})_2\text{C}=\text{C}(\text{NO}_2)-(\text{O})\text{NO}\cdots\text{Cp}_2\text{HfCH}_3^+$ complex, contributing 52.2% to the total attractive interactions. The dispersion interactions are more prominent in complexes of type $(\text{O}_2\text{N})_2\text{C}=\text{C}(\text{NH}_2)-\text{H}_2\text{N}\cdots\text{Cp}_2\text{MCH}_3^+$, this component seems to play a major role in stabilising these complexes. The largest value (-16.73 kcal/mol) is achieved for the $(\text{O}_2\text{N})_2\text{C}=\text{C}(\text{NH}_2)-\text{H}_2\text{N}\cdots\text{Cp}_2\text{TiCH}_3^+$ complex, providing 23.61% of the total attractive interactions. The contribution of dispersion interactions is relatively small in complexes of type $(\text{H}_2\text{N})_2\text{C}=\text{C}(\text{NO}_2)-(\text{O})\text{NO}\cdots\text{Cp}_2\text{MCH}_3^+$, varying narrowly from 8.3 to 11.0%. The Pauli repulsion between like-spin electrons plays a destabilising role and naturally leads to a decrease in electron density in the bonding region.

The $(\text{H}_2\text{N})_2\text{C}=\text{C}(\text{NO}_2)-(\text{O})\text{NO}\cdots\text{Cp}_2\text{TiCH}_3^+$ and $(\text{H}_2\text{N})_2\text{C}=\text{C}(\text{NO}_2)-(\text{O})\text{NO}\cdots\text{Cp}_2\text{HfCH}_3^+$ complexes exhibit this effect more significantly, with values reaching up to 52.06 and 51.12 kcal/mol , respectively. However, this destabilising energy is compensated by the electrostatic interaction as their magnitudes are fairly similar. Based on the aforementioned contributions, it may be concluded that the $\{\text{O}, \text{N}\} = \text{X}\cdots\text{M} = \{\text{Ti}, \text{Zr}, \text{Hf}\}$ bond is more covalent in $(\text{O}_2\text{N})_2\text{C}=\text{C}(\text{NH}_2)-\text{H}_2\text{N}\cdots\text{Cp}_2\text{MCH}_3^+$, whereas it is more ionic in $(\text{H}_2\text{N})_2\text{C}=\text{C}(\text{NO}_2)-(\text{O})\text{NO}\cdots\text{Cp}_2\text{MCH}_3^+$.

Subsequently, the density deformation due to the orbital interaction described by the first two NOCV orbitals have been analysed in detail. Visualising deformation densities helps to understand which interaction plays primary and secondary roles between the interacting species. The isosurface maps of $\Delta\rho(\mathbf{r})^{(1)}$ and $\Delta\rho(\mathbf{r})^{(2)}$ associated to the σ -donation and π -backdonation of the first two NOCV pairs are shown in Figures IV.8 and IV.9. The orbital interaction energy contributions from the first two NOCV pairs are also indicated. The deformation density map reveals the change in electron density distribution during the interaction between the two molecular fragments. The direction of the charge flow is highlighted by arrows (from red to blue). The red and blue isosurfaces show the regions of concentration and depletion of electron density caused by the orbital interaction due to the first two NOCV pairs, respectively. From these Figures, it is readily apparent that the overall effect of the interaction between FOX-7 and MMCs induces an increase in electron density in the bonding region. The breakdown of the orbital term enables quantifying the donation and backdonation strength of MMCs in each complex, which can be classified according to their donor or acceptor properties.

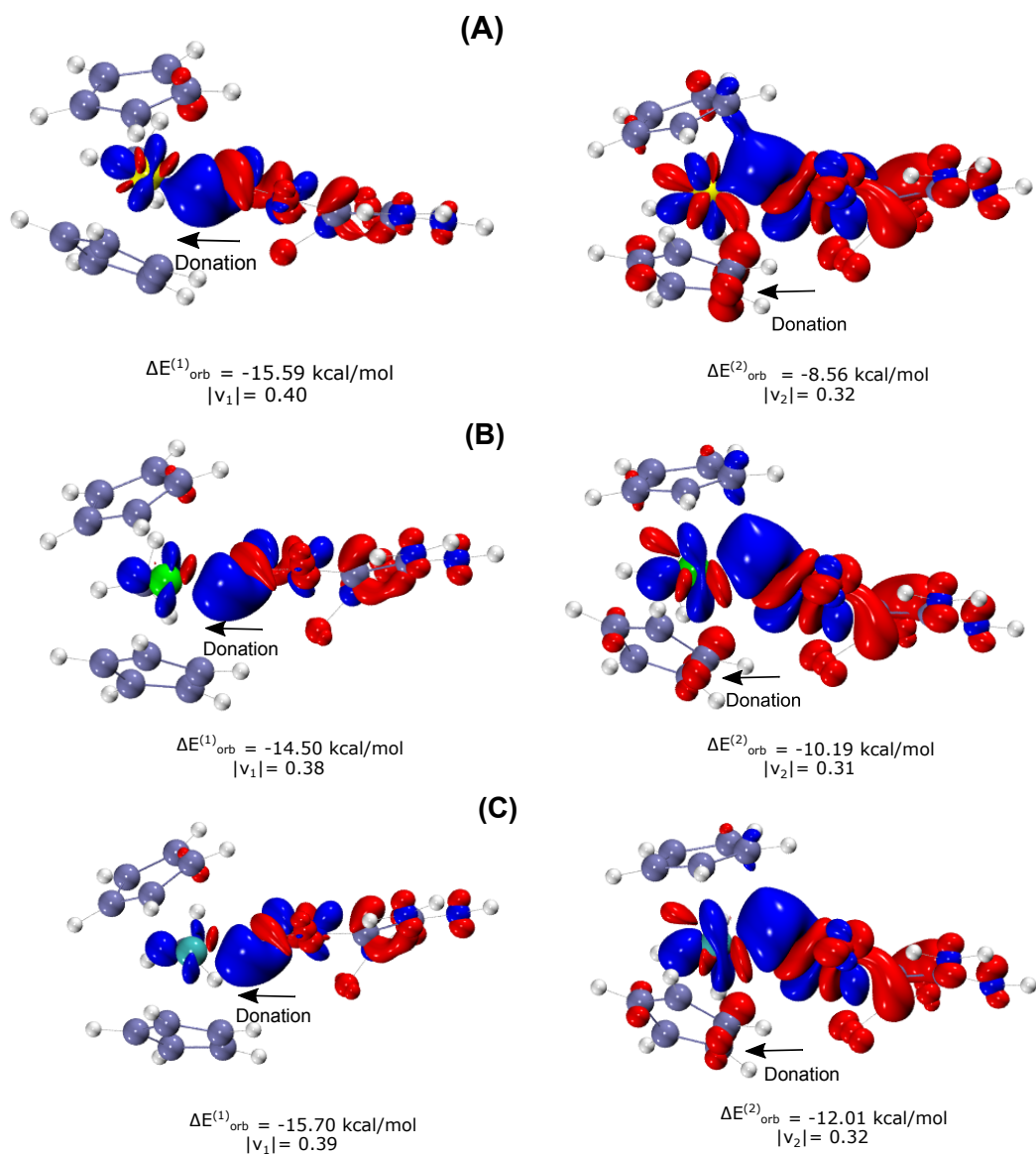


Figure IV.8: ETS-NOCV deformation densities in complexes $(\text{H}_2\text{N})_2\text{C}=\text{C}(\text{NO}_2)-(\text{O})\text{NO}\cdots\text{Cp}_2\text{MCH}_3^+$. (A): $(\text{H}_2\text{N})_2\text{C}=\text{C}(\text{NO}_2)-(\text{O})\text{NO}\cdots\text{Cp}_2\text{TiCH}_3^+$, (B): $(\text{H}_2\text{N})_2\text{C}=\text{C}(\text{NO}_2)-(\text{O})\text{NO}\cdots\text{Cp}_2\text{ZrCH}_3^+$ and (C): $(\text{H}_2\text{N})_2\text{C}=\text{C}(\text{NO}_2)-(\text{O})\text{NO}\cdots\text{Cp}_2\text{HfCH}_3^+$. The red and blue contours correspond to accumulation and depletion of electron density, respectively. Direction of the negative charge flow: red \rightarrow blue. The eigenvalues $|\nu|$ yield the extent of the charge flow. The deformation densities were plotted with the contour values 0.002 a.u. for $\Delta\rho(\mathbf{r})^{(1)}$ and 0.0006 a.u. for $\Delta\rho(\mathbf{r})^{(2)}$.

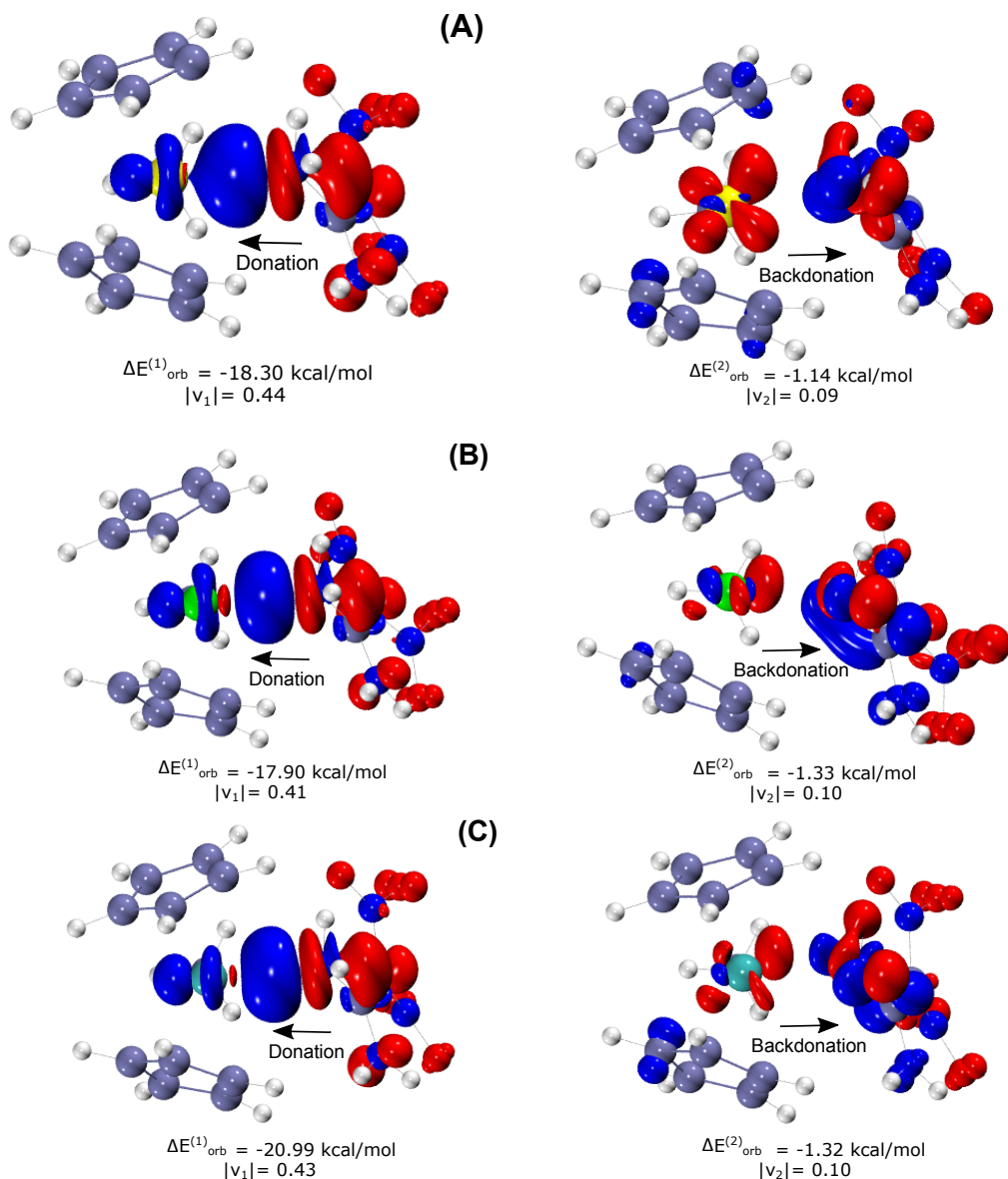


Figure IV.9: ETS-NOCV deformation densities in complexes $(\text{O}_2\text{N})_2\text{C}=\text{C}(\text{NH}_2)\text{-H}_2\text{N}\cdots\text{Cp}_2\text{MCH}_3^+$. (A): $(\text{O}_2\text{N})_2\text{C}=\text{C}(\text{NH}_2)\text{-H}_2\text{N}\cdots\text{Cp}_2\text{TiCH}_3^+$, (B): $(\text{O}_2\text{N})_2\text{C}=\text{C}(\text{NH}_2)\text{-H}_2\text{N}\cdots\text{Cp}_2\text{ZrCH}_3^+$ and (C): $(\text{O}_2\text{N})_2\text{C}=\text{C}(\text{NH}_2)\text{-H}_2\text{N}\cdots\text{Cp}_2\text{HfCH}_3^+$. The red and blue contours correspond to accumulation and depletion of electron density, respectively. Direction of the negative charge flow: red \rightarrow blue. The eigenvalues $|\nu|$ yield the extent of the charge flow. The deformation densities were plotted with the contour values 0.002 a.u. for $\Delta\rho(\mathbf{r})^{(1)}$ and 0.0006 a.u. for $\Delta\rho(\mathbf{r})^{(2)}$.

The σ -donations from occupied orbitals of nitrogen ($\text{N} \rightarrow \text{Cp}_2\text{MCH}_3^+$) are significantly stronger than π -backdonation from $\text{Cp}_2\text{MCH}_3^+$ to N ($\text{Cp}_2\text{MCH}_3^+ \rightarrow \text{N}$) in complexes of type $(\text{O}_2\text{N})_2\text{C}=\text{C}(\text{NH}_2)\text{-H}_2\text{N}\cdots\text{Cp}_2\text{MCH}_3^+$. This result is expected since NH_2 is an electron-rich species that tends to donate electrons to the electron-deficient species $\text{M} = \{\text{Ti}, \text{Zr}, \text{Hf}\}$ that tends to accept electrons through its unoccupied $(n-1)d$ orbital. The charge transfer ($\text{N} \rightarrow \text{Cp}_2\text{MCH}_3^+$) occurs in a fairly narrow range, from $|0.41|$ to $|0.44|$. In these complexes, the effect of backdonation is very small, its contribu-

tion is almost negligible since the energy of the second NOCV pair is ~ -1.0 kcal/mol. The situation is different concerning the $(\text{H}_2\text{N})_2\text{C}=\text{C}(\text{NO}_2)\text{-(O)NO}\cdots\text{Cp}_2\text{MCH}_3^+$ complexes (see Figure IV.8), where both charge transfers correspond to the σ -donation. The second NOCV contributions to deformation density show that the σ -component also corresponds to the donation from the lone electron pair of oxygen into a vacant orbital of $\text{M}=\{\text{Hf}, \text{Zr}, \text{Ti}\}$. The oxygen atom acts as a Lewis base donating its lone electron pair to the metal centre. The two charge transfers reinforce each other, resulting in increased stability for $(\text{H}_2\text{N})_2\text{C}=\text{C}(\text{NO}_2)\text{-(O)NO}\cdots\text{Cp}_2\text{MCH}_3^+$. This seems to strengthen the $(\text{H}_2\text{N})_2\text{C}=\text{C}(\text{NO}_2)\text{-(O)NO}\cdots\text{M}=\{\text{Hf}, \text{Zr}, \text{Ti}\}$ bond, which may explain the high stability of $(\text{H}_2\text{N})_2\text{C}=\text{C}(\text{NO}_2)\text{-(O)NO}\cdots\text{Cp}_2\text{MCH}_3^+$ compared to $(\text{O}_2\text{N})_2\text{C}=\text{C}(\text{NH}_2)\text{-H}_2\text{N}\cdots\text{Cp}_2\text{MCH}_3^+$. The interaction between the $(\text{H}_2\text{N})_2\text{C}=\text{C}(\text{NO}_2)\text{-(O)NO}$ ligand and the $\text{M}=\{\text{Hf}, \text{Zr}, \text{Ti}\}$ moiety is dominated by the σ forward donation, indicating the σ -donating ability of this ligand. The strong σ -donor achieves good overlap with the metal orbital, and the resulting interaction is low-energy.

IV.4 Conclusion

The local chemical reactivity of FOX-7 towards nucleophilic and electrophilic reagents was characterised through a quantitative analysis of the ESP on the molecular surface. As expected, significant negative ESP values are found over the nitro groups, while positive ESP values are located above the C-NO₂ bonds indicating a decrease in electron density due to the high electron-withdrawing effect of NO₂ group. The central regions are characterised by large positive ESP, typical of energetic molecules.

Results derived from QTAIM showed that the C-NO₂ bonds are influenced by the $\text{O}\cdots\text{M} = \{\text{Ti}, \text{Zr}, \text{Hf}\}$ bonding. Indeed, the formation of complexes of type $(\text{H}_2\text{N})_2\text{C}=\text{C}(\text{NO}_2)\text{-(O)NO}\cdots\text{Cp}_2\text{MCH}_3^+$ strengthens the C-NO₂ bond, which provides additional stability to the molecular structure of FOX-7. In addition, the shorter distances of C-NO₂ observed in $(\text{H}_2\text{N})_2\text{C}=\text{C}(\text{NO}_2)\text{-(O)NO}\cdots\text{Cp}_2\text{MCH}_3^+$ confirm the strengthening of these bonds after interaction with MMCs. Furthermore, the interaction $\text{O}\cdots\text{M}$ rules the complex formation when a nitro group interacts with MMCs, which is reactive through its transition metal.

The interaction energies calculated by EDA-NOCV revealed that the $(\text{H}_2\text{N})_2\text{C}=\text{C}(\text{NO}_2)\text{-(O)NO}\cdots\text{Cp}_2\text{MCH}_3^+$ complexes are significantly more structurally stable (by about 21.8 kcal/mol) than the $(\text{O}_2\text{N})_2\text{C}=\text{C}(\text{NH}_2)\text{-H}_2\text{N}\cdots\text{Cp}_2\text{MCH}_3^+$ complexes. The electrostatic terms varying from 51.1 to 52.2% are clearly more dominant in complexes of type $(\text{H}_2\text{N})_2\text{C}=\text{C}(\text{NO}_2)\text{-(O)NO}\cdots\text{Cp}_2\text{MCH}_3^+$ compared to the set of complexes like $(\text{O}_2\text{N})_2\text{C}=\text{C}(\text{NH}_2)\text{-H}_2\text{N}\cdots\text{Cp}_2\text{MCH}_3^+$ (from 36.2 to 39.9%). In contrast, the orbital

terms are slightly predominant in complexes of type $(\text{O}_2\text{N})_2\text{C}=\text{C}(\text{NH}_2)\text{-H}_2\text{N}\cdots\text{Cp}_2\text{MCH}_3^+$ and contribute 40.1 – 41.3% to the total attractive interactions. Overall, the dispersion interactions are less important compared to the other attractive terms, but are slightly higher in $(\text{O}_2\text{N})_2\text{C}=\text{C}(\text{NH}_2)\text{-H}_2\text{N}\cdots\text{Cp}_2\text{MCH}_3^+$ ranging from 18.7 to 23.6 %.

Based on the first NOCV pair energy, the σ -donor character is more prominent in $(\text{O}_2\text{N})_2\text{C}=\text{C}(\text{NH}_2)\text{-H}_2\text{N}\cdots\text{Cp}_2\text{MCH}_3^+$ compared to $(\text{H}_2\text{N})_2\text{C}=\text{C}(\text{NO}_2)\text{-(O)NO}\cdots\text{Cp}_2\text{MCH}_3^+$. This seems to strengthen the $(\text{H}_2\text{N})_2\text{C}=\text{C}(\text{NO}_2)\text{-(O)NO}\cdots\text{M}=\{\text{Hf}, \text{Zr}, \text{Ti}\}$ bond, which may explain the high stability of $(\text{H}_2\text{N})_2\text{C}=\text{C}(\text{NO}_2)\text{-(O)NO}\cdots\text{Cp}_2\text{MCH}_3^+$ compared to $(\text{O}_2\text{N})_2\text{C}=\text{C}(\text{NH}_2)\text{-H}_2\text{N}\cdots\text{Cp}_2\text{MCH}_3^+$.

This study allows us to further understand the effect of these intermolecular interactions on the stabilisation of such bonds, for designing less sensitive energetic molecules allowing more secure handling. In addition, if we cannot prevent the explosive behaviour of molecules like FOX-7, at least we can diminish their sensitivity for safer handling through the formation of these types of complexes with MMCs.

Bibliography

- [1] Roman V Tsyshevsky, Onise Sharia, and Maija M Kuklja. Thermal decomposition mechanisms of nitroesters: Ab initio modeling of pentaerythritol tetranitrate. *The Journal of Physical Chemistry C*, 117(35):18144–18153, 2013.
- [2] Roman V Tsyshevsky, Onise Sharia, and Maija M Kuklja. Molecular theory of detonation initiation: insight from first principles modeling of the decomposition mechanisms of organic nitro energetic materials. *Molecules*, 21(2):236, 2016.
- [3] Ying Xiong, Kai Zhong, and Chao-yang Zhang. Trigger linkage mechanism: Two or multiple steps initiate the spontaneous decay of energetic materials. *Energetic Materials Frontiers*, 3(1):38–46, 2022.
- [4] Thomas B Brill and Kenneth J James. Kinetics and mechanisms of thermal decomposition of nitroaromatic explosives. *Chemical Reviews*, 93(8):2667–2692, 1993.
- [5] Peter Politzer and Jane S Murray. C–NO₂ dissociation energies and surface electrostatic potential maxima in relation to the impact sensitivities of some nitroheterocyclic molecules. *Molecular Physics*, 86(2):251–255, 1995.
- [6] Peter Politzer and Jane S Murray. Relationships between dissociation energies and electrostatic potentials of C–NO₂ bonds: Applications to impact sensitivities. *Journal of Molecular Structure*, 376(1-3):419–424, 1996.
- [7] Maija M Kuklja, Eugene V Stefanovich, and A Barry Kunz. An excitonic mechanism of detonation initiation in explosives. *The Journal of Chemical Physics*, 112(7):3417–3423, 2000.
- [8] Svatopluk Zeman. Sensitivities of high energy compounds. *High Energy Density Materials*, pages 195–271, 2007.
- [9] Jane S Murray, Monica C Concha, and Peter Politzer. Links between surface electrostatic potentials of energetic molecules, impact sensitivities and C–NO₂/N–NO₂ bond dissociation energies. *Molecular Physics*, 107(1):89–97, 2009.

- [10] MJ Kamlet and HG Adolph. The relationship of impact sensitivity with structure of organic high explosives. ii. polynitroaromatic explosives. *Propellants, Explosives, Pyrotechnics*, 4(2):30–34, 1979.
- [11] Peter Politzer and Jane S Murray. Detonation performance and sensitivity: a quest for balance. In *Advances in quantum chemistry*, volume 69, pages 1–30. Elsevier, 2014.
- [12] Scott A Shackelford. Role of thermochemical decomposition in energetic material initiation sensitivity and explosive performance. Technical report, AIR FORCE RESEARCH LAB EDWARDS AFB CA, 2007.
- [13] Jacqueline Akhavan. *The Chemistry of Explosives*. Royal Society of Chemistry, 2011.
- [14] Laurence E Fried, M Riad Manaa, Philip F Pagoria, and Randall L Simpson. Design and synthesis of energetic materials. *Annual Review of Materials Research*, 31(1):291–321, 2001.
- [15] Sury Iyer and Norman Slagg. *Molecular Aspects in Energetic Materials*. VCH Publishers, New York, 1988.
- [16] Peter Politzer, Pat Lane, and Jane S Murray. Electrostatic potentials, intralattice attractive forces and crystal densities of nitrogen-rich C, H, N, O salts. *Crystals*, 6(1):7, 2016.
- [17] Anna V Kimmel, Peter V Sushko, Alexander L Shluger, and Maija M Kuklja. Effect of charged and excited states on the decomposition of 1,1-diamino-2,2-dinitroethylene molecules. *The Journal of Chemical Physics*, 126(23):234711, 2007.
- [18] Jun Tao and Xiaofeng Wang. Theoretical investigation on the interaction mechanism of FOX-7/AP mixed crystals. *Molecular Simulation*, 46(2):155–161, 2020.
- [19] Betsy M Rice and Jennifer J Hare. A quantum mechanical investigation of the relation between impact sensitivity and the charge distribution in energetic molecules. *The Journal of Physical Chemistry A*, 106(9):1770–1783, 2002.
- [20] Joaquín O Singh, Jorge D Anunziata, and Juana J Silber. n - π electron donor–acceptor complexes. ii. aliphatic amines with dinitrobenzenes. *Canadian Journal of Chemistry*, 63(4):903–907, 1985.
- [21] Divyakant L. Patel, James Dillon, and Noel Wright. In-situ landmine neutralization using chemicals to initiate low order burning of main charge. 2006.

- [22] Nikolai V Latypov, Jan Bergman, Abraham Langlet, Ulf Wellmar, and Ulf Bemm. Synthesis and reactions of 1,1-diamino-2,2-dinitroethylene. *Tetrahedron*, 54(38):11525–11536, 1998.
- [23] Yu Zhang, Qian Sun, Kangzhen Xu, Jirong Song, and Fengqi Zhao. Review on the reactivity of 1,1-diamino-2,2-dinitroethylene (FOX-7). *Propellants, Explosives, Pyrotechnics*, 41(1):35–52, 2016.
- [24] Dan C Sorescu, Jerry A Boatz, and Donald L Thompson. Classical and quantum-mechanical studies of crystalline FOX-7 (1,1-diamino-2,2-dinitroethylene). *The Journal of Physical Chemistry A*, 105(20):5010–5021, 2001.
- [25] Xue-Hai Ju, He-Ming Xiao, and Qi-Ying Xia. A density functional theory investigation of 1,1-diamino-2,2-dinitroethylene dimers and crystal. *The Journal of Chemical Physics*, 119(19):10247–10255, 2003.
- [26] Jijun Zhao and Hong Liu. High-pressure behavior of crystalline FOX-7 by density functional theory calculations. *Computational Materials Science*, 42(4):698–703, 2008.
- [27] Jorge M. del Campo and Jorge Ignacio Martínez-Araya. Possible use of group 4 metallocene methyl cations as potential neutralizers for FOX-7. *Propellants, Explosives, Pyrotechnics*, 39(6):890–896, 2014.
- [28] Steven Hunter, Paul L Coster, Alistair J Davidson, David IA Millar, Stewart F Parker, William G Marshall, Ronald I Smith, Carole A Morrison, and Colin R Pulham. High-pressure experimental and DFT-D structural studies of the energetic material FOX-7. *The Journal of Physical Chemistry C*, 119(5):2322–2334, 2015.
- [29] Zbigniew A Dreger, Yuchuan Tao, and Yogendra M Gupta. Phase diagram and decomposition of 1,1-diamino-2,2-dinitroethene single crystals at high pressures and temperatures. *The Journal of Physical Chemistry C*, 120(20):11092–11098, 2016.
- [30] Yongxing Tang, Wei Huang, Gregory H Imler, Damon A Parrish, and Jeanne M Shreeve. Enforced planar FOX-7-like molecules: a strategy for thermally stable and insensitive π -conjugated energetic materials. *Journal of the American Chemical Society*, 142(15):7153–7160, 2020.
- [31] Haixiang Gao and M Shreeve Jean’ne. Recent progress in taming FOX-7 (1,1-diamino-2,2-dinitroethene). *RSC Advances*, 6(61):56271–56277, 2016.

- [32] Yang Liu, Feng Li, and Huai Sun. Thermal decomposition of FOX-7 studied by ab initio molecular dynamics simulations. In *Guosen Yan*, pages 165–175. Springer, 2015.
- [33] Yingzhe Liu, Yiding Ma, Tao Yu, Weipeng Lai, Wangjun Guo, Zhongxue Ge, and Zhinan Ma. Structural rearrangement of energetic materials under an external electric field: A case study of nitromethane. *The Journal of Physical Chemistry A*, 122(8):2129–2134, 2018.
- [34] Ludmila Simkova, Frantisek Liska, and Jiri Ludvik. 2,2-dinitroethene-1,1-diamine. *Current Organic Chemistry*, 15(17):2983–2995, 2011.
- [35] P Cossee. Ziegler-natta catalysis i. Mechanism of polymerisation of α -olefins with Ziegler-Natta catalysts. *Journal of Catalysis*, 3(1):80–88, 1964.
- [36] EJ Arlman. Ziegler-Natta catalysis ii. Surface structure of layer-lattice transition metal chlorides. *Journal of Catalysis*, 3(1):89–98, 1964.
- [37] Nassima Bachir, Samir Kenouche, and Jorge I Martínez-Araya. Theoretical investigation of the effect of $O \cdots M = \{Ti, Zr, Hf\}$ interactions on the sensitivity of energetic N-nitro compounds. *Journal of Molecular Graphics and Modelling*, 118:108341, 2023.
- [38] Waldemar A Trzciński, Stanisław Cudziło, Zbigniew Chyłek, and Leszek Szymańczyk. Detonation properties of 1,1-diamino-2,2-dinitroethene (DADNE). *Journal of Hazardous Materials*, 157(2-3):605–612, 2008.
- [39] Qiong Wu, Weihua Zhu, and Heming Xiao. DFT study on crystalline 1,1-diamino-2,2-dinitroethylene under high pressures. *Journal of Molecular Modeling*, 19(9):4039–4047, 2013.
- [40] Peter Politzer, Monica C Concha, M Edward Grice, Jane S Murray, and Pat Lane. Computational investigation of the structures and relative stabilities of amino/nitro derivatives of ethylene. *Journal of Molecular Structure: THEOCHEM*, 452(1-3):75–83, 1998.
- [41] Yu-Ran Luo. *Comprehensive Handbook of Chemical Bond Energies*. CRC press, 2007.
- [42] Miroslav Pospíšil, Pavel Vávra, Monica C Concha, Jane S Murray, and Peter Politzer. Sensitivity and the available free space per molecule in the unit cell. *Journal of Molecular Modeling*, 17(10):2569–2574, 2011.
- [43] Peter Politzer and Jane S Murray. Some perspectives on sensitivity to initiation of detonation. *Green Energetic Materials*, pages 45–62, 2014.

- [44] F Matthias Bickelhaupt, Célia Fonseca Guerra, Mariusz Paweł Mitoraj, Filip Sagan, Artur Michalak, Sudip Pan, and Gernot Frenking. Clarifying notes on the bonding analysis adopted by the energy decomposition analysis. *Physical Chemistry Chemical Physics*, 2022.
- [45] Peter Politzer, Robert Parr. Some new energy formulas for atoms and molecules. *The Journal of Chemical Physics*, 61(10), pages 4258–4262, 1974.
- [46] Peter Politzer, Jane S. Murray. The fundamental nature and role of the electrostatic potential in atoms and molecules. *Theoretical Chemistry Accounts*, 108, pages 134–142, 2002.
- [47] Peter Politzer Atomic and molecular energies as functionals of the electrostatic potential. *Theoretical Chemistry Accounts*, 111, pages 395–399, 2004.
- [48] Jane S. Murray, Peter Politzer The electrostatic potential: An overview. *WIREs Computational Molecular Science*, 1(2), pages 153–163, 2011.
- [49] Peter Politzer, Pat Lane, and Jane S Murray. Tricyclic polyazine n-oxides as proposed energetic compounds. *Central European Journal of Energetic Materials*, 10(3), 2013.
- [50] Anton Hammerl, Thomas M Klapötke, Heinrich Nöth, Markus Warchhold, and Gerhard Holl. Synthesis, structure, molecular orbital and valence bond calculations for tetrazole azide, CHN_7 . *Propellants, Explosives, Pyrotechnics: An International Journal Dealing with Scientific and Technological Aspects of Energetic Materials*, 28(4):165–173, 2003.
- [51] Thomas M Klapötke, Andreas Nordheider, and Jörg Stierstorfer. Synthesis and reactivity of an unexpected highly sensitive 1-carboxymethyl-3-diazonio-5-nitrimino-1, 2, 4-triazole. *New Journal of Chemistry*, 36(7):1463–1468, 2012.
- [52] Elif Gökçınar, Thomas M Klapötke, and Anthony J Bellamy. Computational study on 2, 6-diamino-3, 5-dinitropyrazine and its 1-oxide and 1,4-dioxide derivatives. *Journal of Molecular Structure: THEOCHEM*, 953(1-3):18–23, 2010.
- [53] Jane S Murray, Tore Brinck, Pat Lane, Kirn Paulsen, and Peter Politzer. Statistically-based interaction indices derived from molecular surface electrostatic potentials: A general interaction properties function (gipf). *Journal of Molecular Structure: THEOCHEM*, 307:55–64, 1994.
- [54] Peter Politzer, Jorge Martinez, Jane S. Murray, Monica C. Concha, Alejandro Toro-Labbé An electrostatic interaction correction for improved crystal density prediction. *Molecular Physics*, 107:2095–2101, 2009.

- [55] Peter Politzer, Jorge Martinez, Jane S. Murray, Monica C. Concha. An electrostatic correction for improved crystal density predictions of energetic ionic compounds. *Molecular Physics*, 108:1391–1396, 2010.
- [56] A. Luna, B. Amekraz, J.-P. Morizur, J. Tortajada, O. Mó, and M. Yáñez. Reactions between guanidine and Cu^+ in the gas phase. an experimental and theoretical study. *The Journal of Physical Chemistry A*, 101(33):5931–5941, 1997.
- [57] J.-L. M. Abboud, I. Alkorta, J. Z. Dávalos, J.-F. Gal, M. Herreros, P.-C. Maria, O. Mó, M. T. Molina, R. Notario, and M. Yáñez. The $\text{P}_4 \cdots \text{Li}^+$ ion in the gas phase: A planetary system. *Journal of the American Chemical Society*, 122(18):4451–4454, 2000.
- [58] Manuel Alcamí, Alberto Luna, Otilia Mó, Manuel Yáñez, Jeanine Tortajada, and Badia Amekraz. Unimolecular reactivity of strong metal–cation complexes in the gas phase: Ethylenediamine– Cu^+ . *Chemistry–A European Journal*, 10(12):2927–2934, 2004.
- [59] Sai Manoj NVT Gorantla and Kartik Chandra Mondal. Uncovering the hidden reactivity of benzyne/aryne precursors utilized under milder condition: Bonding and stability studies by EDA–NOCV analyses. *Journal of Computational Chemistry*, 43(23):1543–1560, 2022.
- [60] Kavita Devi, Sai Manoj NVT Gorantla, and Kartik Chandra Mondal. EDA–NOCV analysis of carbene-borylene bonded dinitrogen complexes for deeper bonding insight: A fair comparison with a metal-dinitrogen system. *Journal of Computational Chemistry*, 43(11):757–777, 2022.
- [61] Kenouche Samir, Bachir Nassima, and Jorge I Martínez-Araya, Explaining the High Catalytic Activity in Bis (indenyl) methyl Zirconium Cation Using Combined EDA–NOCV/QTAIM Approach. *ChemPhysChem*, 24(2):e202200488, 2023.
- [62] Sai Manoj NVT Gorantla and Kartik Chandra Mondal. EDA–NOCV calculation for efficient N_2 binding to the reduced Ni_3S_8 complex: Estimation of Ni– N_2 intrinsic interaction energies. *ACS Omega*, 6(49):33389–33397, 2021.
- [63] Tom Ziegler and Arvi Rauk. Carbon monoxide, carbon monosulfide, molecular nitrogen, phosphorus trifluoride, and methyl isocyanide as. sigma. donors and. pi. acceptors. a theoretical study by the Hartree-Fock-Slater transition-state method. *Inorganic Chemistry*, 18(7):1755–1759, 1979.

- [64] Tom Ziegler and Arvi Rauk. A theoretical study of the ethylene-metal bond in complexes between copper (1+), silver (1+), gold (1+), platinum (0) or platinum (2+) and ethylene, based on the Hartree-Fock-Slater transition-state method. *Inorganic Chemistry*, 18(6):1558–1565, 1979.
- [65] Mariusz Mitoraj and Artur Michalak. Donor–acceptor properties of ligands from the natural orbitals for chemical valence. *Organometallics*, 26(26):6576–6580, 2007.
- [66] Mariusz Mitoraj and Artur Michalak. Applications of natural orbitals for chemical valence in a description of bonding in conjugated molecules. *Journal of Molecular Modeling*, 14(8):681–687, 2008.
- [67] Gernot Frenking and F Matthias Bickelhaupt. The EDA perspective of chemical bonding. *The Chemical Bond: Fundamental Aspects of Chemical Bonding*, pages 121–157, 2014.
- [68] Lili Zhao, Markus Hermann, WH Schwarz, and Gernot Frenking. The Lewis electron-pair bonding model: Modern energy decomposition analysis. *Nature Reviews Chemistry*, 3(1):48–63, 2019.
- [69] Moritz von Hopffgarten and Gernot Frenking. Energy decomposition analysis. *Wiley Interdisciplinary Reviews: Computational Molecular Science*, 2(1):43–62, 2012.
- [70] HB Schlegel, GE Scuseria, MA Robb, JR Cheeseman, G Scalmani, V Barone, GA Petersson, H Nakatsuji, X Li, M Caricato, et al. Gaussian 16, revision b. 01, Gaussian. Inc., Wallingford CT.[*Google Scholar*], 2016.
- [71] Takeshi Yanai, David P Tew, and Nicholas C Handy. A new hybrid exchange–correlation functional using the coulomb-attenuating method (CAM-B3LYP). *Chemical physics letters*, 393(1-3):51–57, 2004.
- [72] Jeng-Da Chai and Martin Head-Gordon. Long-range corrected hybrid density functionals with damped atom–atom dispersion corrections. *Physical Chemistry Chemical Physics*, 10(44):6615–6620, 2008.
- [73] Patricio Fuentealba, Heinzwerner Preuss, Hermann Stoll, and Laszlo Von Szentpaly. A proper account of core-polarisation with pseudopotentials: Single valence-electron alkali compounds. *Chemical Physics Letters*, 89(5):418–422, 1982.
- [74] G Te Velde, F Matthias Bickelhaupt, Evert Jan Baerends, C Fonseca Guerra, Stan JA van Gisbergen, Jaap G Snijders, and Tom Ziegler. Chemistry with ADF. *Journal of Computational Chemistry*, 22(9):931–967, 2001.

- [75] John P Perdew, Kieron Burke, and Matthias Ernzerhof. Generalized gradient approximation made simple. *Physical Review Letters*, 77(18):3865, 1996.
- [76] Stefan Grimme, Stephan Ehrlich, and Lars Goerigk. Effect of the damping function in dispersion corrected density functional theory. *Journal of Computational Chemistry*, 32(7):1456–1465, 2011.
- [77] Lars Goerigk, Andreas Hansen, Christoph Bauer, Stephan Ehrlich, Asim Najibi, and Stefan Grimme. A look at the density functional theory zoo with the advanced GMTKN55 database for general main group thermochemistry, kinetics and noncovalent interactions. *Physical Chemistry Chemical Physics*, 19(48):32184–32215, 2017.
- [78] Erik Van Lenthe and Evert Jan Baerends. optimised Slater-type basis sets for the elements 1–118. *Journal of Computational Chemistry*, 24(9):1142–1156, 2003.
- [79] Mirko Franchini, Pierre Herman Theodoor Philipsen, and Lucas Visscher. The Becke fuzzy cells integration scheme in the Amsterdam density functional program suite. *Journal of Computational Chemistry*, 34(21):1819–1827, 2013.
- [80] E van Lenthe, Evert-Jan Baerends, and Jaap G Snijders. Relativistic regular two-component hamiltonians. *The Journal of Chemical Physics*, 99(6):4597–4610, 1993.
- [81] W Humphrey, A Dalke, and K Schulten. VMD: Visual molecular dynamics. *Journal of Molecular Graphics*, 14(1):33–38, 1996.
- [82] Tian Lu and Feiwu Chen. Multiwfn: A multifunctional wavefunction analyser. *Journal of Computational Chemistry*, 33(5):580–592, 2012.
- [83] RFW Bader, W H Henneker, and Paul E Cade. Molecular charge distributions and chemical binding. *The Journal of Chemical Physics*, 46(9):3341–3363, 1967.
- [84] Peter Politzer, Jane S Murray, Jorge M Seminario, Pat Lane, M Edward Grice, and Monica C Concha. Computational characterization of energetic materials. *Journal of Molecular Structure: THEOCHEM*, 573(1-3):1–10, 2001.
- [85] Richard FW Bader and Hanno Essén. The characterization of atomic interactions. *The Journal of Chemical Physics*, 80(5):1943–1960, 1984.
- [86] Richard FW Bader and Preston J MacDougall. Toward a theory of chemical reactivity based on the charge density. *Journal of the American Chemical Society*, 107(24):6788–6795, 1985.

- [87] Richard FW Bader. A bond path: A universal indicator of bonded interactions. *The Journal of Physical Chemistry A*, 102(37):7314–7323, 1998.
- [88] Richard FW Bader. Pauli repulsions exist only in the eye of the beholder. *Chemistry—A European Journal*, 12(10):2896–2901, 2006.
- [89] Zhaoxu Wang, Yi Liu, Baishu Zheng, Fengxiang Zhou, Yinchun Jiao, Yuan Liu, XunLei Ding, and Tian Lu. A theoretical investigation on Cu/Ag/Au bonding in $\text{XH}_2\text{P}\cdots\text{MY}$ ($\text{X} = \text{H}, \text{CH}_3, \text{F}, \text{CN}, \text{NO}_2$; $\text{M} = \text{Cu}, \text{Ag}, \text{Au}$; $\text{Y} = \text{F}, \text{Cl}, \text{Br}, \text{I}$) complexes. *The Journal of Chemical Physics*, 148(19):194106, 2018.
- [90] Baishu Zheng, Yi Liu, Zhaoxu Wang, Fengxiang Zhou, Yuan Liu, XunLei Ding, and Tian Lu. Regium bonds formed by MX ($\text{M} = \text{Cu}, \text{Ag}, \text{Au}$; $\text{X} = \text{F}, \text{Cl}, \text{Br}$) with phosphine-oxide/phosphinous acid: Comparisons between oxygen-shared and phosphine-shared complexes. *Molecular Physics*, 117(18):2443–2455, 2019.
- [91] Samir Kenouche and Jorge I Martínez-Araya. A combined QTAIM/IRI topological analysis of the effect of axial/equatorial positions of NH_2 and CN substituents in the $[(\text{PY}_5\text{Me}_2)\text{MoO}]^+$ complex. *Journal of Molecular Graphics and Modelling*, 116:108273, 2022.
- [92] Enrique Espinosa, Ibon Alkorta, José Elguero, and Elies Molins. From weak to strong interactions: A comprehensive analysis of the topological and energetic properties of the electron density distribution involving $\text{X-H}\cdots\text{F-Y}$ systems. *The Journal of Chemical Physics*, 117(12):5529–5542, 2002.
- [93] Ignacy Cukrowski, Jurgens H de Lange, and Mariusz Mitoraj. Physical nature of interactions in Zn^{II} complexes with 2,2'-bipyridyl: Quantum theory of atoms in molecules (QTAIM), interacting quantum atoms (IQA), noncovalent interactions (NCI), and extended transition state coupled with natural orbitals for chemical valence (ETS-NOCV) comparative studies. *The Journal of Physical Chemistry A*, 118(3):623–637, 2014.

General conclusion

The main goal of this work is to improve the safety of ECs, which are widely used in various civil and military sectors. This task may contribute to public security by designing insensitive ECs, thereby minimising the risks of possible unpredictable explosions and their associated tragic events. The sensitive nature of ECs makes experimental investigations a very difficult and dangerous task, as the detonation process occurs almost instantaneously and is highly exothermic. Accordingly, theoretical studies using quantum chemical methods can be a very useful way to study such compounds.

Our first work outlines the role of intermolecular interactions involving group 4 transition metals in stabilising the N–NO₂ trigger bonds. A quantitative analysis using Molecular Electrostatic Potential (MEP) evidenced anomalies arising from the marked depletion of negative charge distribution of RDX and HMX. The Energy Decomposition Analysis with Natural Orbitals for Chemical Valence (EDA-NOCV) results reveal that the electrostatic and orbital contributions are the dominant factors driving the assembly of the M = {Ti, Zr, Hf}-based complexes. Sensitivity of the N–NO₂ trigger bonds is investigated by using the Quantum Theory of Atoms in Molecules (QTAIM). The QTAIM topological analysis showed that the O···M = {Ti, Zr, Hf} interaction strengthens these trigger bonds, revealing an increased stability to decomposition. This effect is more marked in the Hf- and Zr-based complexes. Finally, the results based on Interaction Indicator Region (IRI) are fully consistent with those generated from QTAIM analysis.

The second work highlights the effect of $\{O, N\} = X \cdots M = \{Ti, Zr, Hf\}$ interactions on the stability of C–NO₂ trigger bonds in FOX-7. In this study, three types of interactions were examined: oxygen and nitrogen from a nitro group interacting with the metal atom, as well as nitrogen from an amino group interacting with the same metal atom. Topological analysis based on Bader’s theory and the EDA-NOCV method were performed in order to quantify the different intermolecular interactions. Furthermore, the local chemical reactivity of FOX-7 was elucidated through a quantitative study of the electrostatic potential on the molecular surface. Unlike (O₂N)₂C=C(NH₂)-H₂N···Cp₂MCH₃⁺ complexes, which exhibit both σ -donor and π -acceptor features, the situation is different concerning the (H₂N)₂C=C(NO₂)-(O)NO···Cp₂MCH₃⁺ complexes, where both charge transfers correspond to the σ -donation. The two charge transfers reinforce each other, resulting in increased stability for (H₂N)₂C=C(NO₂)-(O)NO···Cp₂MCH₃⁺. This seems

to strengthen the $(\text{H}_2\text{N})_2\text{C}=\text{C}(\text{NO}_2)\text{-(O)NO}\cdots\text{Cp}_2\text{MCH}_3^+$ bond, which may explain the high stability of $(\text{H}_2\text{N})_2\text{C}=\text{C}(\text{NO}_2)\text{-(O)NO}\cdots\text{Cp}_2\text{MCH}_3^+$ compared to $(\text{O}_2\text{N})_2\text{C}=\text{C}(\text{NH}_2)\text{-H}_2\text{N}\cdots\text{Cp}_2\text{MCH}_3^+$. Results from topological analysis revealed that the decreased sensitivity to decomposition of C–NO₂ bonds depends on the chemical nature of the interacting metal, and the best achievements are obtained for the Hf-based complex. Our results demonstrate that the interaction of {Ti, Zr, Hf} with C–NO₂ is more favorable than that with C–NH₂, this specific action on the trigger bond may support the use of Metallocene Methyl Cations (MMCs) as possible neutralisers.

This work allows us to further understand the effect of intermolecular interactions on the stabilisation of trigger bonds, for designing less sensitive energetic molecules allowing more secure handling. In addition, if we cannot prevent the explosive behaviour of ECs, at least we can diminish their sensitivity for safer handling through the formation of these types of complexes. As perspectives, we aim to establish correlations between our theoretical findings and experimental studies. This will enhance our understanding of the intermolecular interactions within RDX-Cp₂M(CH₃)⁺, HMX-Cp₂M(CH₃)⁺ and FOX-7-Cp₂M(CH₃)⁺ complexes, and their influence on the neutralisation of ECs as well as the stabilisation of trigger bonds. Additionally, as other potential theoretical investigations, we can employ a relaxed scan procedure or intrinsic reaction coordinate (IRC), to check whether the explosion path of these complexes is altered compared with that of isolated molecules.

Appendix A

Optimised Structures

To perform geometrical optimisations, we used Gaussian 16 on each structure. The route section for the optimisation jobs was set as follows:

```
CAM-B3LYP/GenECP NoSymm SCF=(MaxCyc=100,NoVarAcc,XQC)
Int=(Grid=Ultrafine,acc2e=12) Opt=(CalcAll,MaxCycle=200,Tight)
Guess=Huckel
```

The options specified for the SCF command either speed-up or guarantee convergence of the SCF cycles: We defined the maximum number of 100 SCF cycles to ensure meeting the convergence criterion. The NoVarAcc option allows maintaining a high accuracy from the very beginning of calculations instead of the default option, so the calculations' accuracy increases with each step. The XQC option applies a quadratic convergence on the SCF [1] process, therefore helping to guarantee the process's convergence. The initial parameters for the SCF calculations were obtained with the Guess=Huckel command. For the integration process, the grid parameter to Ultrafine [2] was defined, thus meaning that integration grids achieve a level of accuracy of 99 radial shells and 590 points per shell [3]. Furthermore, we have imposed the option acc2e=12 which sets two-electron integral accuracy parameter to 10^{-12} Hartree. On the other hand, the convergence accuracy for the geometrical optimisation calculations was set at $1.5 \cdot 10^{-5}$ for maximum force, $1.0 \cdot 10^{-5}$ for RMS force (root mean square of force), $6.0 \cdot 10^{-5}$ for maximum displacement, and $4.0 \cdot 10^{-5}$ for RMS displacement with the Tight command. The CalcAll option of the Opt command computes the force constant at every point, and we set up the maximum number of geometrical optimisation steps as 200 through the MaxCyc option. Besides, we set up a net charge equals +1, and a spin-multiplicity equals 1 (closed-shell systems) for each metallocene methyl cation, and RDX/HMX-MMCs complex. For each energetic molecule alone (RDX, and HMX), the net charge was set up equals 0 and the spin-multiplicity equals 1. We selected the CAM-B3LYP density functional following the concept proposed by [4, 5, 6].

The effective core potential MDF10 for Ti-based complexes guarantees that an external number of electrons is 12 ($22 - 10 = 12$, because 10 inner electrons are simulated employing pseudopotential) which are responsible for local reactivity.

The effective core potential MWB28 for Zr-based complexes guarantees that an external number of electrons is 12 ($40 - 28 = 12$, because 28 inner electrons are simulated utilizing pseudopotential) which are responsible for local reactivity.

The effective core potential MWB60 for Hf-based complexes guarantee that an external number of electrons is 12 ($72 - 60 = 12$, because 60 inner electrons are simulated employing pseudopotential) which are responsible for local reactivity.

So, all of these metallocene cations have a metal atom each providing 12 external electrons and then the description of local reactivity could be compared among the three types of metallocenes.

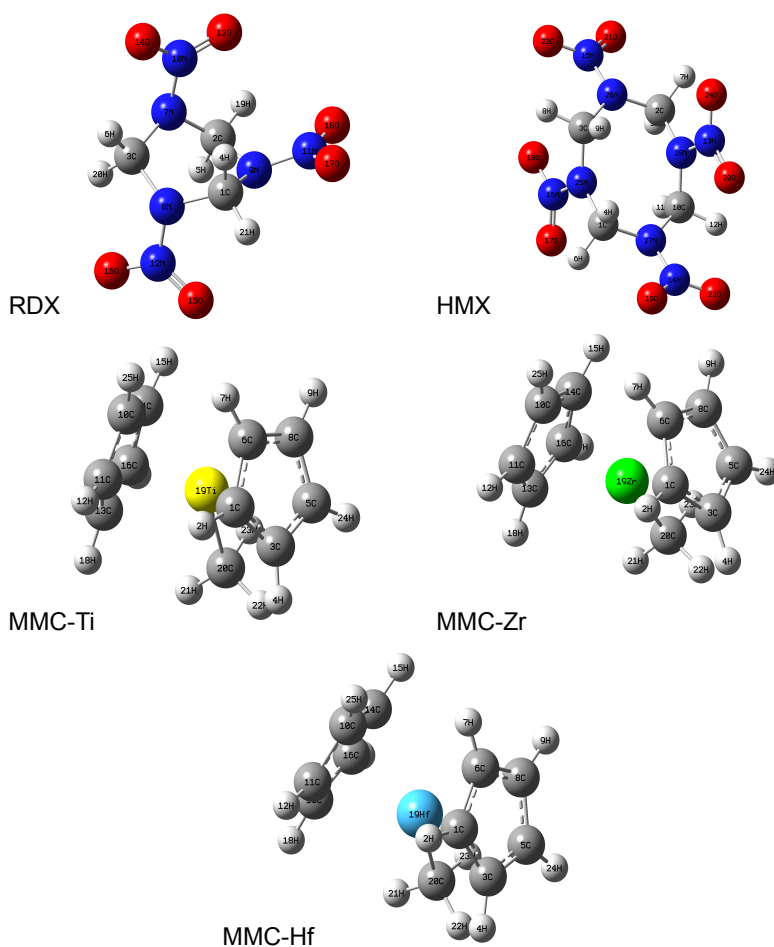


Figure 1: Optimised geometrical structures for the isolated molecules along with their numerical labeling on atoms.

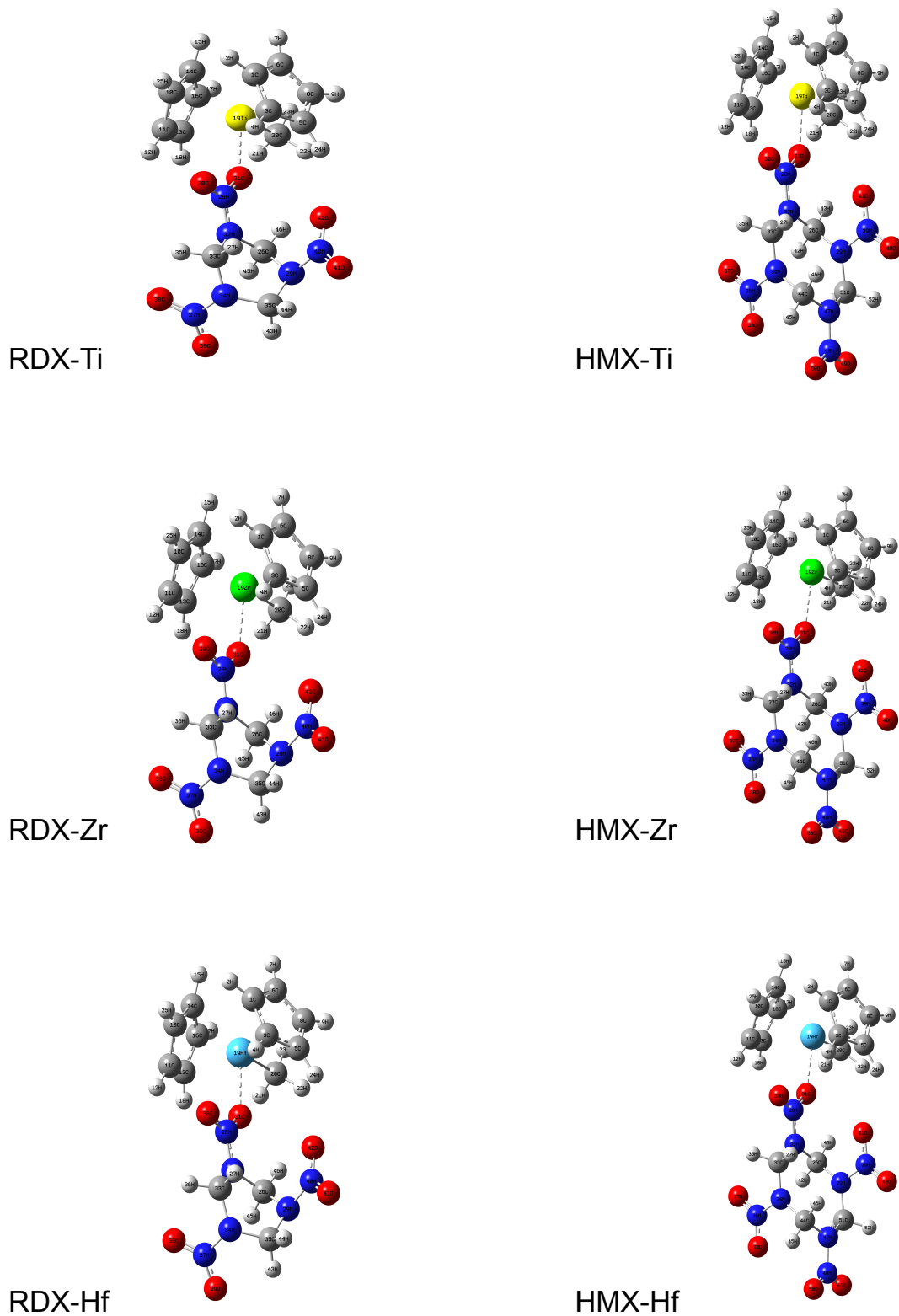


Figure 2: Optimised geometrical structures for the complexes along with their numerical labeling on atoms.

Dihedral angle of N-NO₂ bonds

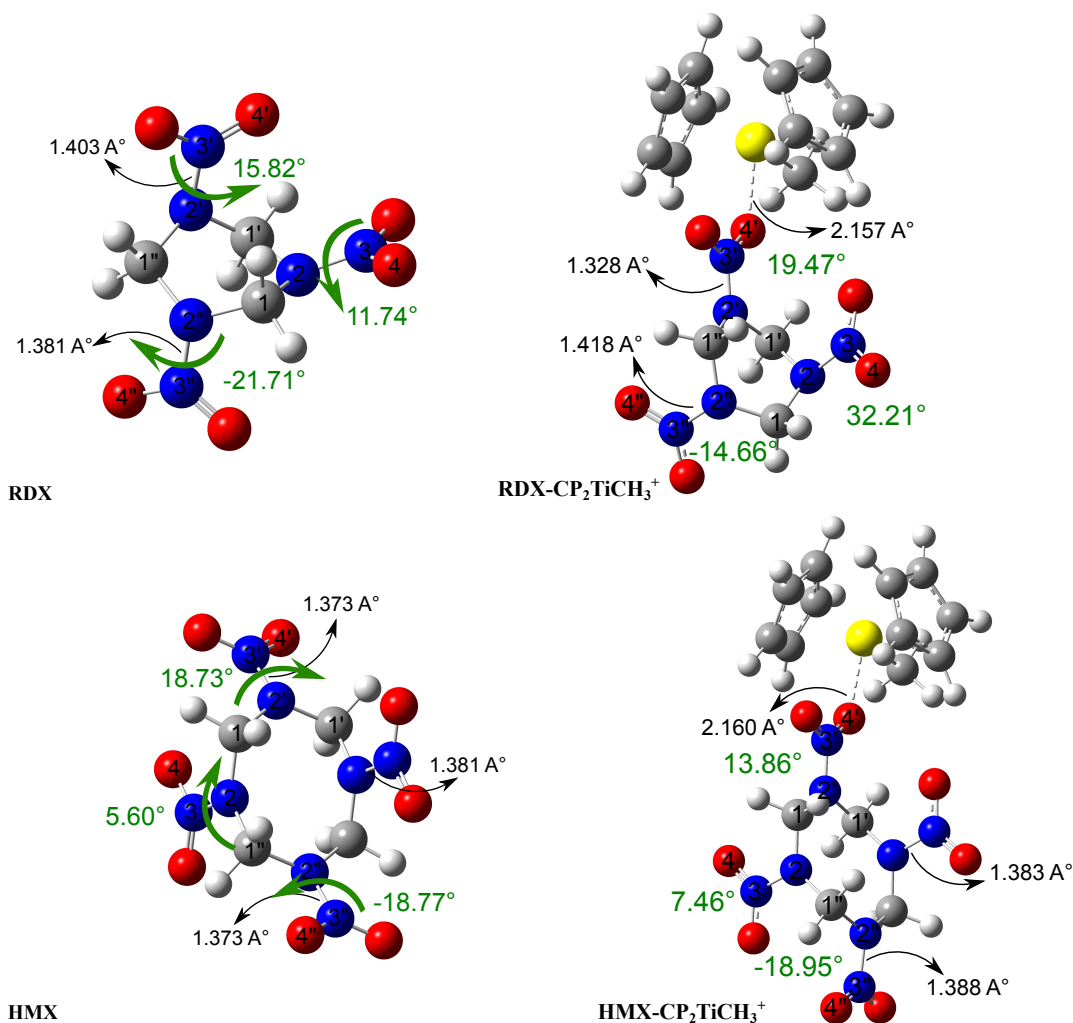


Figure 3: Dihedral angle values of some N-NO₂ bonds.

Table 1: Dihedral angle values (in °) of some N-NO₂ bonds in the isolated molecules and complexes

Atom label	RDX	RDX-Cp ₂ Ti(CH ₃) ⁺	RDX-Cp ₂ Zr(CH ₃) ⁺	RDX-Cp ₂ Hf(CH ₃) ⁺
1C-2N-3N-4O	11.74	32.21	32.98	32.79
1'C-2'N-3'N-4'O	15.82	19.47	19.95	19.17
1''C-2''N-3''N-4''O	-21.71	-14.66	-14.45	-14.29
Atom label	HMX	HMX-Cp ₂ Ti(CH ₃) ⁺	HMX-Cp ₂ Zr(CH ₃) ⁺	HMX-Cp ₂ Hf(CH ₃) ⁺
1C-2N-3N-4O	5.60	7.46	7.63	7.68
1'C-2'N-3'N-4'O	18.73	13.86	14.29	13.88
1''C-2''N-3''N-4''O	-18.77	-18.95	-18.93	-18.82

For RDX... MMCs complexes, the dihedral angle involving the nitro group influenced by the $O \cdots M = \{Ti, Zr, Hf\}$ interactions, increases from 15.8° to 19.9°. In contrast,

the adjacent NO₂ group (defined by atoms 1C-2N-3N-4O) increases from 11.7° to 32.9°. For HMX···MMCs complexes, the dihedral angle involving the nitro group impacted by the $O\cdots M = \{Ti, Zr, Hf\}$ interactions, decreases from 18.7° to 13.8°. Unlike the previous case, the intermolecular interaction seems to favor planarity by reducing the dihedral angle. While, the adjacent NO₂ group increases from 5.6° to 7.6°. The dihedral angle defined by atoms 1" C-2" N-3" N-4" O in HMX almost hasn't changed after complexation, and seems to correlate with the N-NO₂ bond lengths which are roughly the same before and after complexation. In light of these results, the hypothesis of activation of adjacent N-NO₂ bonds caused by an increase in the dihedral angle seems to be conclusive, especially for RDX···MMCs complexes where the effect is more pronounced. Although, it is not straightforward to separate the individual contributions of steric effects, electron withdrawing effect of NO₂ groups, and enhancement of the dihedral angles. Probably, all these effects act concurrently.

Table 2: Topological properties of the electron density calculated at the (3,-1) bond critical point of the N-NO₂ bonds.

Comp.	Bonds	dist. ^a	$\rho(r_B)^b$	$\nabla^2\rho(r_B)^c$	$H(r_B)^d$	$V(r_B)^e$	$G(r_B)^f$	$-V(r_B)/G(r_B)^g$	
RDX	N7—N10	1.403	0.3363	-0.6040	-0.3205	-0.49001	0.16950	2.8909	
	N8—N12	1.400	0.3382	-0.6089	-0.3231	-0.49396	0.17086	2.8910	
	N9—N11	1.376	0.3567	-0.6848	-0.3530	-0.53491	0.18184	2.9416	
	RDX-Cp ₂ Ti(CH ₃) ⁺	N28—N32	1.328	0.3938	-0.8294	-0.4222	-0.63721	0.21492	2.9648
		N34—N37	1.418	0.3263	-0.5723	-0.3050	-0.46699	0.16195	2.8835
RDX-Cp ₂ Zr(CH ₃) ⁺	N29—N40	1.406	0.3355	-0.6082	-0.3202	-0.48839	0.16817	2.9041	
	N28—N32	1.323	0.3977	-0.8440	-0.4299	-0.64890	0.21893	2.9639	
	N34—N37	1.419	0.3256	-0.5694	-0.3037	-0.46521	0.16142	2.8819	
RDX-Cp ₂ Hf(CH ₃) ⁺	N29—N40	1.407	0.3345	-0.6050	-0.3186	-0.48612	0.16742	2.9035	
	N28—N32	1.321	0.3993	-0.8497	-0.4329	-0.65338	0.22048	2.9634	
	N34—N37	1.420	0.3254	-0.5688	-0.3035	-0.46479	0.16129	2.8817	
RDX-Cp ₂ Hf(CH ₃) ⁺	N29—N40	1.408	0.3340	-0.6034	-0.3179	-0.48502	0.16708	2.9029	
	HMX	N14—N27	1.374	0.3581	-0.6868	-0.3549	-0.53828	0.18328	2.9369
		N13—N28	1.380	0.3535	-0.6674	-0.3475	-0.52816	0.18065	2.9236
N15—N26		1.374	0.3581	-0.6868	-0.3549	-0.53828	0.18328	2.9369	
N16—N25		1.380	0.3535	-0.6674	-0.3475	-0.52816	0.18065	2.9236	
HMX-Cp ₂ Ti(CH ₃) ⁺		N28—N32	1.328	0.3938	-0.8272	-0.4223	-0.63778	0.21548	2.9598
	N29—N39	1.383	0.3520	-0.6690	-0.3462	-0.52526	0.17900	2.9344	
	N47—N48	1.388	0.3479	-0.6556	-0.3390	-0.51412	0.17510	2.9361	
HMX-Cp ₂ Zr(CH ₃) ⁺	N34—N36	1.389	0.3476	-0.6536	-0.3388	-0.51426	0.17542	2.9315	
	N28—N32	1.323	0.3978	-0.8422	-0.4301	-0.64976	0.21960	2.9588	
	N29—N39	1.384	0.3511	-0.6656	-0.3447	-0.52298	0.17828	2.9334	
HMX-Cp ₂ Hf(CH ₃) ⁺	N47—N48	1.389	0.3475	-0.6540	-0.3383	-0.51308	0.17478	2.9355	
	N34—N36	1.390	0.3469	-0.6510	-0.3376	-0.51246	0.17485	2.9308	
	N28—N32	1.322	0.3989	-0.8462	-0.4323	-0.65312	0.22078	2.9582	
HMX-Cp ₂ Hf(CH ₃) ⁺	N29—N39	1.384	0.3508	-0.6644	-0.3441	-0.52213	0.17800	2.9333	
	N47—N48	1.389	0.3474	-0.6537	-0.3381	-0.51288	0.17472	2.9354	
	N34—N36	1.390	0.3468	-0.6505	-0.3373	-0.51209	0.17473	2.9307	

^aBond distance (Å), ^bElectron density ($e\text{Å}^{-3}$), ^cLaplacian of the electron density ($e\text{Å}^{-5}$), ^dTotal electron energy density ($\text{hartree}\text{Å}^{-3}$), ^ePotential electron energy density ($V(r_B)$, $\text{hartree}\text{Å}^{-3}$), ^fKinetic electron energy density ($G(r_B)$, $\text{hartree}\text{Å}^{-3}$). The vector r_B locates the position of the critical point, ^g where $R = -V(r_B)/G(r_B)$.

Appendix B

Optimised geometrical structures

For molecular optimisation, we set up a net charge equals +1, and a spin–multiplicity equals 1 (closed–shell systems) for each metallocene methyl cation, and FOX-7···MMC complex. For FOX-7, the net charge was set up equals 0 and the spin–multiplicity equals 1.

Table 3: Topological properties of the electron density calculated at the (3,-1) bond critical point of the C-NO₂ trigger bonds.

Compound	Bond	dist. ^a	$\rho(r_B)^b$	$\nabla^2\rho(r_B)^c$	$H(r_B)^d$	$V(r_B)^e$	$G(r_B)^f$	$-V(r_B)/G(r_B)$
CAM-B3LYP								
FOX-7	C2-N10	1.4255	0.2868	-0.7904	-0.4091	-0.6207	0.2115	2.9347
	C2-N9	1.4255	0.2868	-0.7904	-0.4091	-0.6206	0.2115	2.9342
(H ₂ N) ₂ C=C(NO ₂)-(O)NO···Cp ₂ TiCH ₃ ⁺	C26-N34	1.3730	0.3057	-0.3639	-0.4885	-0.8862	0.3976	2.2288
	C26-N33	1.4501	0.2789	-0.8201	-0.3587	-0.5123	0.1536	3.3352
(H ₂ N) ₂ C=C(NO ₂)-(O)NO···Cp ₂ ZrCH ₃ ⁺	C26-N34	1.3664	0.3090	-0.3261	-0.4957	-0.9100	0.4142	2.1970
	C26-N33	1.4535	0.2780	-0.8180	-0.3501	-0.4957	0.1456	3.4045
(H ₂ N) ₂ C=C(NO ₂)-(O)NO···Cp ₂ HfCH ₃ ⁺	C26-N34	1.3644	0.3100	-0.3125	-0.4977	-0.9172	0.4195	2.1864
	C26-N33	1.4545	0.2778	-0.8174	-0.3475	-0.4907	0.1431	3.4290
(O ₂ N) ₂ C=C(NH ₂)-(H)HN···Cp ₂ TiCH ₃ ⁺	C25-N27	1.4480	0.2805	-0.8341	-0.3608	-0.5132	0.1523	3.3696
	C25-N28	1.4365	0.2826	-0.8092	-0.3915	-0.5808	0.1892	3.0697
(O ₂ N) ₂ C=C(NH ₂)-(H)HN···Cp ₂ ZrCH ₃ ⁺	C25-N27	1.4436	0.2827	-0.8427	-0.3673	-0.5240	0.1566	3.3461
	C25-N28	1.4375	0.2816	-0.7983	-0.3927	-0.5858	0.1931	3.0336
(O ₂ N) ₂ C=C(NH ₂)-(H)HN···Cp ₂ HfCH ₃ ⁺	C25-N27	1.4485	0.2805	-0.8355	-0.3590	-0.5091	0.1501	3.3917
	C25-N28	1.4369	0.2824	-0.8104	-0.3905	-0.5785	0.1879	3.0787
WB97X-D								
FOX-7	C2-N10	1.4269	0.2883	-0.7831	-0.3994	-0.6314	0.2123	2.9741
	C2-N9	1.4269	0.2883	-0.7831	-0.3994	-0.6314	0.2123	2.9741
(H ₂ N) ₂ C=C(NO ₂)-(O)NO···Cp ₂ TiCH ₃ ⁺	C26-N34	1.3732	0.3047	-0.3489	-0.4852	-0.8833	0.3980	2.2193
	C26-N33	1.4517	0.2776	-0.8098	-0.3541	-0.5058	0.1517	3.3342
(H ₂ N) ₂ C=C(NO ₂)-(O)NO···Cp ₂ ZrCH ₃ ⁺	C26-N34	1.3638	0.3078	-0.3126	-0.4920	-0.9058	0.4138	2.1889
	C26-N33	1.4548	0.2768	-0.8075	-0.3462	-0.4906	0.1444	3.3975
(H ₂ N) ₂ C=C(NO ₂)-(O)NO···Cp ₂ HfCH ₃ ⁺	C26-N34	1.3646	0.3089	-0.2988	-0.4943	-0.9139	0.4196	2.1780
	C26-N33	1.4557	0.2766	-0.8069	-0.3439	-0.4862	0.1422	3.4191
(O ₂ N) ₂ C=C(NH ₂)-(H)HN···Cp ₂ TiCH ₃ ⁺	C25-N27	1.4482	0.2798	-0.8265	-0.3591	-0.5117	0.1525	3.3554
	C25-N28	1.4374	0.2816	-0.8017	-0.3878	-0.5752	0.1873	3.0710
(O ₂ N) ₂ C=C(NH ₂)-(H)HN···Cp ₂ ZrCH ₃ ⁺	C25-N27	1.4478	0.2801	-0.8275	-0.3596	-0.5123	0.1527	3.3549
	C25-N28	1.4367	0.2819	-0.8022	-0.3893	-0.5781	0.1887	3.0635
(O ₂ N) ₂ C=C(NH ₂)-(H)HN···Cp ₂ HfCH ₃ ⁺	C25-N27	1.4481	0.2801	-0.8283	-0.3585	-0.5100	0.1514	3.3685
	C25-N28	1.4372	0.2817	-0.8028	-0.3881	-0.5755	0.1874	3.0709

^aBond distance (Å), ^bElectron density ($e\text{Å}^{-3}$), ^cLaplacian of the electron density ($e\text{Å}^{-5}$), ^dTotal electron energy density ($\text{hartree}\text{Å}^{-3}$), ^ePotential electron energy density ($V(r_B)$, $\text{hartree}\text{Å}^{-3}$), ^fKinetic electron energy density ($G(r_B)$, $\text{hartree}\text{Å}^{-3}$). The vector r_B locates the position of the critical point. The atoms in bold (Bond column) denote the C-NO₂ bond, for which the carbon atom is not interacting with MMC.

Table 4: Topological properties of the electron density calculated at the (3,-1) bond critical point for the $\{O, N\} = X \cdots M = \{Ti, Zr, Hf\}$ bonding.

Compound	Bond	dist. ^a	$\rho(r_B)^b$	$\nabla^2\rho(r_B)^c$	$H(r_B)^d$	$V(r_B)^e$	$G(r_B)^f$	$-V(r_B)/G(r_B)$
CAM-B3LYP								
$(H_2N)_2C=C(NO_2)-(O)NO \cdots C_{P_2}TiCH_3^+$	Ti39...O37	2.1002	0.0625	0.2990	0.0001	-0.0744	0.0746	0.9973
$(H_2N)_2C=C(NO_2)-(O)NO \cdots C_{P_2}ZrCH_3^+$	Zr39...O37	2.2255	0.0580	0.3005	0.0041	-0.0667	0.0709	0.9407
$(H_2N)_2C=C(NO_2)-(O)NO \cdots C_{P_2}HfCH_3^+$	Hf39...O37	2.2050	0.0622	0.3383	0.0042	-0.0680	0.0722	0.9418
$(O_2N)_2C=C(NH_2)-(H)HN \cdots C_{P_2}TiCH_3^+$	Ti31...N30	2.3060	0.0426	0.1292	-0.0027	-0.0378	0.0351	1.0769
$(O_2N)_2C=C(NH_2)-(H)HN \cdots C_{P_2}ZrCH_3^+$	Zr31...N30	2.4512	0.0418	0.1507	0.0008	-0.0359	0.0367	0.9782
$(O_2N)_2C=C(NH_2)-(H)HN \cdots C_{P_2}HfCH_3^+$	Hf31...N30	2.4055	0.0453	0.1663	0.0002	-0.0369	0.0371	0.9946
WB97X-D								
$(H_2N)_2C=C(NO_2)-(O)NO \cdots C_{P_2}TiCH_3^+$	Ti39...O37	2.1071	0.0614	0.2935	0.0003	-0.0726	0.0730	0.9945
$(H_2N)_2C=C(NO_2)-(O)NO \cdots C_{P_2}ZrCH_3^+$	Zr39...O37	2.2356	0.0571	0.2926	0.0040	-0.0649	0.0690	0.9405
$(H_2N)_2C=C(NO_2)-(O)NO \cdots C_{P_2}HfCH_3^+$	Hf39...O37	2.2084	0.0618	0.3357	0.0042	-0.0674	0.0716	0.9413
$(O_2N)_2C=C(NH_2)-(H)HN \cdots C_{P_2}TiCH_3^+$	Ti31...N30	2.3058	0.0491	0.1514	-0.0040	-0.0460	0.0419	1.0978
$(O_2N)_2C=C(NH_2)-(H)HN \cdots C_{P_2}ZrCH_3^+$	Zr31...N30	2.4294	0.0468	0.1710	0.0002	-0.0422	0.0425	0.9929
$(O_2N)_2C=C(NH_2)-(H)HN \cdots C_{P_2}HfCH_3^+$	Hf31...N30	2.4076	0.0499	0.1871	-0.0004	-0.0427	0.0423	1.0094

^aBond distance (\AA), ^bElectron density ($e \text{\AA}^{-3}$), ^cLaplacian of the electron density ($e \text{\AA}^{-5}$), ^dTotal electron energy density ($\text{hartree} \text{\AA}^{-3}$), ^ePotential electron energy density ($V(r_B)$, $\text{hartree} \text{\AA}^{-3}$), ^fKinetic electron energy density ($G(r_B)$, $\text{hartree} \text{\AA}^{-3}$). The vector r_B locates the position of the critical point. All quantities are in atomic units.

Table 5: Topological properties of the electron density calculated at the (3,-1) bond critical point of the C-NH₂ bonds.

Comp	Bond	Dist. ^a	$\rho(r_B)^b$	$\nabla^2\rho(r_B)^c$	$H(r_B)^d$	$V(r_B)^e$	$G(r_B)^f$	$-V(r_B)/G(r_B)$
CAM-B3LYP								
FOX-7	C1-N3	1.3390	0.3449	-1.1856	-0.5536	-0.8108	0.2572	3.1524
	C1-N6	1.3390	0.3449	-1.1855	-0.5536	-0.8108	0.2572	3.1524
$(H_2N)_2C=C(NO_2)-(O)NO \cdots C_{P_2}TiCH_3^+$	C25-N30	1.3300	0.3495	-1.0903	-0.5826	-0.8926	0.3100	2.8793
$(H_2N)_2C=C(NO_2)-(O)NO \cdots C_{P_2}ZrCH_3^+$	C25-N27	1.3296	0.3504	-1.1121	-0.5836	-0.8892	0.3056	2.9096
	C25-N30	1.3289	0.3502	-1.0864	-0.5848	-0.8981	0.3132	2.8674
$(H_2N)_2C=C(NO_2)-(O)NO \cdots C_{P_2}HfCH_3^+$	C25-N27	1.3288	0.3510	-1.1105	-0.5853	-0.8929	0.3076	2.9027
	C25-N30	1.3286	0.3504	-1.0852	-0.5853	-0.8994	0.3140	2.8643
$(O_2N)_2C=C(NH_2)-(H)HN \cdots C_{P_2}TiCH_3^+$	C25-N27	1.3286	0.3512	-1.1103	-0.5857	-0.8939	0.3081	2.9013
	C26-N30	1.4172	0.3025	-1.0128	-0.3783	-0.5035	0.1251	4.0247
$(O_2N)_2C=C(NH_2)-(H)HN \cdots C_{P_2}ZrCH_3^+$	C26-N29	1.3271	0.3509	-1.0514	-0.5878	-0.9127	0.3249	2.8091
	C26-N30	1.4162	0.3020	-1.0198	-0.3837	-0.5125	0.1287	3.9821
$(O_2N)_2C=C(NH_2)-(H)HN \cdots C_{P_2}HfCH_3^+$	C26-N29	1.3266	0.3513	-1.0604	-0.5881	-0.9111	0.3230	2.8207
	C26-N30	1.4227	0.2982	-0.9874	-0.3699	-0.4930	0.1230	4.0081
	C26-N29	1.3262	0.3518	-1.0574	-0.5898	-0.9153	0.3254	2.8128
WB97XD								
FOX-7	C1-N3	1.3394	0.3450	-1.1863	-0.5637	-0.8125	0.2531	3.2109
	C1-N6	1.3394	0.3450	-1.1863	-0.5637	-0.8125	0.2531	3.2109
$(H_2N)_2C=C(NO_2)-(O)NO \cdots C_{P_2}TiCH_3^+$	C25-N30	1.3310	0.3464	-1.0451	-0.5756	-0.8900	0.3143	2.8316
$(H_2N)_2C=C(NO_2)-(O)NO \cdots C_{P_2}ZrCH_3^+$	C25-N27	1.3309	0.3472	-1.0674	-0.5762	-0.8857	0.3094	2.8626
	C25-N30	1.3300	0.3471	-1.0413	-0.5777	-0.8950	0.3173	2.8206
$(H_2N)_2C=C(NO_2)-(O)NO \cdots C_{P_2}HfCH_3^+$	C25-N27	1.3301	0.3478	-1.0658	-0.5779	-0.8894	0.3114	2.8561
	C25-N30	1.3296	0.3473	-1.0400	-0.5783	-0.8966	0.3183	2.8168
$(O_2N)_2C=C(NH_2)-(H)HN \cdots C_{P_2}TiCH_3^+$	C25-N27	1.3299	0.3479	-1.0655	-0.5783	-0.8903	0.3119	2.8544
	C26-N30	1.4145	0.3024	-1.0177	-0.3861	-0.5179	0.1317	3.9324
$(O_2N)_2C=C(NH_2)-(H)HN \cdots C_{P_2}ZrCH_3^+$	C26-N29	1.3287	0.3476	-1.0120	-0.5795	-0.9060	0.3265	2.7748
	C26-N30	1.4151	0.3009	-1.0121	-0.3868	-0.5206	0.1338	3.8908
$(O_2N)_2C=C(NH_2)-(H)HN \cdots C_{P_2}HfCH_3^+$	C26-N29	1.3285	0.3479	-1.0194	-0.5799	-0.9049	0.3250	2.7843
	C26-N30	1.4118	0.2990	-0.9986	-0.3807	-0.5117	0.1310	3.9061
	C26-N29	1.3279	0.3484	-1.0187	-0.5812	-0.9077	0.3265	2.7800

^aBond distance (\AA), ^bElectron density ($e \text{\AA}^{-3}$), ^cLaplacian of the electron density ($e \text{\AA}^{-5}$), ^dTotal electron energy density ($\text{hartree} \text{\AA}^{-3}$), ^ePotential electron energy density ($V(r_B)$, $\text{hartree} \text{\AA}^{-3}$), ^fKinetic electron energy density ($G(r_B)$, $\text{hartree} \text{\AA}^{-3}$). The vector r_B locates the position of the critical point. The atoms in bold (Bond column) denote the C-NH₂ bond, for which the carbon atom is not interacting with MMC.

Table 6: Results of the EDA-NOCV calculations at DFT/revPBE-D3(BJ)/TZ2P^[a] level of theory. All the values are in *kcal/mol*.

Complex	ΔE_{Pauli}	ΔE_{orb}	ΔE_{elstat}	ΔE_{disp}	ΔE_{int}
CAM-B3LYP^[b]					
(H ₂ N) ₂ C=C(NO ₂)-(O)NO... Cp ₂ TiCH ₃ ⁺	52.06	-36.71	-50.07	-10.76	-45.48
(H ₂ N) ₂ C=C(NO ₂)-(O)NO... Cp ₂ ZrCH ₃ ⁺	45.10	-35.40	-49.40	-8.77	-50.47
(H ₂ N) ₂ C=C(NO ₂)-(O)NO... Cp ₂ HfCH ₃ ⁺	51.12	-41.58	-55.04	-8.76	-54.26
(O ₂ N) ₂ C=C(NH ₂)-(H)HN... Cp ₂ TiCH ₃ ⁺	45.88	-28.44	-25.67	-16.73	-24.96
(O ₂ N) ₂ C=C(NH ₂)-(H)HN... Cp ₂ ZrCH ₃ ⁺	40.47	-28.14	-25.55	-15.18	-28.40
(O ₂ N) ₂ C=C(NH ₂)-(H)HN... Cp ₂ HfCH ₃ ⁺	46.58	-32.19	-31.04	-14.55	-31.20
WB97X-D^[b]					
(H ₂ N) ₂ C=C(NO ₂)-(O)NO... Cp ₂ HfCH ₃ ⁺	52.69	-36.39	-50.54	-10.96	-45.20
(H ₂ N) ₂ C=C(NO ₂)-(O)NO... Cp ₂ ZrCH ₃ ⁺	45.64	-36.84	-49.93	-9.12	-50.25
(H ₂ N) ₂ C=C(NO ₂)-(O)NO... Cp ₂ HfCH ₃ ⁺	51.94	-41.40	-55.55	-9.07	-54.08
(O ₂ N) ₂ C=C(NH ₂)-(H)HN... Cp ₂ TiCH ₃ ⁺	54.26	-32.61	-32.12	-17.65	-28.12
(O ₂ N) ₂ C=C(NH ₂)-(H)HN... Cp ₂ ZrCH ₃ ⁺	47.70	-31.45	-30.76	-16.01	-30.52
(O ₂ N) ₂ C=C(NH ₂)-(H)HN... Cp ₂ HfCH ₃ ⁺	54.57	-35.37	-37.57	-15.74	-34.11

[a] The EDA-NOCV method was conducted from a single point calculation at DFT/revPBE-D3(BJ)/TZ2P level of theory. [b] The molecular structures were fully optimized with CAM-B3LYP and WB97X-D density functionals.

Table 7: Results of the EDA-NOCV calculations obtained using several density functionals^[a]. All the values are in *kcal/mol*.

Complex	Functional	ΔE_{Pauli}	ΔE_{orb}	ΔE_{elstat}	ΔE_{disp}	$\Delta E_{int}^{[b]}$
		(3.01) ^[c]	(0.74) ^[c]	(0.83) ^[c]	(3.25) ^[c]	(0.55) ^[c]
$(O_2N)_2C=C(NH_2)-(H)HN \cdots Cp_2TiCH_3^+$	BLYP-D3BJ	46.01	-28.59 (39.95%)	-26.95 (37.66%)	-16.02 (22.38%)	-25.54
	PBE-D3BJ	39.43	-29.29 (45.94%)	-26.04 (40.84%)	-8.42 (13.20%)	-24.32
	TPSS-D3BJ	40.03	-28.95 (44.30%)	-25.41 (38.88%)	-10.98 (16.80%)	-25.31
	B3LYP-D3BJ	42.79	-27.58 (40.43%)	-27.21 (39.89%)	-13.41 (19.66%)	-25.41
		(2.65) ^[c]	(0.64) ^[c]	(0.79) ^[c]	(3.10) ^[c]	(0.80) ^[c]
$(O_2N)_2C=C(NH_2)-(H)HN \cdots Cp_2ZrCH_3^+$	BLYP-D3BJ	40.70	-28.45 (40.41%)	-26.86 (38.15%)	-15.09 (21.43%)	-29.71
	PBE-D3BJ	34.60	-28.90 (45.11%)	-25.91 (41.34%)	-7.86 (12.54%)	-28.08
	TPSS-D3BJ	35.74	-28.70 (44.50%)	-25.41 (39.40%)	-10.37 (16.08%)	-28.74
	B3LYP-D3BJ	37.51	-27.44 (40.80%)	-27.11 (40.31%)	-12.70 (18.88%)	-29.74
		(2.94) ^[c]	(0.79) ^[c]	(0.90) ^[c]	(2.98) ^[c]	(0.57) ^[c]
$(O_2N)_2C=C(NH_2)-(H)HN \cdots Cp_2HfCH_3^+$	BLYP-D3BJ	47.27	-32.56 (40.87%)	-32.58 (40.90%)	-14.51 (18.21%)	-32.38
	PBE-D3BJ	40.83	-32.99 (45.83%)	31.42 (43.65%)	-7.57 (10.51%)	-31.15
	TPSS-D3BJ	41.27	-32.53 (44.45%)	-30.68 (41.92%)	-9.97 (13.62%)	-31.91
	B3LYP-D3BJ	43.47	-31.16 (41.09%)	-32.42 (42.75%)	-12.24 (16.14%)	-32.34
		(2.33) ^[c]	(0.89) ^[c]	(1.26) ^[c]	(2.10) ^[c]	(0.49) ^[c]
$(H_2N)_2C=C(NO_2)-(O)NO \cdots Cp_2TiCH_3^+$	BLYP-D3BJ	51.08	-36.97 (37.11%)	-52.14 (52.34%)	-10.49 (10.53%)	-47.80
	PBE-D3BJ	46.04	-37.33 (40%)	-50.40 (54.01%)	-5.58 (5.98%)	-47.28
	TPSS-D3BJ	46.37	-37.00 (39.14%)	-50.22 (53.13%)	-7.30 (7.72%)	-48.14
	B3LYP-D3BJ	48.53	-35.35 (36.46%)	-52.76 (54.42%)	-8.83 (9.10%)	-48.42
		(2.21) ^[c]	(0.67) ^[c]	(1.09) ^[c]	(1.78) ^[c]	(0.76) ^[c]
$(H_2N)_2C=C(NO_2)-(O)NO \cdots Cp_2ZrCH_3^+$	BLYP-D3BJ	45.11	-37.88 (38.55%)	-51.42 (52.34%)	-8.94 (9.10%)	-53.13
	PBE-D3BJ	40.08	-37.91 (41.09%)	-49.60 (53.76%)	-4.74 (5.13%)	-52.18
	TPSS-D3BJ	40.78	-37.65 (40.19%)	-49.75 (53.11%)	-6.26 (6.68%)	-52.88
	B3LYP-D3BJ	41.74	-36.49 (38.10%)	-51.69 (53.98%)	-7.57 (7.90%)	-54.02
		(2.57) ^[c]	(0.82) ^[c]	(1.15) ^[c]	(1.80) ^[c]	(0.56) ^[c]
$(H_2N)_2C=C(NO_2)-(O)NO \cdots Cp_2HfCH_3^+$	BLYP-D3BJ	51.52	-42.08 (38.81%)	-57.37 (52.91%)	-8.96 (8.26%)	-56.88
	PBE-D3BJ	46.04	-42.11 (41.20%)	-55.34 (54.15%)	-4.74 (4.63%)	-56.15
	TPSS-D3BJ	46.11	-41.70 (40.45%)	-55.12 (53.47%)	-6.26 (6.07%)	-56.97
	B3LYP-D3BJ	47.51	-40.35 (38.41%)	-57.10 (54.36%)	-7.59 (7.22%)	-57.53

[a] The calculated standard deviations are fairly high for ΔE_{disp} and ΔE_{Pauli} . Dispersive term is associated with a relatively high standard deviation. It is well known in the literature that the dispersion corrections are density functional dependent. Indeed, in DFT calculation, the dispersion interaction is frequently modeled using an energy correction that implies empirically fitted parameters for all-atom pairs of the chemical system under study. On the other hand, the Pauli term expresses an energy increase due to the repulsion between the occupied molecular orbitals of the two fragments. This term is also known as the exchange-repulsion term. Thus it strongly depends upon the exchange part of the considered functional. [b] The interaction energy is calculated according to: $\Delta E_{int} = \Delta E_{Pauli} + \Delta E_{orb} + \Delta E_{elstat} + \Delta E_{disp}$. The percentages in parentheses indicate the contribution to the stabilising interactions (attractive terms). [c] The numbers in parentheses highlight the standard deviation (σ_{n-1}) for each energetic term.

Table 8: Atomic coordinates for $(\text{H}_2\text{N})_2\text{C}=\text{C}(\text{NO}_2)-(\text{O})\text{NO}\cdots\text{Cp}_2\text{MCH}_3^+$ (CAM-B3LYP).

Compound	$(\text{H}_2\text{N})_2\text{C}=\text{C}(\text{NO}_2)-(\text{O})\text{NO}\cdots\text{Cp}_2\text{TiCH}_3^+$			$(\text{H}_2\text{N})_2\text{C}=\text{C}(\text{NO}_2)-(\text{O})\text{NO}\cdots\text{Cp}_2\text{ZrCH}_3^+$			$(\text{H}_2\text{N})_2\text{C}=\text{C}(\text{NO}_2)-(\text{O})\text{NO}\cdots\text{Cp}_2\text{HfCH}_3^+$		
Atom labels	X	Y	Z	X	Y	Z	X	Y	Z
C1	-0.6813	-1.3582	0.7015	-0.7664	-1.3068	0.8294	0.7210	-1.2983	0.8263
H2	-0.1050	-2.2172	1.0122	-0.1908	-2.1669	1.1425	-0.1259	-2.1473	1.1330
C3	-0.2232	-0.0285	0.6643	-0.3148	0.0300	0.8053	-0.2919	0.0465	0.7912
H4	0.7810	0.2958	0.8990	0.6804	0.3642	1.0670	0.7004	0.3979	1.0403
C5	-1.2828	0.7915	0.2210	-1.3846	0.8494	0.3703	-1.3811	0.8468	0.3699
C6	-2.0425	-1.3593	0.2971	-2.1278	-1.3130	0.4202	-2.0883	-1.3286	0.4387
H7	-2.6921	-2.2218	0.2580	-2.7740	-2.1793	0.3797	-2.7203	-2.2057	0.4088
C8	-2.4124	-0.0281	0.0070	-2.5094	0.0224	0.1490	-2.4948	-0.0005	0.1668
H9	-3.3835	0.3044	-0.3299	-3.4862	0.3529	-0.1745	-3.4802	0.3129	-0.1481
C10	-0.3529	-3.0391	-1.7748	-0.2144	-3.0878	-1.8820	-0.2576	-3.0994	-1.8687
C11	0.6462	-2.3706	-2.5007	0.6807	-2.3838	-2.7133	0.6821	-2.4085	-2.6615
H12	1.7021	-2.3727	-2.2660	1.7536	-2.3309	-2.5818	1.7504	-2.3795	-2.4907
C13	0.0241	-1.6766	-3.5703	-0.0693	-1.7694	-3.7501	-0.0166	-1.7770	-3.7247
C14	-1.6018	-2.7465	-2.3791	-1.5242	-2.9086	-2.4021	-1.5435	-2.8899	-2.4338
H15	-2.5649	-3.1277	-2.0698	-2.4289	-3.3567	-2.0139	-2.4714	-3.3193	-2.0802
C16	-1.3596	-1.9280	-3.5065	-1.4268	-2.1111	-3.5687	-1.3862	-2.0907	-3.5937
H17	-2.1060	-1.5539	-4.1904	-2.2478	-1.8109	-4.2036	-2.1775	-1.7676	-4.2545
H18	0.5171	-1.0375	-4.2901	0.3286	-1.1474	-4.5414	0.4213	-1.1611	-4.4994
C19	-1.9604	0.6356	-2.7045	-2.2112	0.6416	-2.7810	-2.1857	0.6719	-2.7847
H20	-1.4877	0.7520	-3.6829	-1.8130	0.7637	-3.7953	-1.7997	0.8044	-3.8028
H21	-1.9795	1.6074	-2.2073	-2.2767	1.6338	-2.3203	-2.2647	1.6651	-2.3277
H22	-2.9938	0.3116	-2.8557	-3.2358	0.2670	-2.8805	-3.2099	0.2926	-2.8847
H23	-1.2343	1.8584	0.0539	-1.3532	1.9230	0.2394	-1.3702	1.9201	0.2340
H24	-0.1993	-3.6637	-0.9073	0.0510	-3.6804	-1.0175	-0.0369	-3.6986	-0.9964
C25	4.1918	1.8141	-2.1308	4.3334	1.8223	-2.1165	4.3064	1.8132	-2.1207
C26	2.8240	1.5088	-2.4741	2.9557	1.5618	-2.4673	2.9279	1.5560	-2.4722
N27	4.8089	2.8432	-2.7037	4.9856	2.8278	-2.6906	4.9583	2.8205	-2.6915
H28	4.2718	3.4924	-3.2692	4.4716	3.4960	-3.2558	4.4441	3.4931	-3.2513
H29	5.7881	3.0196	-2.5326	5.9676	2.9782	-2.5099	5.9404	2.9707	-2.5103
N30	4.8591	1.0685	-1.2546	4.9679	1.0558	-1.2357	4.9401	1.0418	-1.2439
H31	5.7901	1.3277	-0.9617	5.9078	1.2791	-0.9407	5.8809	1.2617	-0.9491
H32	4.4047	0.2588	-0.8489	4.4796	0.2686	-0.8242	4.4512	0.2537	-0.8349
N33	2.1873	2.1531	-3.6064	2.3474	2.2317	-3.6048	2.3212	2.2316	-3.6085
N34	2.0801	0.5762	-1.7942	2.1809	0.6592	-1.7949	2.1531	0.6527	-1.8047
O35	2.4779	3.3325	-3.8145	2.6642	3.4076	-3.7907	2.6306	3.4113	-3.7807
O36	1.4465	1.4962	-4.3101	1.6080	1.5955	-4.3261	1.5923	1.5953	-4.3396
O37	0.8320	0.5750	-1.9658	0.9316	0.6771	-1.9953	0.9023	0.6729	-2.0113
O38	2.6054	-0.2137	-0.9948	2.6633	-0.1329	-0.9724	2.6303	-0.1415	-0.9819
M39={ Ti,Zr,Hf}	-0.7763	-0.7134	-1.5606	-0.8045	-0.6565	-1.5951	-0.8108	-0.6529	-1.5998

Table 9: Atomic coordinates for $(\text{O}_2\text{N})_2\text{C}=\text{C}(\text{NH}_2)-(\text{H})\text{HN}\cdots\text{Cp}_2\text{TiCH}_3^+$ (CAM-B3LYP).

Compound	$(\text{O}_2\text{N})_2\text{C}=\text{C}(\text{NH}_2)-(\text{H})\text{HN}\cdots\text{Cp}_2\text{TiCH}_3^+$			$(\text{O}_2\text{N})_2\text{C}=\text{C}(\text{NH}_2)-(\text{H})\text{HN}\cdots\text{Cp}_2\text{ZrCH}_3^+$			$(\text{O}_2\text{N})_2\text{C}=\text{C}(\text{NH}_2)-(\text{H})\text{HN}\cdots\text{Cp}_2\text{HfCH}_3^+$		
Atom labels	X	Y	Z	X	Y	Z	X	Y	Z
C1	-0.9514	-1.7503	0.4318	-0.5766	-1.6009	0.7814	-0.8845	-1.6258	0.7039
H2	-0.6268	-2.7726	0.5569	-0.0435	-2.5205	0.9790	-0.4466	-2.5897	0.9227
C3	-0.2599	-0.6074	0.8637	-0.1120	-0.3010	1.0663	-0.3364	-0.3722	1.0442
H4	0.6974	-0.6028	1.3715	0.8463	-0.0601	1.5114	0.5948	-0.2146	1.5757
C5	-1.0494	0.5272	0.5381	-1.1300	0.6192	0.6989	-1.2477	0.6340	0.6214
C6	-2.1528	-1.3283	-0.1930	-1.8838	-1.4888	0.2326	-2.1300	-1.3997	0.0573
H7	-2.9156	-1.9721	-0.6085	-2.5284	-2.3126	-0.0444	-2.8170	-2.1634	-0.2825
C8	-2.2236	0.0806	-0.0950	-2.2299	-0.1157	0.2035	-2.3612	-0.0016	0.0316
H9	-3.0360	0.7012	-0.4425	-3.1700	0.2972	-0.1346	-3.2357	0.4919	-0.3689
C10	0.5401	-2.6067	-1.9879	0.4483	-2.7877	-2.0589	0.5823	-2.7530	-1.9568
C11	1.3636	-1.6546	-2.6132	1.4133	-1.9033	-2.5822	1.4684	-1.8274	-2.5475
H12	2.3980	-1.4651	-2.3626	2.4537	-1.8607	-2.2831	2.4963	-1.6653	-2.2495
C13	0.6013	-0.9971	-3.6065	0.7955	-1.1385	-3.6090	0.7850	-1.1825	-3.6117
C14	-0.7389	-2.5468	-2.6009	-0.7716	-2.5679	-2.7531	-0.6544	-2.6822	-2.6538
H15	-1.5840	-3.1797	-2.3704	-1.6917	-3.1195	-2.6109	-1.5225	-3.3016	-2.4717
C16	-0.6930	-1.5594	-3.6093	-0.5466	-1.5630	-3.7262	-0.5185	-1.7228	-3.6873
H17	-1.5072	-1.2781	-4.2620	-1.2719	-1.1932	-4.4369	-1.2779	-1.4513	-4.4077
H18	0.9481	-0.2118	-4.2636	1.2811	-0.4018	-4.2357	1.1980	-0.4408	-4.2826
C19	-1.4749	0.9888	-2.6200	-1.7075	0.9581	-2.5787	-1.5784	0.9976	-2.7334
H20	-1.0112	1.2001	-3.5874	-1.2784	1.2531	-3.5444	-1.1567	1.1975	-3.7258
H21	-1.5764	1.9174	-2.0466	-1.9286	1.8647	-2.0011	-1.7473	1.9556	-2.2222
H22	-2.4927	0.6501	-2.8395	-2.6819	0.5118	-2.8131	-2.5864	0.6079	-2.9324
H23	-0.8204	1.5574	0.7811	-1.0993	1.6937	0.8315	-1.1451	1.7005	0.7807
H24	0.8460	-3.2834	-1.2036	0.6174	-3.5252	-1.2867	0.8187	-3.4240	-1.1427
C25	3.4667	1.1378	-2.2138	3.3960	1.1649	-2.3401	3.4667	1.2312	-2.3312
C26	2.1327	1.5309	-2.2049	2.1082	1.6863	-2.4024	2.1297	1.6003	-2.2533
N27	4.3143	1.4057	-3.3570	4.3900	1.4771	-3.3393	4.2331	1.4700	-3.5369
N28	4.1036	0.5019	-1.0941	3.8064	0.2729	-1.2902	4.1811	0.6344	-1.2365
N29	1.5950	2.3491	-3.1008	1.6475	2.4240	-3.4042	1.5125	2.3727	-3.1372
N30	1.2502	1.0621	-1.1998	1.1881	1.4151	-1.3605	1.3212	1.1436	-1.1753
M31={ Ti,Zr,Hf}	-0.4128	-0.5034	-1.5178	-0.3630	-0.4806	-1.4570	-0.4120	-0.4934	-1.4957
O32	5.2125	0.6320	-3.6030	5.5602	1.3810	-3.0511	5.1269	0.7025	-3.8150
O33	4.0214	2.3863	-4.0505	3.9659	1.8746	-4.4336	3.8757	2.4203	-4.2419
O34	5.3017	0.5744	-0.9778	4.6604	-0.5517	-1.5215	5.3830	0.7145	-1.2029
O35	3.3665	-0.0775	-0.2630	3.2118	0.3512	-0.1958	3.5048	0.0784	-0.3388
H36	2.2108	2.7952	-3.7765	2.2562	2.5717	-4.2068	2.0693	2.8018	-3.8726
H37	0.5950	2.4894	-3.1302	0.6983	2.7694	-3.4068	0.5047	2.4596	-3.1263
H38	0.7418	1.8498	-0.8015	0.5513	2.2013	-1.2318	0.8501	1.9398	-0.7429
H39	1.8385	0.6058	-0.4773	1.7372	1.2515	-0.5021	1.9742	0.7033	-0.4918

Table 10: Atomic coordinates for $(\text{H}_2\text{N})_2\text{C}=\text{C}(\text{NO}_2)-(\text{O})\text{NO}\cdots\text{Cp}_2\text{MCH}_3^+$ (wB97X-D).

Compound	$(\text{H}_2\text{N})_2\text{C}=\text{C}(\text{NO}_2)-(\text{O})\text{NO}\cdots\text{Cp}_2\text{TiCH}_3^+$			$(\text{H}_2\text{N})_2\text{C}=\text{C}(\text{NO}_2)-(\text{O})\text{NO}\cdots\text{Cp}_2\text{ZrCH}_3^+$			$(\text{H}_2\text{N})_2\text{C}=\text{C}(\text{NO}_2)-(\text{O})\text{NO}\cdots\text{Cp}_2\text{HfCH}_3^+$		
Atom labels	X	Y	Z	X	Y	Z	X	Y	Z
C1	-0.6521	-1.3552	0.6984	-0.6874	-1.2662	0.8268	-0.6755	-1.2796	0.8275
H2	-0.0469	-2.1976	0.9996	-0.0267	-2.0683	1.1257	-0.0152	-2.0842	1.1210
C3	-0.2340	-0.0102	0.6645	-0.3663	0.1106	0.8023	-0.3519	0.0974	0.8102
H4	0.7619	0.3430	0.8923	0.5957	0.5385	1.0503	0.6109	0.5221	1.0610
C5	-1.3196	0.7794	0.2270	-1.5139	0.8245	0.3799	-1.4999	0.8163	0.3969
C6	-2.0168	-1.3954	0.3004	-2.0487	-1.4015	0.4347	-2.0393	-1.4105	0.4420
H7	-2.6381	-2.2783	0.2550	-2.6069	-2.3267	0.3925	-2.5998	-2.3345	0.3973
C8	-2.4268	-0.0742	0.0132	-2.5581	-0.1076	0.1660	-2.5466	-0.1137	0.1816
H9	-3.4063	0.2303	-0.3262	-3.5631	0.1293	-0.1537	-3.5523	0.1273	-0.1342
C10	-0.3935	-3.0326	-1.7622	-0.2139	-3.0344	-1.8864	-0.2655	-3.0512	-1.8726
C11	0.6518	-2.3734	-2.4331	0.7076	-2.3100	-2.6725	0.7107	-2.3462	-2.6101
H12	1.6949	-2.3942	-2.1481	1.7747	-2.2539	-2.5005	1.7707	-2.3252	-2.3928
C13	0.0916	-1.6584	-3.5253	-0.0093	-1.6764	-3.7234	0.0588	-1.6873	-3.6890
C14	-1.6089	-2.7071	-2.4176	-1.5071	-2.8468	-2.4471	-1.5273	-2.8209	-2.4856
H15	-2.5938	-3.0634	-2.1495	-2.4248	-3.2975	-2.0938	-2.4722	-3.2480	-2.1767
C16	-1.2999	-1.8830	-3.5264	-1.3724	-2.0261	-3.5955	-1.3180	-1.9968	-3.6218
H17	-2.0073	-1.4883	-4.2395	-2.1727	-1.7130	-4.2500	-2.0801	-1.6542	-4.3068
H18	0.6266	-1.0195	-4.2147	0.4123	-1.0329	-4.4845	0.5302	-1.0543	-4.4293
C19	-1.9668	0.6435	-2.6896	-2.2549	0.6584	-2.7441	-2.2086	0.7049	-2.7470
H20	-1.4804	0.7846	-3.6596	-1.8497	0.8225	-3.7513	-1.8095	0.8788	-3.7553
H21	-2.0168	1.6096	-2.1814	-2.3681	1.6354	-2.2588	-2.3304	1.6828	-2.2643
H22	-2.9915	0.2993	-2.8634	-3.2626	0.2438	-2.8666	-3.2189	0.2945	-2.8769
H23	-1.3013	1.8468	0.0584	-1.5848	1.8954	0.2452	-1.5709	1.8881	0.2700
H24	-0.2934	-3.6655	-0.8927	0.0216	-3.6373	-1.0203	-0.0856	-3.6664	-1.0019
C25	4.1881	1.7964	-2.1559	4.3410	1.7600	-2.1376	4.3173	1.7546	-2.1633
C26	2.8138	1.5048	-2.4817	2.9545	1.5364	-2.4759	2.9250	1.5276	-2.4757
N27	4.8087	2.8195	-2.7385	5.0254	2.7244	-2.7465	4.9838	2.7276	-2.7780
H28	4.2717	3.4792	-3.2897	4.5335	3.3964	-3.3245	4.4763	3.4044	-3.3367
H29	5.7914	2.9850	-2.5840	6.0122	2.8458	-2.5769	5.9730	2.8541	-2.6268
N30	4.8597	1.0431	-1.2879	4.9530	0.9991	-1.2346	4.9502	0.9877	-1.2804
H31	5.7929	1.2954	-1.0003	5.8967	1.2031	-0.9420	5.8995	1.1918	-1.0060
H32	4.4031	0.2386	-0.8764	4.4413	0.2417	-0.7987	4.4505	0.2250	-0.8400
N33	2.1689	2.1518	-3.6099	2.3653	2.1840	-3.6379	2.3095	2.1842	-3.6199
N34	2.0635	0.5880	-1.7872	2.1468	0.6895	-1.7699	2.1366	0.6723	-1.7622
O35	2.4474	3.3340	-3.8094	2.7012	3.3474	-3.8547	2.6264	3.3552	-3.8226
O36	1.4348	1.4907	-4.3158	1.6228	1.5360	-4.3451	1.5664	1.5359	-4.3256
O37	0.8157	0.6151	-1.9462	0.9003	0.7629	-1.9652	0.8847	0.7432	-1.9399
O38	2.5823	-0.2082	-0.9917	2.5979	-0.1001	-0.9289	2.6026	-0.1192	-0.9326
M39={ Ti,Zr,Hf}	-0.7761	-0.7072	-1.5482	-0.8134	-0.6201	-1.5797	-0.8165	-0.6175	-1.5772

Table 11: Atomic coordinates for $(\text{O}_2\text{N})_2\text{C}=\text{C}(\text{NH}_2)-(\text{H})\text{HN}\cdots\text{Cp}_2\text{MCH}_3^+$ (wB97X-D).

Compound	$(\text{O}_2\text{N})_2\text{C}=\text{C}(\text{NH}_2)-(\text{H})\text{HN}\cdots\text{Cp}_2\text{TiCH}_3^+$			$(\text{O}_2\text{N})_2\text{C}=\text{C}(\text{NH}_2)-(\text{H})\text{HN}\cdots\text{Cp}_2\text{ZrCH}_3^+$			$(\text{O}_2\text{N})_2\text{C}=\text{C}(\text{NH}_2)-(\text{H})\text{HN}\cdots\text{Cp}_2\text{HfCH}_3^+$		
Atom labels	X	Y	Z	X	Y	Z	X	Y	Z
C1	-0.8864	-1.8016	0.4777	-0.8529	-1.6679	0.6772	-0.8939	-1.6429	0.6537
H2	-0.6011	-2.8393	0.5666	-0.3974	-2.6274	0.8788	-0.4448	-2.6027	0.8672
C3	-0.1248	-0.6953	0.8960	-0.3340	-0.4100	1.0504	-0.3732	-0.3844	1.0244
H4	0.8552	-0.7363	1.3558	0.5928	-0.2439	1.5870	0.5462	-0.2195	1.5741
C5	-0.8840	0.4770	0.6280	-1.2595	0.5872	0.6332	-1.2922	0.6142	0.5944
C6	-2.0867	-1.3189	-0.1016	-2.0948	-1.4525	0.0167	-2.1281	-1.4271	-0.0213
H7	-2.8808	-1.9225	-0.5200	-2.7581	-2.2224	-0.3545	-2.7923	-2.1970	-0.3916
C8	-2.0969	0.0922	0.0251	-2.3537	-0.0577	0.0143	-2.3821	-0.0308	-0.0323
H9	-2.8966	0.7502	-0.2799	-3.2316	0.4265	-0.3894	-3.2540	0.4547	-0.4479
C10	0.7489	-2.5686	-1.8364	0.6846	-2.6939	-1.9701	0.6710	-2.6919	-1.9454
C11	1.4849	-1.5881	-2.5260	1.5469	-1.7333	-2.5425	1.5535	-1.7388	-2.5004
H12	2.5052	-1.3074	-2.3063	2.5680	-1.5459	-2.2370	2.5677	-1.5569	-2.1698
C13	0.6559	-1.0412	-3.5342	0.8488	-1.0882	-3.5980	0.8885	-1.1002	-3.5817
C14	-0.5436	-2.6385	-2.4250	-0.5521	-2.6460	-2.6724	-0.5456	-2.6448	-2.6822
H15	-1.3362	-3.3156	-2.1392	-1.4052	-3.2884	-2.4995	-1.4051	-3.2843	-2.5301
C16	-0.5926	-1.7015	-3.4819	-0.4403	-1.6640	-3.6891	-0.4001	-1.6721	-3.7043
H17	-1.4392	-1.5128	-4.1264	-1.2048	-1.4001	-4.4065	-1.1431	-1.4106	-4.4452
H18	0.9270	-0.2613	-4.2324	1.2415	-0.3186	-4.2498	1.3037	-0.3409	-4.2317
C19	-1.5596	0.8150	-2.6019	-1.5937	0.9642	-2.7148	-1.5738	0.9871	-2.7704
H20	-1.1583	0.9867	-3.6058	-1.1499	1.1827	-3.6945	-1.1333	1.1958	-3.7544
H21	-1.6932	1.7768	-2.0902	-1.7842	1.9096	-2.1864	-1.7729	1.9428	-2.2626
H22	-2.5647	0.4007	-2.7433	-2.5874	0.5503	-2.9343	-2.5696	0.5764	-2.9926
H23	-0.6034	1.4892	0.8900	-1.1756	1.6524	0.8100	-1.2088	1.6799	0.7689
H24	1.1203	-3.1736	-1.0223	0.9362	-3.3694	-1.1643	0.8980	-3.3632	-1.1289
C25	3.3291	1.2722	-2.3585	3.3964	1.1991	-2.3012	3.4074	1.1808	-2.2572
C26	1.9821	1.6167	-2.3341	2.0843	1.6549	-2.2457	2.0929	1.6284	-2.2231
N27	4.1144	1.4362	-3.5643	4.1501	1.2709	-3.5353	4.1808	1.2614	-3.4789
N28	4.0313	0.7632	-1.2122	4.0790	0.6284	-1.1730	4.0763	0.6136	-1.1185
N29	1.3779	2.3294	-3.2788	1.5086	2.4007	-3.1824	1.5265	2.3762	-3.1630
N30	1.1527	1.1975	-1.2677	1.2519	1.3013	-1.1572	1.2438	1.2628	-1.1473
M31={ Ti,Zr,Hf}	-0.3569	-0.5355	-1.4545	-0.3668	-0.4823	-1.4742	-0.3902	-0.4689	-1.5049
O32	5.0046	0.6443	-3.7796	4.9543	0.3961	-3.7681	4.9920	0.3909	-3.7024
O33	3.7762	2.3424	-4.3315	3.8681	2.1929	-4.3062	3.9068	2.1858	-4.2495
O34	5.2294	0.8877	-1.1575	5.2844	0.6257	-1.1585	5.2811	0.6161	-1.0872
O35	3.3515	0.2387	-0.3021	3.3791	0.1830	-0.2353	3.3655	0.1665	-0.1898
H36	1.9453	2.7364	-4.0164	2.0821	2.7474	-3.9456	2.1085	2.7294	-3.9167
H37	0.3719	2.4140	-3.2878	0.5080	2.5411	-3.1813	0.5236	2.5003	-3.1808
H38	0.5855	1.9793	-0.9468	0.7281	2.1121	-0.8294	0.7319	2.0780	-0.8096
H39	1.7735	0.8585	-0.5122	1.8668	0.9316	-0.4084	1.8554	0.8823	-0.3984

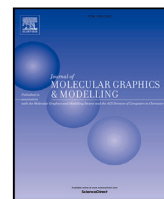
Bibliography

- [1] George B Bacskay. A quadratically convergent hartree—fock (qc-scf) method. application to closed shell systems. *Chemical Physics*, 61(3):385–404, 1981.
- [2] Matthias Krack and Andreas M Köster. An adaptive numerical integrator for molecular integrals. *The Journal of chemical physics*, 108(8):3226–3234, 1998.
- [3] Vyacheslav Ivanovich Lebedev and AL Skorokhodov. Quadrature formulas of orders 41, 47, and 53 for the sphere. In *Russian Acad. Sci. Dokl. Math*, volume 45, pages 587–592, 1992.
- [4] Juan Frau, Francisco Muñoz, and Daniel Glossman-Mitnik. A molecular electron density theory study of the chemical reactivity of cis-and trans-resveratrol. *Molecules*, 21(12):1650, 2016.
- [5] Juan Frau and Daniel Glossman-Mitnik. A conceptual dft study of the molecular properties of glycating carbonyl compounds. *Chemistry Central Journal*, 11(1):1–8, 2017.
- [6] Daniel Glossman-Mitnik and Jorge I Martínez-Araya. Kid procedure applied on the [(py5me2) moo]⁺ complex. *ACS omega*, 5(47):30549–30555, 2020.



Contents lists available at ScienceDirect

Journal of Molecular Graphics and Modelling

journal homepage: www.elsevier.com/locate/jmglmTheoretical investigation of the effect of $O \cdots M = \{Ti, Zr, Hf\}$ interactions on the sensitivity of energetic N-nitro compoundsNassima Bachir^a, Samir Kenouche^a, Jorge I. Martínez-Araya^{b,*}^a Group of Modeling of Chemical Systems using Quantum Calculations, Applied Chemistry Laboratory (LCA), University M. Khider of Biskra, 07000 Biskra, Algeria^b Departamento de Ciencias Químicas, Facultad de Ciencias Exactas, Universidad Andres Bello (UNAB), Av. República 275, 8370146 Santiago, Chile

ARTICLE INFO

Keywords:

Energetic material
 Metallocene methyl cation
 MEP analysis
 EDA-NOCV analysis
 QTAIM analysis
 IRI analysis
 N-NO₂ trigger bonds

ABSTRACT

This paper outlines the role of intermolecular interactions involving group 4 transition metals in stabilising the N-NO₂ trigger bonds. Minimising sensitivity is the foremost priority in designing energetic compounds. A quantitative analysis with Molecular Electrostatic Potential (MEP) evidenced anomalies arising from the marked depletion of negative charge distribution of RDX and HMX. The Energy Decomposition Analysis with Natural Orbitals for Chemical Valence (EDA-NOCV) results reveal that the electrostatic and orbital contributions are the dominant factors driving the assembly of the $M = \{Ti, Zr, Hf\}$ -based complexes. Sensitivity of the N-NO₂ trigger bonds is investigated by using the Quantum Theory of Atoms in Molecules (QTAIM). The QTAIM topological analysis showed that the $O \cdots M = \{Ti, Zr, Hf\}$ interaction strengthens these trigger bonds, revealing an increased stability to decomposition. This effect is more marked in the Hf- and Zr-based complexes. Finally, the results based on Interaction Indicator Region (IRI) are fully consistent with those generated from QTAIM analysis.

1. Introduction

All nations subscribed to the Ottawa Landmine Treaty [1,2] have compromised to destroy their antipersonnel mines. Furthermore, this treaty prohibits its use and stockpiles [3]. Such a process is known as humanitarian demining (HD). Nevertheless, HD is a hazardous procedure. It is also an expensive and slow method for cleaning the lands contaminated from munitions because several types of munitions contain energetic materials. A molecule is classified as energetic molecule, when its molecular structure includes one or more substituent groups called explosophores. An explosophore provides the oxygen needed to turn the energetic molecule into small molecules (like N₂, CO, H₂O) in short periods to release energy through heat and pressure. As time goes by, the ageing of energetic molecules makes them unstable compounds, decomposing partially into other molecules and increasing the risk of explosion caused by possible unsuitable handling.

A first step in identifying or designing a neutraliser for a particular energetic compound involves characterising its local chemical reactivity. This approach can reveal regions of the energetic molecule under study that are likely to be susceptible to undergoing electrophilic or nucleophilic attacks through non-covalent and covalent interactions. HMX (mass density 1.96 g/cm³, detonation velocity 9.1 km/s, and detonation pressure 381 kbar) and RDX (mass density 1.82 g/cm³, detonation velocity 8.8 km/s, and detonation pressure 342 kbar) are emblematic

energetic molecules [4] that can be used to test the influence of a possible neutraliser. Metallocene methyl cations (MMCs) originally involved in the catalysis for ethylene polymerisation, were theoretically assessed as possible neutralisers of FOX-7 [5]. This energetic compound is a derivative of ethylene, was thought to be highly reactive against MMCs through double bond π -electrons. However, after proper investigations, we realised that π -electrons from the double bond were less reactive when compared against those of oxygens of nitro groups. We found that a stable complex between FOX-7 and MMC is formed. Such an article opened the possibility to explore interactions with any energetic molecule bearing at least one nitro group under the assumption that this substituent group can favourably interact with a cation like MMCs. If so, we can postulate MMCs as neutralisers of any energetic organic molecule.

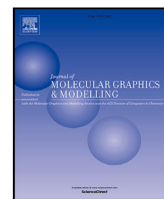
However, the assessment through following a trajectory on the potential energy surface (PES) implies a computational cost that we would like to reduce by using alternative methodologies that should lead to similar conclusions without performing a relaxed scan procedure or intrinsic reaction coordinate (IRC) method along the PES. Indeed, the present study intends to support these findings by exploring other energetic molecules (HMX and RDX depicted in Fig. 1) through quantum chemical methods that provide more chemically useful information. Further, we resorted to IRI (Interaction Indicator Region),

* Correspondence to: Av. República 275, Santiago, Chile.
 E-mail address: jorge.martinez@unab.cl (J.I. Martínez-Araya).



Contents lists available at ScienceDirect

Journal of Molecular Graphics and Modelling

journal homepage: www.elsevier.com/locate/jmglm

The effect of $\{O, N\} = X \cdots M = \{Ti, Zr, Hf\}$ interactions on the sensitivity of C–NO₂ trigger bonds in FOX-7: Approach based on the QTAIM/EDA-NOCV analysis

Nassima Bachir^a, Samir Kenouche^a, Jorge I. Martínez-Araya^{b,c,*}^a Group of Modeling of Chemical Systems using Quantum Calculations, Applied Chemistry Laboratory (LCA). University M. Khider of Biskra, 07000 Biskra, Algeria^b Departamento de Ciencias Químicas, Facultad de Ciencias Exactas, Universidad Andres Bello (UNAB), Av. República 275, 8370146 Santiago, Chile^c Centro de Química Teórica y Computacional (CQT&C). Facultad de Ciencias Exactas, Santiago, Chile

ARTICLE INFO

Keywords:

Energetic molecules
Sensitivity of trigger bonds
FOX-7 or DADNE
Metallocene methyl cations
ESP/EDA-NOCV/QTAIM analysis

ABSTRACT

The local chemical reactivity of FOX-7 (1,1-diamino-2,2-nitroethylene, also known as DADNE from DiAmino-DiNitroEthylene) was elucidated through a quantitative study of the electrostatic potential on the molecular surface, topological analysis based on Bader's theory, and the EDA-NOCV method. Unlike $(O_2N)_2C=C(NH_2)-H_2N \cdots Cp_2MCH_3^+$ complexes, which exhibit both σ -donor and π -acceptor features, the situation is different concerning the $(H_2N)_2C=C(NO_2)-(O)NO \cdots Cp_2MCH_3^+$ complexes, where both charge transfers correspond to the σ -donation. The two charge transfers reinforce each other, resulting in increased stability for $(H_2N)_2C=C(NO_2)-(O)NO \cdots Cp_2MCH_3^+$. This seems to strengthen the $(H_2N)_2C=C(NO_2)-(O)NO \cdots M = \{Ti, Zr, Hf\}$ bond, which may explain the high stability of $(H_2N)_2C=C(NO_2)-(O)NO \cdots Cp_2MCH_3^+$ compared to $(O_2N)_2C=C(NH_2)-H_2N \cdots Cp_2MCH_3^+$. Results from topological analysis revealed that the decreased sensitivity to decomposition of C–NO₂ bonds depends on the chemical nature of the interacting metal, and the best achievements are obtained for the Hf-based complex. Our results demonstrate that the interaction of $M = \{Ti, Zr, Hf\}$ with C–NO₂ is more favourable than that with C–NH₂, this specific action on the trigger bond may support the use of Metallocene Methyl Cations (MMC) as possible neutralisers.

1. Introduction

Understanding the decomposition process is an increasingly crucial factor in the field of energetic materials (EM) [1–3]. The trigger bond, also known as the “trigger linkage mechanism”, is a widely accepted concept in the decomposition mechanism of such materials [4–9]. This concept was first defined by Kamlet and Adolph [10], and allows to understand the impact sensitivity of EM from a molecular perspective. The trigger bond is a concept referred to as the trend presented by certain bonds to break apart in EM as a response to energy input from an external stimulus; their rupture “triggers” the exothermic decomposition that characterises detonation [11]. Sensitivity to detonation is an essential characteristic of EM. This property refers to the vulnerability of these compounds to unexpected detonation due to an involuntary stimulus (sparks, friction, shock, etc.) [12–14]. An explosion caused by these molecules occurs when a highly exothermic reaction takes place, instantly releasing a large amount of heat along with a large amount of gas, which expands and moves at high speed [15,16].

One of the main challenges in EM is reducing the sensitivity without losing the detonation efficiency, although these two objectives seem intrinsically contradictory. From a practical point of view, an optimal balance between these two fundamental characteristics achieves this task. Other essential facts, such as cost of synthesis and transformability are considered for designing new energetic molecules.

Non-explosive reaction channels for the decomposition of EM have been proposed [11,17,18], which could be attained by selecting specific chemical compounds to react on certain sites of an energetic molecule, and preventing the latter from following its normal explosion channel. The surfaces of EM are prone to possessing quite positive electrostatic potentials [19], suggesting reactivity towards nucleophiles. It is a well known fact that nitroaromatics react with amines [20]. The 2,4,6-trinitrotoluene (TNT) can be neutralised by exposure to aliphatic amines, leading to hypergolic combustion of the TNT [21]. In this study, we define a neutraliser as a molecule able to form a complex with an energetic molecule, thus preventing the latter from following its

* Corresponding author at: Departamento de Ciencias Químicas, Facultad de Ciencias Exactas, Universidad Andres Bello (UNAB), Av. República 275, 8370146 Santiago, Chile.

E-mail address: jorge.martinez@unab.cl (J.I. Martínez-Araya).

¹ Present address: Av. República 275, Santiago-Chile.

<https://doi.org/10.1016/j.jmglm.2023.108645>

Received 28 March 2023; Received in revised form 27 September 2023; Accepted 27 September 2023

Available online 4 October 2023

1093-3263/© 2023 Published by Elsevier Inc.

Explaining the High Catalytic Activity in Bis(indenyl)methyl Zirconium Cation Using Combined EDA-NOCV/QTAIM Approach

Samir Kenouche⁺,^[a] Nassima Bachir⁺,^[a] and Jorge I. Martínez-Araya^{*[b]}

This article is dedicated to Prof. Dr. Peter Politzer, respected and outstanding scientist, who passed away on Friday, June 10, 2022. He served University of New Orleans for 40 years as a brilliant, dedicated teacher who will be remembered as an internationally-recognized researcher in theoretical and computational chemistry.

The main purpose of this study is to elucidate some discrepancies already observed in the catalytic activity values of some zirconocene methyl cations. The EDA-NOCV scheme was employed for a theoretical description of the interactions between an ethylene molecule and five catalysts of zirconocene methyl cation. The nature of the chemical interactions has been elucidated through the QTAIM topological analysis. The steric hindrance due to the ligands was evaluated qualitatively by means of an IRI-based analysis and quantitatively through Fisher information. The findings prove that the indenyl ligand seems to favor the orbital interaction between the ethylene molecule and the metal centre of zirconocene methyl cation. Both

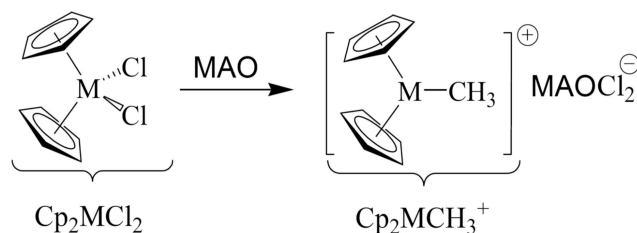
electrostatic and orbital contributions play a crucial role in stabilising the studied complexes. Based on the NOCV deformation density contributions, the strongest orbital interaction is reached with the bis(indenyl)methyl zirconium cation, which is the only one exhibiting covalent interactions. Especially, the strong contribution of π -back donation (occurring from the occupied orbitals of the zirconium atom to the π^* anti-bonding orbital of ethylene) may be a key to understand why this catalyst has a higher polymerisation yield than the other studied catalysts. This work suggests a perspective for predicting values of catalytic activity when theoretically designing novel catalysts of zirconocene type.

Introduction

Metallocene methyl cations of group 4 usually have been employed as catalysts of polymerisation reactions.^[1–12] The polymerisation implies a multistep process where three types of stages take place: initiation, propagation, and termination.^[13] Researchers involved in the computational study of the polymerisation processes resort to the Cossée-Arlman's^[14–16] mechanism when low monomer concentrations are assumed; while, at high monomer concentrations, the Ystenes' mechanism is taken into account^[17,18] instead. The monomer is an olefin molecule; then, the catalysis is driven by the affinity for π -electrons presented by the metallic atom of the metallocene methyl cation,^[1,16,19,20] thus leading to coordination of the olefin onto the metallic atom. Commonly, metallocene methyl cations

based on Zirconium are called zirconocene methyl cations. These cations are produced *in situ* from neutral dichlorozirconocenes through an interaction with a co-catalyst^[21–23] the latter being a Lewis acid so that it can replace the two chlorine atoms with one methyl group as Scheme 1 depicts. The co-catalyst that is usually employed corresponds to methylaluminoxane (MAO).^[24] Furthermore, the solvent employed is *n*-pentane.^[25] We have assumed that co-catalyst and solvent are constant factors and do not influence the chemical reactions as stated in the respective reference.^[25]


Generally speaking, a zirconocene methyl cation can be represented as $[L_1L_2ZrCH_3]^+$, where L_1 , and L_2 are commonly ligands, usually cyclopentadienyl (Cp), indenyl (Ind), or fluorenyl (Flu), and all their possible derivatised versions (i.e. including substituent groups) in the Scheme 1, we have that




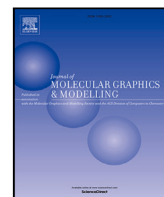
Scheme 1. MAO co-catalyst can replace two chlorine atoms with one methyl group. The resulting cationic species has catalytic properties through its ability to coordinate one olefin molecule.

[a] Dr. S. Kenouche,⁺ N. Bachir⁺
Group of Modeling of Chemical Systems using Quantum Calculations,
Applied Chemistry Laboratory (LCA), University of M. Khider of Biskra, BP
145 RP, 07000 Biskra, Algeria
E-mail: samir.kenouche@univ-biskra.dz
nassima.bachir@univ-biskra.dz

[b] Dr. J. I. Martínez-Araya
Departamento de Ciencias Químicas, Facultad de Ciencias Exactas,
Universidad Andres Bello (UNAB), Av. República 275, 8370146 Santiago,
Chile
E-mail: jorge.martinez@unab.cl

 These authors contributed equally.

 Supporting information for this article is available on the WWW under
https://doi.org/10.1002/cphc.202200488



Aromaticity of six-membered nitro energetic compounds through molecular electrostatic potential, magnetic, electronic delocalization and reactivity-based indices

Samir Kenouche^a, Nassima Bachir^a, Wissam Bouchal^b, Jorge I. Martínez-Araya^{c,d,*}

^a Group of Modeling of Chemical Systems using Quantum Calculations, Applied Chemistry Laboratory (LCA). University M. Khider of Biskra, 07000 Biskra, Algeria

^b Molecular Chemistry and Environment Laboratory, University of Mohammed Khider of Biskra, BP 145 RP, Biskra 07000, Algeria

^c Departamento de Ciencias Químicas, Facultad de Ciencias Exactas, Universidad Andres Bello (UNAB), Av. República 275, 8370146 Santiago, Chile

^d Centro de Química Teórica y Computacional (CQT&C). Facultad de Ciencias Exactas, Santiago, Chile

ARTICLE INFO

Keywords:

Aromaticity indices
Nitro energetic molecules
ESP analysis
Resonance energy

ABSTRACT

The electron density depletion associated with π -hole at the ring center typical of energetic compounds was clearly revealed by the molecular electrostatic potential (ESP). In addition, the spatial arrangement of NO₂ groups appears to affect the ESP value in the ring center, and therefore sensitivity to detonation. Indeed, for monocyclic nitrobenzene compounds with the same number of NO₂ groups, the ESP value in the ring center decreases as the NO₂ groups are more closely spaced. As expected, the central rings become less aromatic as NO₂ groups are added. The MCI, PDI, PLR, NICS_{zz}(1), FLU indices are all strongly correlated with the ESP values observed in the ring center of the set of nitrobenzenes. Aromaticity indices based on electron delocalization criteria appear to be very sensitive to small variations in aromaticity. Among magnetic-based indices, only NICS_{zz}(1) is capable to predict small changes in aromaticity. The PLR index derived from conceptual DFT is quite relevant for predicting small variations in aromaticity. According to our results, the most suitable aromaticity index is not based on a single criterion, and that selecting it is more subtle. Therefore, it is important to combine information from several criteria to obtain a more complete description of the aromaticity of the studied compounds.

1. Introduction

Nitroaromatic compounds are largely derived from human activities and are rarely found in nature. These compounds are widely used in manufacturing, particularly in the synthesis of dyes, polymers, pesticides and explosives [1–4]. The reactivity of these compounds is mainly governed by the electron-withdrawing nature of the nitro groups. The high electronegativity of the nitro group arises through the simultaneous action of the two electron-deficient oxygen atoms bonded to the partially positive nitrogen atom. When such a substituent is attached to a benzene ring, the NO₂ group tends to delocalize the ring's π -electrons to overcome its intrinsic charge deficiency. The delocalization of π electrons directly affects many aspects of the properties of these compounds, such as thermodynamic stability, and reactive sites.

Conjugated cyclic compounds show high diamagnetic susceptibility, and this magnetic irregularity is associated with the ring current [5]. The difficulty lies in quantifying the π -electron delocalization that causes this ring current [6]. Since Hückel's rules of thumb on aromaticity describing the electronic cyclic delocalization, it is definitely

accepted that the aromatic character of a molecule implies a higher stability compared to molecules with similar structures but not aromatic [7–9]. Pauling and Sherman were the first to describe aromaticity in quantitative terms, through the concept of resonance energy [10]. Although aromaticity is a fundamental concept in modern chemistry, its exact definition is still not established [11]. As aromaticity is not a measurable magnitude, it is commonly assessed indirectly by quantifying a property which reveals the aromatic nature of the whole or portions of a molecule. However, it is commonly accepted that aromaticity is akin to electronic delocalization in conjugated chemical bonds that form closed loops, either in two or three dimensions [12,13]. The idea behind this concept is that aromaticity is proportional to the ring current strength induced by the π -electrons delocalization. Certainly, the concept of aromaticity plays a major role in rationalizing reactivity of aromatic compounds, and represents a stabilizing factor [14]. Recently, several descriptors based on energetic, magnetic, structural and chemical reactivity criteria have been proposed to quantify aromatic

* Correspondence to: Av. República 275, Santiago, Chile.
E-mail address: jorge.martinez@unab.cl (J.I. Martínez-Araya).